An investigation into the relaxation response of a self-healing dual network polymer through controlled introduction of strain damage

Caspar Bartholome Roth

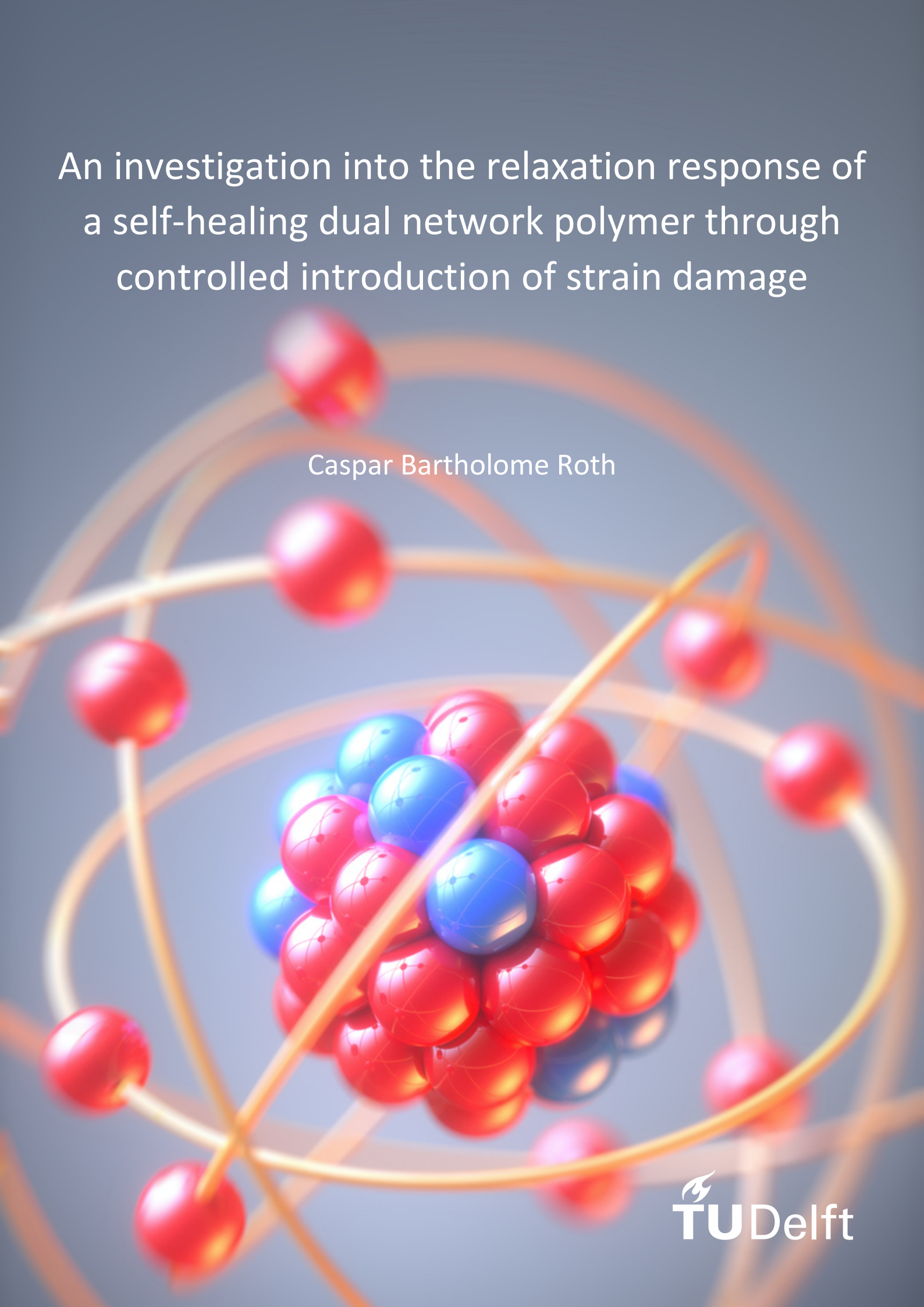

TU Delft

Title page image credits: University of Nottingham Press Office

An investigation into the relaxation response of a self-healing dual network polymer through controlled introduction of strain damage

by

Caspar Bartholome Roth

in partial fulfilment of the requirements for the degree of

Master of Science

in Aerospace Engineering

at the Delft University of Technology,

to be defended publicly on Friday August 27 2021 at 13:00.

GRADUATION COMMITTEE

Chair holder	Prof. dr. ir. Sybrand van der Zwaag
Committee members	Dr. Santiago J. Garcia (supervisor)
	Dr. Marlies Nijemeisland
	Ir. Jos Sinke

TU Delft

[This page is intentionally left blank]

ACKNOWLEDGEMENTS

This work concludes my time as a student, which stretched across eight wonderful years. I fully realize that most people will never get to experience a single year of student life, let alone eight, and I am extremely grateful to have been given this opportunity. A wise man once told me that I would be alright if I just took my time. I think my student years are a testimony to that. This is not the same as idleness: my journey here at TU Delft has taken me from the Netherland to the United States, from Australia to Portugal, from robotics to studying molecules, and from building a solar car to walking a catwalk. I am fully convinced that these experiences have made me a more well-rounded person, and I look back on my time at TU Delft with satisfaction and gratitude.

The realization of this thesis was not an easy task, and I would like to thank those who helped me get though this last part of my academic journey. First and foremost, I would like to thank my supervisor, Santiago Garcia. You stimulated me to think beyond the obvious, and to go the extra mile. You gave me the freedom to explore by myself, which is invaluable in grooming an independent researcher. With you at the wheel, academia will not soon run out of ideas. Sybrand van der Zwaag, chairholder of the Novel Aerospace Materials group. Your wealth of knowledge and calm demeanor were an inspiration. Thanks for always making time for me. Marlies Nijemeisland, thank you so much for your support in all the practical challenges that a thesis brings. You were my lifeline during rheometer and DMA experiments. Shanta Visser, thank you for being the spider in the web of NovAM, and helping me arrange all things necessary to graduate. Paul Denissen, thanks for your advice and tips, and for generously introducing me to the world of CNC machining! Yasir Khan, a big shoutout for being the ultimate rubber duck! My brothers Siddharth Yoshi, Krishna Rawat, Mark Ablonczy, Nikhil Bhootpur, and Anuj Kumthekar. Still don't know who the imposter is. Everyone at NovAM, thank you for being so very approachable and helping me discover research and academia. My housemate, Tawfik. You're such a positive soul. I'm sorry but I really cannot leave your phone number here. My lovely girlfriend, Anna. Thank you for never-ending adventures, laughs and love. And finally, my parents, Louis and Patricia Roth. Thank you for being the most supportive parents I could wish for.

ABSTRACT

Self-healing ability in polymers is typically probed by monitoring restorative properties after localized macroscopic damage or repetitive cycles of destructive testing followed by a healing cycle (e.g. cut-and-heal tests). However, the restoration of homogeneously distributed damage before ultimate failure remains largely unattended in literature. This work investigates whether damage degree and damage restoration after plastic deformation in self-healing polymer networks can be identified via continuous relaxation spectra from rheology, which were recently successfully employed to identify energy contributions in self-healing polyurethanes. As a model system a self-healing epoxy-silane dual network with dynamic sulfur-sulfur bonds is used together with a non-healing reference epoxy. Three levels of deformation are probed: pristine, partially plastic (near yield), and fully plastic (near failure).

Compared to the non-healing reference epoxy, the self-healing epoxy is observed to have faster dynamics of the main relaxation peak and to dissipate more energy at very fast (10^{-9} s) relaxation times. It is found that any level of plastic deformation (near yield or near failure) induces clear changes in the energy profile compared to the pristine state (e.g. relaxation peak height drop). Between the two levels of plastic deformation, no clear distinction could be made. An oven treatment, intended to repair any induced damage by stimulating network mobility through sulfur-sulfur bond reshuffling above T_g, was found to shift the energy profile to longer relaxation times for both pristine and plastically deformed samples not observed in the non-healing polymer. However, this time shift could be undone by allowing a one week recovery period after the oven treatment. It is proposed that the observed behavior can be explained by trapping, in self-healing polymers, a non-equilibrium polymer state through quenching. Despite the necessary further research, the results confirm the potential of continuous relaxation spectra to evaluate damage degree and damage restoration in plastically deformed self-healing polymers.

TABLE OF CONTENTS

LIST OF FIGURES

1. INTRODUCTION

1.1. Self-healing materials

Similar to natural systems like skin tissue and bone, artificial self-healing materials have the ability to restore damage, thereby extending their lifetime [1]. Since the trailblazing publications by White et al. [2] in the early 2000s, an abundance of such self-healing materials have been developed across polymers, metals and ceramics [3]. Regardless of the materials choice, self-healing systems must have the ability to provide local, temporary mobility. This concept is easily understood by analogy to wound healing (**Figure 1.1**). Here, specialized white blood cells trigger an inflammation reaction at the damage location, resulting in swelling and wound closure. By the time the inflammation reaction seizes, reconstruction of the underlying vascular system and surrounding cell bodies has sufficiently progressed to allow long term recovery of function and strength [4].

Figure 1.1 *Four stages of wound healing. Image retrieved from [4].*

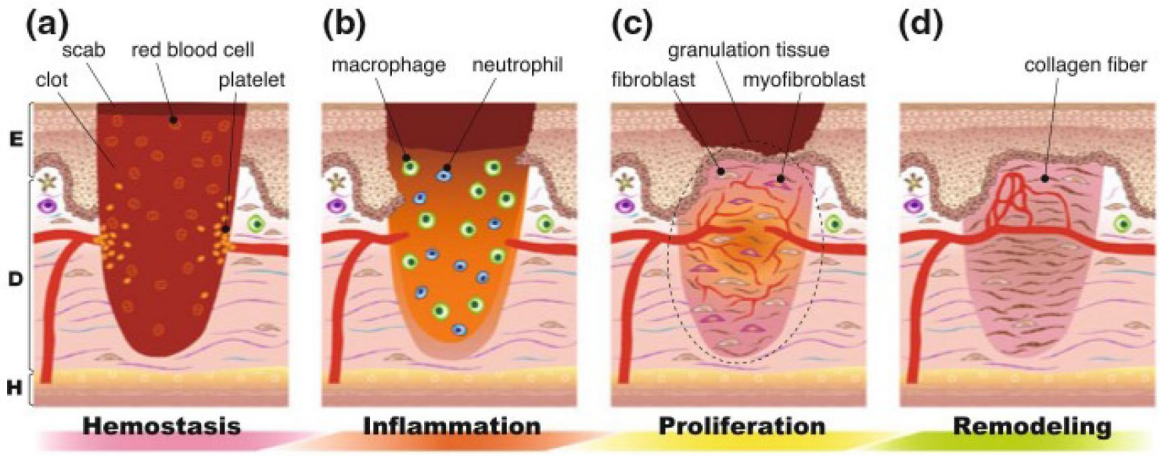

Self-healing materials can be broadly categorized as extrinsic or intrinsic [5], depending on the origin of their healing abilities. In extrinsic healing, healing ability is (mainly) provided by an *external* agent, that is, not by the material matrix itself. A classic example is that of microcapsules containing a healing agent, embedded in an otherwise non-healing material. Upon cracking of the matrix under stress, these microcapsules rupture and release healing agent into the crack plane, where they react with an embedded catalyst or curing agent and eventually close the crack (**Figure 1.2a**). Extrinsic healing has the advantage that in principle any material can be converted into an extrinsic healing material given the right choice of healing agent. On the downside, healing effectiveness strongly depends on the geometry and distribution of the healing capsules, and healing capacity is finite as healing agent depletes with each cracked capsule. Moreover, excessive healing capsules negatively affect the mechanical properties of the matrix, being essentially holes in the matrix structure [6].

In intrinsic healing, healing ability is *integrated* into the material matrix [7]. Materials containing dynamic covalent bonds are a prime example of this category. Such bonds can be broken and healed indefinitely provided an appropriate stimulus (e.g. temperature, UV light, pH). As a result, the number of healing cycles is in principle only limited by deterioration of the dynamic bonds (**Figure 1.2b**). However, the mobility required for and introduced by dynamic bonds typically results in lower mechanical properties [8], and the material matrix must be adaptable to facilitating dynamic bonds.

It is not difficult to understand that a great challenge in self-healing material design lies in optimizing the balance between mechanical properties, healing properties, and function. Indeed, proper design of self-healing materials requires a thorough understanding of the material system and its interplays.

Figure 1.2 (a) *Extrinsic healing.* ***(b)*** *Intrinsic healing. Image retrieved from [9].*

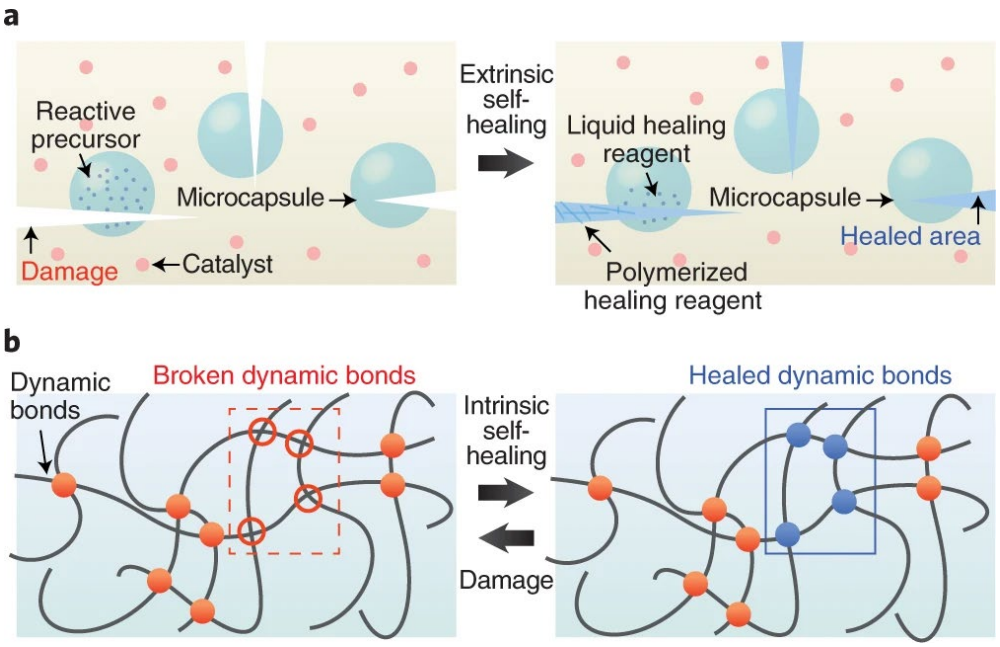

1.2. Assessment of self-healing capability

In polymer literature, several methods exist to examine self-healing capability. A first method involves denting [10] or scratching [11, 12] (**Figure 1.3**) a polymer surface and monitoring healing, again typically promoted by an external stimulus. This method gives insight into *the dynamics of healing for very local (non)destructive damage*. It is particularly suitable for investigating the effects of delayed elasticity [13, 14], where the mobility required for healing is in part provided by energy stored in the damage walls.

Figure 1.3 *Scratch closure of a polyurethane coating. Image retrieved from [13].*

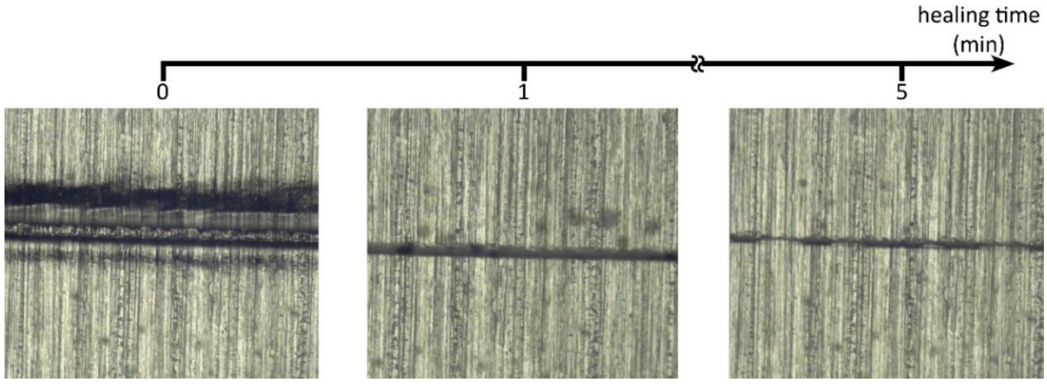

A second, widely used method involves cutting a self-healing polymer in half and / or tensile loading it to failure, placing the two halves back together, and allowing some healing period until (optical) healing is achieved (**Figure 1.4a**). Here, healing is typically promoted by one or more external stimuli that resonate with the self-healing part of the polymer. This cycle of loading and healing is repeated a number of times, and the evolution of the mechanical properties is tracked [15, 16] (**Figure 1.4b**). This method *simultaneously probes the dynamics of healing for homogeneously distributed nondestructive damage throughout the polymer and very local, destructive damage at the fracture site.* Generated data is highly useful for estimating the service lifetime of the self-healing material. Moreover, a change of fracture plane between loading cycles is a direct indicator of full local recovery of mechanical properties.

Figure 1.4 (a) *Room temperature healing of a clean cut self-healing thermoplastic polyurethane elastomer. Image retrieved from [15].* ***(b)*** *Stress-strain curves of three fracture-healing cycles of a dynamically crosslinked polystyrene polymer. Images retrieved from [17].*

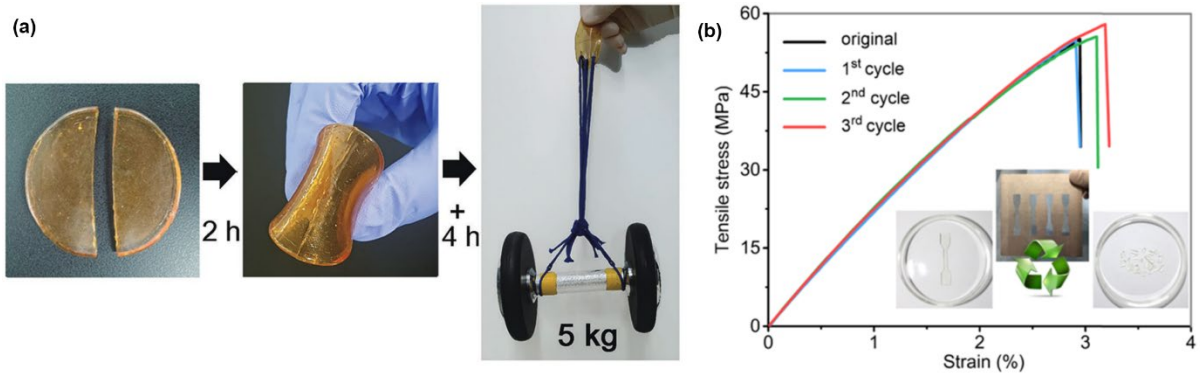

Most studies either focus on healing of small, highly local damages or healing after destructive failure. Interestingly, *the identification and healing of homogeneously distributed damages before ultimate failure* is largely unattended in literature. Studies of this type are important, not only because they can highlight how homogeneously

distributed damage may affect the dynamics of healing at the fracture site, but also because homogeneously distributed non-destructive damage is a very relevant load case for real-life application of self-healing materials.

The topic is not entirely unexplored; several works investigating the healing of non-destructive damages induced by fatigue loading were found. Post et al. [18] embedded Fe_3O_4 nanoparticles into a series of poly(ethylene-*co*-methacrylic acid) zinc ionomers that enabled healing of various degrees of fatigue damage by inductive heating. Here, a combination of optical microscopy, calorimetry, mechanical testing and shear rheology was used to unravel a two-stage healing mechanism specific to ionomers. Hernandez and coworkers [19] explored broadband dielectric spectroscopy (BDS) as a tool to assess healing of strain induced fatigue damages in a disulfide containing natural rubber. For a 50% cured rubber it was found that both fatigue damaging and subsequent healing at optimal disulfide reshuffling temperature led to a distinct broadening of the dielectric loss spectrum. Specifically, fatigue damaging led to a broadening towards higher frequencies, corresponding to an increased presence of more mobile dangling chains generated through bond cleavage. Subsequent healing reduced activity on the high frequency end to pristine levels, but increased low frequency activity far beyond pristine levels. These changes were attributed to the formation of a new polymer architecture with fewer dangling chains and increased hindrance from intermolecular interactions, enabled by increased mobility at the healing temperature due to disulfide reshuffling.

The combination of optical and mechanical test methods utilized by Post et al. to identify damage and healing is well established in the self-healing research field [20]. Additional information about frequency dependency, such as obtained from BDS spectra, can help tremendously in understanding healing behavior. Indeed, the work of Hernandez and coworkers showed that damage and healing can observed directly from dielectric spectra. However, because limited resolution (dielectric spectra represent the average of all chain motions [19]) may limit understanding of the underlying polymer physics. In this regard, continuous relaxation spectra obtained from viscoelastic data may provide an interesting alternative.

1.3. The continuous relaxation spectrum

Continuous relaxation spectra (CRS) show a distribution function of the relaxation intensity (modulus) with time [21] (**Figure 1.5**). They physically represent an idealized experiment wherein a polymer sample is instantaneously strained at a constant reference temperature and the stress relaxation response is observed [22]. Recently, Montano et al. [23] employed continuous relaxation spectra in an attempt to better understand the behavior of a series of self-healing polyurethanes. Specifically, mechanical Maxwell-Weichert modeling was used to identify how the total relaxation energy (area under curve, **Figure 1.5**) was built up from contributions by overlapping relaxation phenomena. Results were validated by correlating the resulting discrete mechanical models to a priori knowledge about the specific molecular structures. From this work by Montano et al. it appears that when correctly used, CRS may

give high resolution information about polymer relaxation processes that is not readily available from other existing characterization techniques.

The stress relaxation response obtained from CRS mirrors the state of stress within the polymer. This state depends on many factors including the temperature, cure cycle, thermal history, load history and, importantly, the internal state of damage. Under plastic deformation, permanent bonds will be broken, thereby altering the equilibrium position of the unstressed polymer. This will in turn change the stress relaxation response. *For this reason it should theoretically be possible to use CRS to identify – and perhaps even quantify – homogeneous non-destructive damage by tracking changes to the stress relaxation response with respect to the pristine state*. Moreover, it could be possible to observe healing as a return of the stress relaxation response to the pristine state. In literature, no other attempts were found at identifying damage and healing through conformal changes to continuous relaxation spectra.

Figure 1.5 *Continuous relaxation spectrum of self-healing epoxy (T_{ref} = 70°C). The area under the curve, highlighted in yellow, represents the energy dissipated in relaxation.*

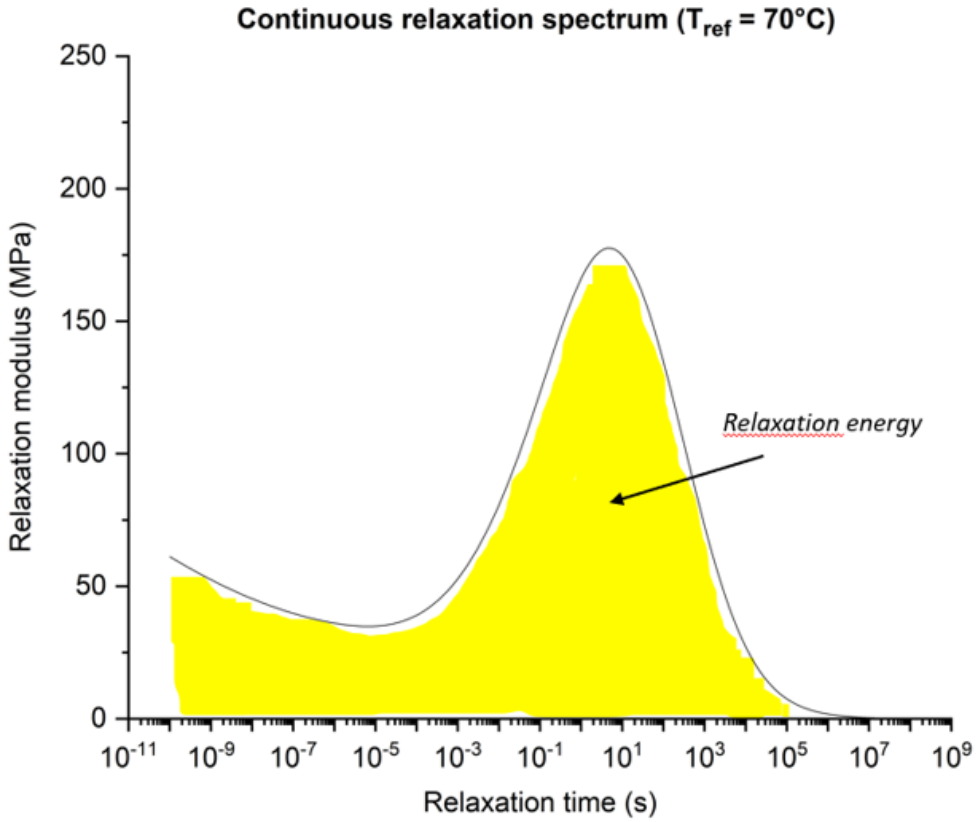

1.4. Research questions

This thesis attempts a novel approach at identifying the presence and healing of homogeneously distributed damage in self-healing materials. It is motivated by the lack of studies on early stage damage restoration and its relevance to practical applications of self-healing materials, where healing of damage before ultimate failure is typically preferred. Specifically, this work aims to provide answers to the following research questions:

RQ1) Can plastic deformation in self-healing polymers be identified using continuous relaxation spectra?

RQ2) Can the effect of a healing treatment be identified using continuous relaxation spectra?

RQ3) Can continuous relaxation spectra be used as a quantification method for measuring plastic deformation and healing in polymers?

1.5. Thesis structure

This concludes the introduction chapter. The remainder of this thesis is structured as follows. **Chapter 2** contains a basic theoretical background on dynamic disulfide bonds, and the derivation and limitations of continuous relaxation spectra. **Chapter 3** explains the materials choice and structure of experiments. **Chapter 4** elaborates on the synthesis and experimental procedures. Results are presented in **Chapter 5** and discussed in detail in **Chapter 6**. Conclusions of this thesis work are drawn in **Chapter 7**, and recommendation for future work are found in **Chapter 8**. Supplementary information is contained in the **Appendices**.

2. THEORETICAL BACKGROUND

2.1. Covalent Adaptable Networks (CANs) and disulfides

Covalent Adaptable Networks (CANs) are dynamic polymers with hybrid properties of thermosets and thermoplastics [24]. They are designed such that under operating conditions they act as a thermoset, showing good mechanical properties and limited creep due to the presence of crosslinks. However, under specific stimuli (e.g. temperature, UV irradiation, pH) they will flow like a thermoplastic, allowing damage to be healed and enabling reshaping and recycling. The secret of this hybrid nature lies in the presence of dynamic bonds. There is a wide variety of these dynamic bonds, of which Diels-Alder and disulfides are some of the most investigated [25]. Dynamic bonds can be grouped based on their mechanism of repositioning as either associative or dissociative. These give rise to different behaviors. Dissociative bonds separate (dissociate) under appropriate stimuli, reducing the number of crosslinks in the polymer. In associatively bonded polymers the crosslink density remains approximately constant. Rather than dissociating, these bonds shuffle in each others proximity - somewhat like switching dancing partners – thereby minimizing the time spent in the dissociated state [26, 27].

Disulfides are a versatile dynamic bond that can be triggered by many stimuli [28], although temperature is the most commonly used trigger. They are broadly applied in self-healing materials for their combination of good mechanical properties with relatively mild healing temperatures [29]. Disulfides display a combination of associative and dissociative behavior (**Figure 2.1**). At room temperature, they are quite stable. However, as energy increases with temperature the bonds may break and very briefly form thiyl radicals [30]. These radicals then recombine (dissociative) to form new disulfide bonds, or they attack a nearby disulfide bond to form a new disulfide bond and a new radical. Alternatively, two disulfide bonds can encounter and reshuffle (associative) to form two new disulfide bonds.

Figure 2.1 *Reshuffling mechanisms in aromatic disulfide bonds. These mechanisms are also representative for aliphatic disulfide bonds. Image retrieved from [24].*

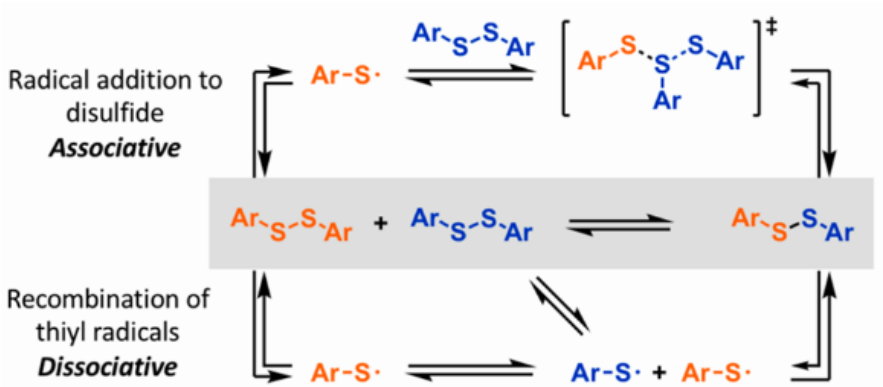

2.2. Time-Temperature Superposition (TTS)

Frequency master curves show the variation of polymer properties with frequency at a given temperature, and are a necessary intermediate step to generating (continuous) relaxation spectra. Problematically, viscoelastic measuring devices (e.g. DMA, rheometer) are typically operated within a very limited frequency band of 0.01 to 100 Hz due to issues associated with higher (cannot be measured) and lower (extremely time-intensive) frequency measurements. The solution to this problem lies in time-temperature Superposition (TTS). This principle uses the equivalence of time and temperature to extrapolate measurements within a narrow frequency range to higher and lower frequencies [31]. At a constant strain loading, stress relaxes faster at higher temperatures because of the greater available energy and thus mobility (**Figure 2.2a**). It has been observed that within the Linear Viscoelastic Range (LVR) there is a linear relationship between time (time = 1 / angular frequency) and temperature, such that the time required for a viscoelastic relaxation at a temperature T_{high} is proportionally shorter than the time it would take for this same relaxation to occur at a lower reference temperature T_{ref} by a factor a_T , such that $t_1 = (1/a_T)t_2$, where t_1 and t_2 are the relaxation times required to reach a certain stress level σ for T_{high} and T_{ref} , respectively. The opposite holds true for low temperatures. This enables extrapolation or 'shifting' of measurements within a narrow frequency band to a much broader frequency band (known as a 'TTS master curve'), if those measurements have been taken over a sufficient range of temperatures (**Figure 2.2b,c**).

Figure 2.2 (a) *Stress relaxation at different temperatures. Within the LVR,* $t_1 = (1/a_T)t_2$. ***(b)*** *Experimental frequency data before TTS, obtained between 0 and 100°C in 5°C steps. The lowest storage modulus curve corresponds to the highest temperature, and vice versa.* ***(c)*** *Experimental frequency data after TTS, shifted to reference temperature* T_{ref} *= 70°C.*

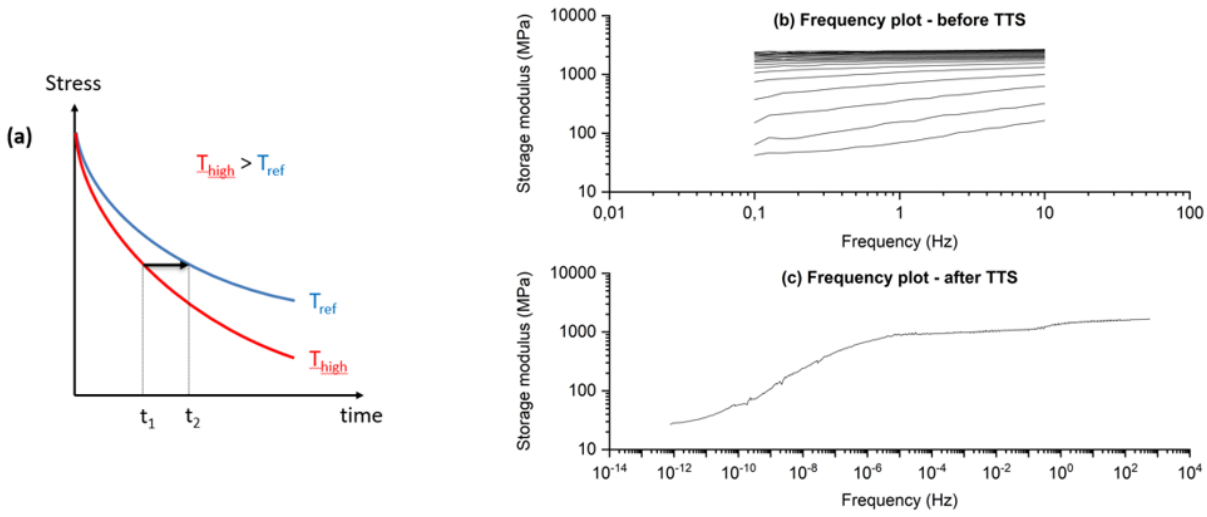

2.3. Limitations of TTS

TTS cannot be universally applied. In principle, it can only be applied to materials displaying thermorheologically simple behavior [32]. This means that a change in mechanical properties obtained by changing the temperature can be identically produced by a change in frequency [33]. This requirement puts restrictions on the material choice. For example, the material must be homogeneous and isotropic because the presence of phases or a significant degree of orientation may result in nonlinear thermal behavior. For the same reason, the material must be amorphous – i.e. not (partially) crystalline. The material must not be strained outside the LVR. Finally, TTS should not be performed near T_g, or any transition temperature for that matter, because the T_g depends on thermal history. There are exceptions to this last condition. For example, Williams, Landel and Ferry [34] proposed an empirical relationship between a_T and temperature in the range (T_g, T_g + 100°C):

$$\ln a_T = -\frac{C_1(T - T_{ref})}{C_2 + (T - T_{ref})} \qquad \textit{Eq. 1}$$

where C_1 and C_2 are constants that depend on the material and reference temperature. This relationship, often known as the Williams-Landel-Ferry (WLF) model, makes TTS much more broadly applicable as it does not exclude measurements near T_g, which are often desirable. It is also the shifting model used in this thesis.

Over the years, TTS has been applied to materials that do not conform to the requirement for thermorheological simplicity. For example, Kirkwood et al. [35] applied TTS to isopropene comb polymers. Bose et al. [36] found that the kinetics of healing of self-healing ionomers closely followed the timescales of network and cluster formation obtained from TTS master curves. More recently, Montano et al. [23] successfully correlated differences in relaxation behavior observed from superposition derived continuous relaxation spectra to controlled variations in the molecular structure of a series of self-healing polyurethanes. Together, these and other works suggest that application of TTS to thermorheologically complex materials is possible, but not without extensive knowledge of the polymer system and physics at hand.

2.4. Generating continuous relaxation spectra from TTS master curves

Continuous relaxation spectra show the relaxation modulus H(τ) as a function of the relaxation time τ. H(τ) can be derived from experimental TTS master curve data by inverting the following pair of Fredholm equations [37]:

$$G'(\omega) = \int_0^{\infty} H(\tau) \frac{\omega^2\tau^2}{1+\omega^2\tau^2} \frac{d\tau}{\tau} \qquad \textit{Eq. 2}$$

$$G''(\omega) = \int_0^{\infty} H(\tau) \frac{\omega\tau}{1+\omega^2\tau^2} \frac{d\tau}{\tau} \qquad \textit{Eq. 3}$$

Here, G'(ω) and G"(ω) are the shear storage and loss modulus, respectively, as a function of the angular frequency ω. This inversion is an ill-posed problem [37], wherefore nonlinear regression methods must be used to find H(τ). Honerkamp and Weese [38] proposed one solution in the form of the following Tikhonov regularization:

$$\begin{aligned} V(\lambda) = & \sum_{i=1}^{n} \frac{1}{\sigma_i'^2} \left[G_i'^{\sigma} - \left(\int_{-\infty}^{+\infty} \frac{\omega_i^2\tau^2}{1+\omega_i^2\tau^2} h(\tau) d(\ln\tau) \right) \right]^2 \\ & + \sum_{i=1}^{n} \frac{1}{\sigma_i''^2} \left[G_i''^{\sigma} - \left(\int_{-\infty}^{+\infty} \frac{\omega_i\tau}{1+\omega_i^2\tau^2} h(\tau) d(\ln\tau) \right) \right]^2 \\ & + \lambda \int_{-\infty}^{+\infty} \left(\frac{d^2}{d\tau^2} h(\tau) \right)^2 d(\ln\tau) \end{aligned} \qquad \textit{Eq. 4}$$

Here, V(λ) is an estimate of the spectrum H(τ). $G_1'^{\sigma}$, …, $G_n'^{\sigma}$ and $G_1''^{\sigma}$, …, $G_n''^{\sigma}$ represent the experimental data for the shear storage and loss modulus G'(ω_1), …, G'(ω_n). G"(ω_1), …, G"(ω_n), and σ_1', …, σ_n' and σ_1'', …, σ_n'' represent the corresponding errors in the fitting. Finally, λ is a fitting parameter. The shear storage and loss modulus G' and G" can analogously be replaced with the 'regular' storage and loss modulus E' and E" as retrieved from DMA analysis, taking into account the straightforward relationship between G and E [37]. When applying Eq. 4, a best estimate is first made of the solution H(τ), from which the storage and loss modulus are then derived using well-known relationships [37]. Then, the best estimate solution and experimental data of the storage and loss modulus are compared, where a greater difference results in a greater 'score'. This process is repeated until the error is minimized and therefore a high goodness-of-fit achieved, where an approximation limit is set by the term involving the fitting parameter λ in Eq. 4.

In this thesis, TTS and conversion to continuous relaxation spectra are performed using TA Instruments TRIOS software accompanying the DMA equipment (**Figure 2.3**)

Figure 2.3 *TA Instruments TRIOS software conversion of TTS master curve to continuous relaxation spectrum.* ***(a)*** *Regression fitting (black line) of experimental data (blue and green lines). Number of polynomial terms and goodness-of-fit are displayed.* ***(b)*** *Continuous relaxation spectrum with one main relaxation peak. Note the 'wobbliness' at very short (< 10^{-3} s) relaxation times, coinciding with the noisy high frequency region on the TTS master plot.*

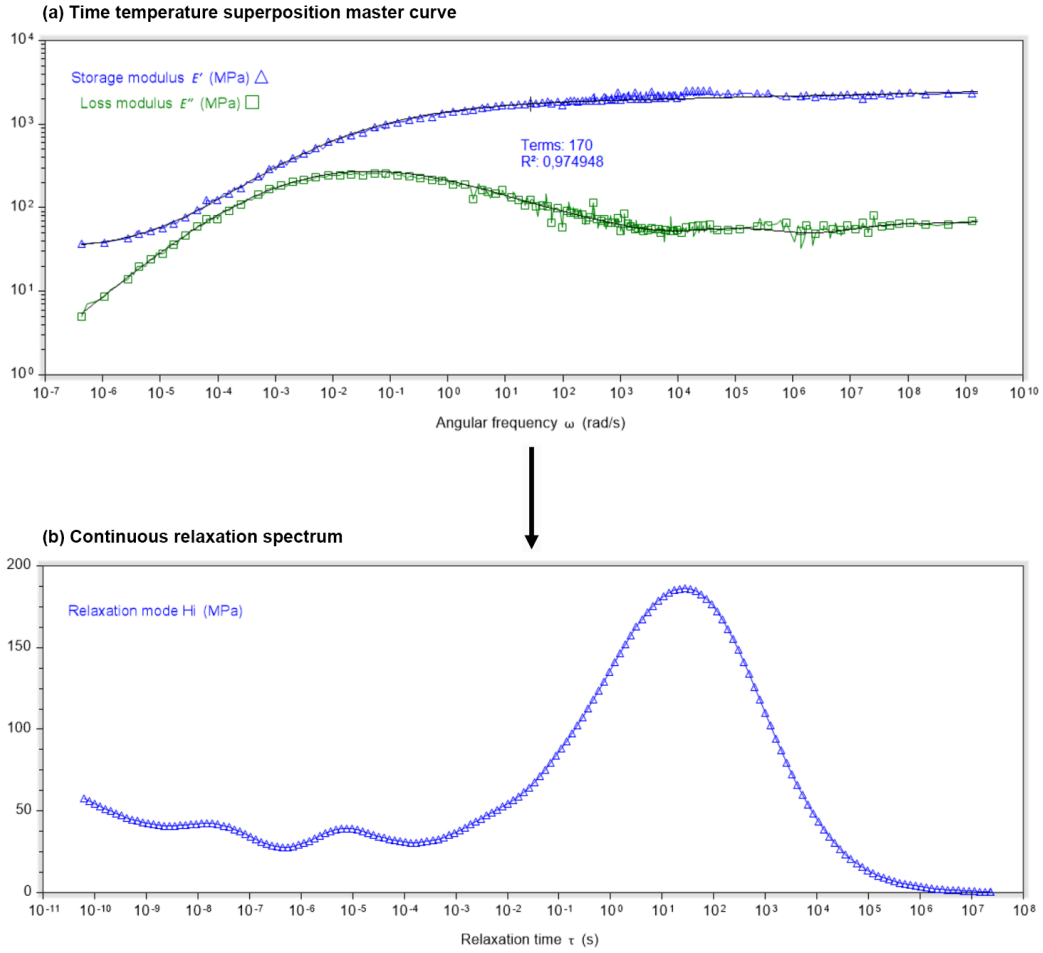

3. MATERIALS AND METHODS

3.1. Materials

The model system of choice is a self-healing epoxy-silane dual network polymer with dynamic disulfide bonds, initially developed by Abdolah Zadeh et al. [29] and characterized further since [39, 40]. The nomenclature 'dual network' originates from a network of organic and inorganic entities that equip the polymer with good mechanical properties, while the dynamic S-S bonds introduce sufficient healing properties. The organic part consists of an epoxy-amine, while the inorganic part encompasses a network of silicone alkoxides (**Figure 3.1a**). Disulfide bonds originate from one of the silicone alkoxide precursors and are therefore principally located in the inorganic part of the network. However, during synthesis the organic and inorganic parts are joined together via several chemical reactions, resulting in an interconnected and interpenetrating network that acts as one single entity (**Figure 3.1b**). For the remainder of this thesis, the dual network polymer with dynamic disulfide bonds is abbreviatedly referred to as 'self-healing epoxy'. Similarly, a non-healing reference model consisting only of an organic epoxy-amine network is referred to as 'non-healing epoxy'.

The self-healing epoxy is a suitable model polymer for several reasons. Compared to other self-healing polymers it is relatively easy to synthesize, requiring few steps and components and only basic laboratory equipment. Moreover, its precursors are relatively cheap, especially the epoxy resin and amine hardener also used to synthesize the non-healing reference epoxy. Both these factors make this model system suitable for a MSc thesis, where limited experience and, in some cases, budget are important considerations. Finally, the self-healing epoxy is a familiar polymer system that has previously been studied extensively within the research group. Consequently, results and findings can more readily be connected to previously observed behavior, contributing to the overall relevance of this thesis.

3.2. Methods

The polymer stress relaxation response, in the form of continuous relaxation spectra, is investigated for three conditions: pristine, damaged, and healed (after damage). Here, the pristine spectrum is a baseline reference from which the effects of damage and healing can be derived. CRS are obtained from a three step DMA procedure, each of which is more elaborately described in the experimental procedures (**Chapter 4)**:

1. Perform temperature-frequency (TF) sweeps
2. Generate time-temperature superposition (TTS) master curves
3. Convert TTS master curves to continuous relaxation spectrum

Figure 3.1 (a) *Two-dimensional chemical structure of self-healing dual network epoxy precursors.* ***(b)*** *Schematic of idealized two-dimensional network structure. Adapted from [29].*

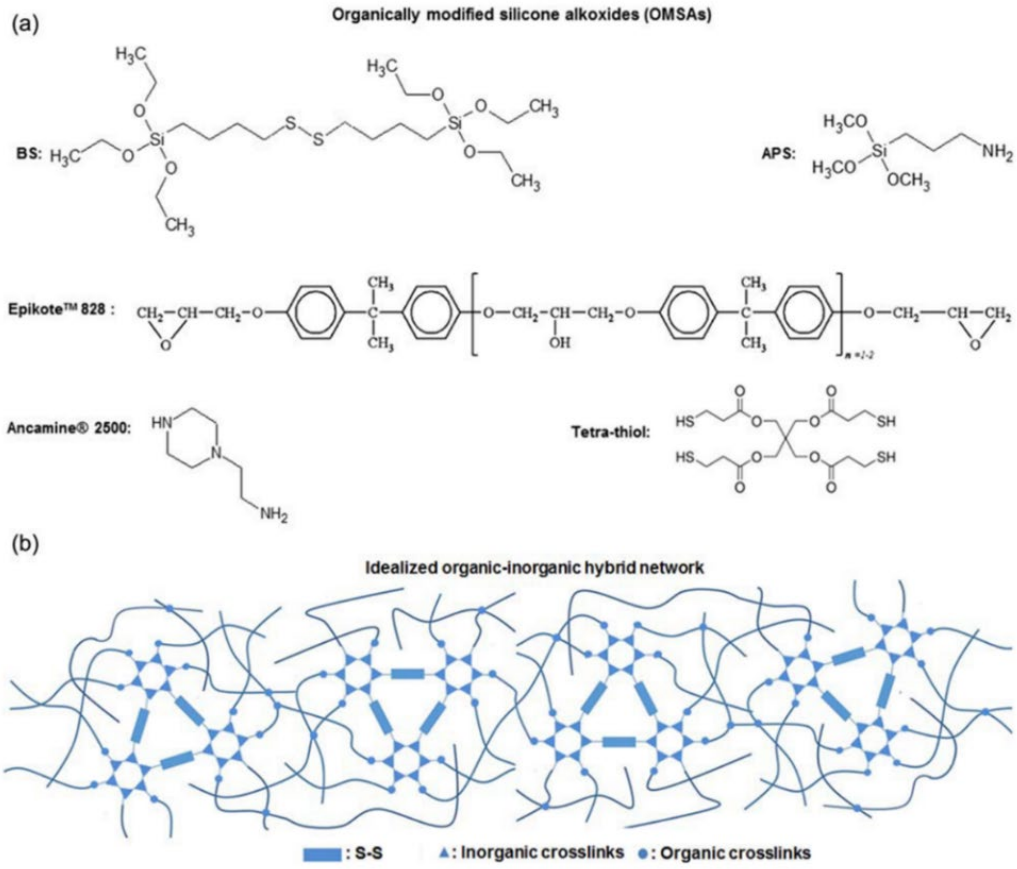

3.2.1. Pristine state experiments

For the pristine baseline, CRS of the self-healing and non-healing epoxy are compared. Tensile stress-strain curves, glass transition temperatures and a Raman spectrum are also obtained for a more complete understanding. T_g is obtained both calorimetrically (DSC) and mechanically (DMA). Raman spectroscopy is performed to confirm the presence of S-S bonds in the self-healing epoxy. Due to time limitations it was not possible to conduct T_g and Raman measurements for the non-healing epoxy. Pristine experiments are summarized in **Table 1**.

Table 1 *Summary of pristine state experiments.*

	CRS	Tensile σ-ε	T_g (DSC)	T_g (DMA)	Raman
SH epoxy	*Yes*	*Yes*	*Yes*	*Yes*	*Yes*
NH epoxy	*Yes*	*Yes*	*No*	*No*	*No*

3.2.2. Straining experiments

To explore the effect of plastic deformation (PD) on the stress relaxation response, self-healing epoxy samples are subjected to one of three levels of tensile strain in the DMA: 0%, 1.5%, 3%. These strains correspond to the polymer in its undeformed (pristine), partially plastically deformed, and fully plastically deformed state, respectively, and are based on preliminary tensile tests where the end of the elastic region and failure strain ranges were determined (**Figure 3.2**). Continuous relaxation spectra are obtained for all three states of deformation, and compared by three parameters related to the main relaxation peak: peak height, peak width at half height, and time at peak height (aka peak time) (**Figure 3.3**). These parameters are from hereon referred to as 'peak parameters'. The sample stiffness is extracted and investigated for its influence on the peak parameters. Finally, a separate experiment is conducted on a dedicated tensile bench where loading-unloading curves are captured for 1.5% and 3% strain deformation. This experiment should confirm the presence or absence of hysteresis and plastic deformation. All these experiments are conducted in threefold. They are summarized in **Table 2**.

Figure 3.2 *Tensile stress-strain curve of SH epoxy with approximate ranges for end of elastic region and failure strain. Black squares indicate selected strain levels: 0% (pristine), 1.5% (partial plastic deformation), 3% (full plastic deformation). Crosses indicate upper and lower limits of the elastic region and failure strain, as determined from a set of 10 samples tested prior to the protocol here presented.*

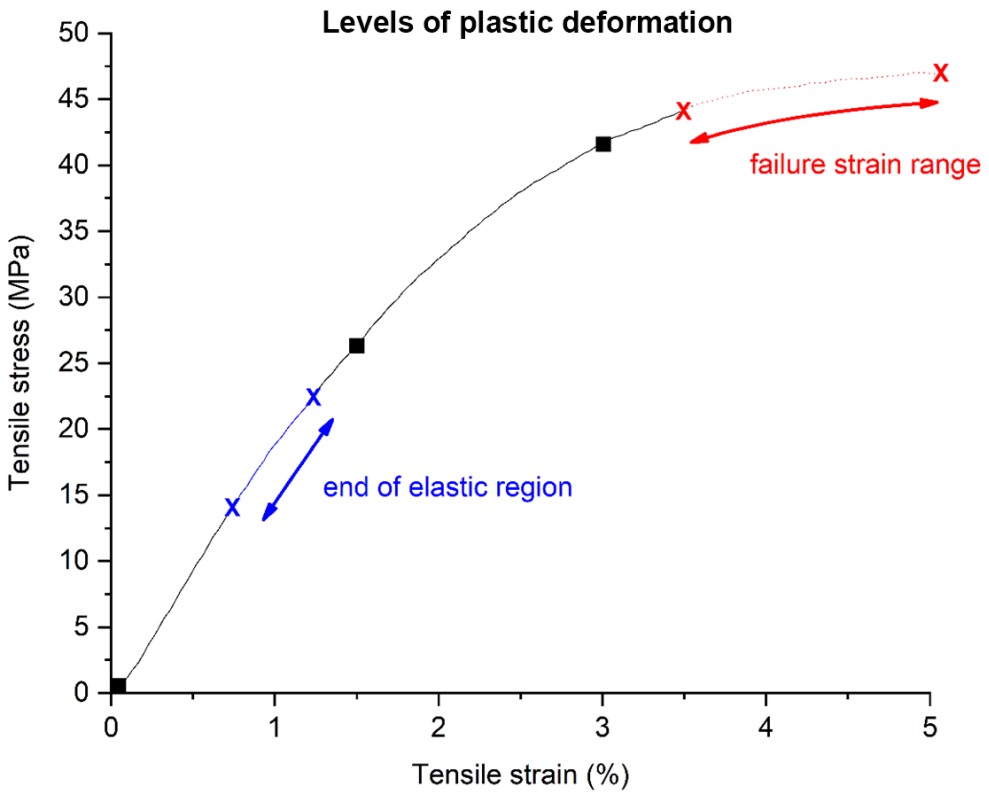

Figure 3.3 *Definition of peak height H_{peak}, peak width at half height $w_{1/2Hpeak}$, and peak time τ_{peak}.*

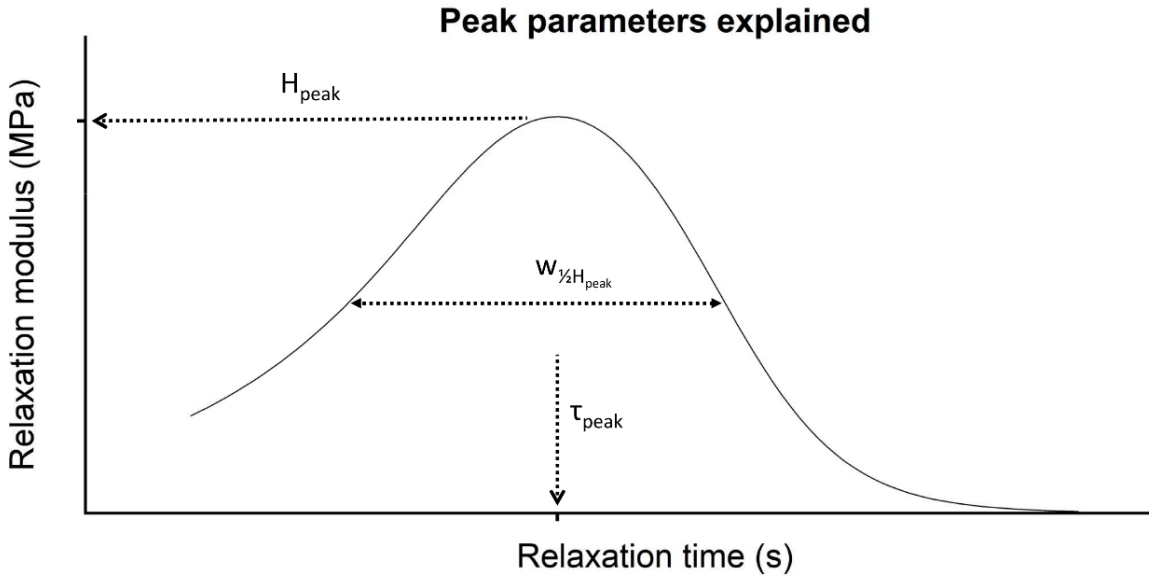

Table 2 *Summary of straining experiments.*
**Stiffness of samples is derived from CRS experiment tensile data, no dedicated samples used.*

Procedure	Step 1	Step 2	Polymer	Strain (%)	# of samples
CRS	Tensile (DMA)	TF sweep (DMA)	SH epoxy	0.0	3
				1.5	3
				3.0	3
Stiffness	Tensile (DMA)	-	SH epoxy	1.5	*
				3.0	*
Hysteresis	Load/unload (Tensile bench)	-	SH epoxy	1.5	3
				3.0	3

3.2.3. Healing experiments

To investigate whether damage healing can be identified through changes in the stress relaxation response, self-healing epoxy samples are subjected to a 2 hour 70°C oven treatment. This temperature enables shuffling of dynamic disulfide bonds above T_g without significant oxidation of free thiol groups [29]. Moreover, within 2 hours at 70°C post-curing and ageing of the constituent (in)organic networks should not significantly alter the mechanical properties [39]. The healing experiment procedure is described here, and summarized in **Table 3**.

A self-healing epoxy sample is strained to 3% (full plastic deformation), and a temperature-frequency sweep is taken to generate a pre-oven CRS. Subsequently, the sample is subjected to a 2 hour 70°C oven treatment, and a second post-oven CRS is generated. For comparison, the same procedure is repeated with an unstrained (pristine) sample, as well as an unstrained non-healing epoxy sample. To isolate the effect of the oven treatment, a third sample is subjected to two consecutive TF sweeps without intermediate oven cycle. Like the first sample, it is fully plastically deformed before the first TF sweep. To exclude post-curing

as a variable, calorimetric temperature sweeps are made in a DSC on a fourth and pristine sample before and after the oven treatment to establish the T_g. Here, the sample was cut in half so that the first calorimetric temperature sweep does not affect the second. Finally, a fifth and fully plastically deformed sample is allowed a one week recovery period after the oven treatment before performing the post-oven TF sweep. In this way, transient i.e. viscoelastic effects of the healing procedure might be identified.

Table 3 *Summary of healing experiments.*

Procedure	Step 1	Step 2	Step 3	Step 4		Polymer	Strain (%)	# of samples
CRS	Tensile (DMA)	TF sweep (DMA)	Oven	TF sweep (DMA)	-	SH epoxy	0.0	1
							3.0	1
						NH epoxy	0.0	1
No oven	Tensile (DMA)	TF sweep (DMA)	TF sweep (DMA)	-	-	SH epoxy	3.0	1
Post-cure check (T_g)	TF sweep (DMA)	T_g (DSC)	Oven	T_g (DSC)	-	SH epoxy	0.0	1
1 week recovery	Tensile (DMA)	TF sweep (DMA)	Oven	Recovery	TF sweep (DMA)	SH epoxy	3.0	1

4. EXPERIMENTAL PROCEDURES

4.1. Polymer components

The self-healing epoxy polymer consists of the following six components. Epikote™828, which is commercial form of diglycidyl ether of bisphenol A (DGEBA) epoxy resin. Ancamine®2500, which is a company secret curing agent mixture of amine monomers including aminoethylpiperazine. (3-aminopropyl)trimethoxysilane, from hereon abbreviated as APTS. Pentaerythritol tetrakis (3-mercaptopropionate), from hereon referred to as tetra-thiol. Triethylamine, from hereon abbreviated as TEA. Bis[3-(triethoxysilyl)propyl]disulfide, from hereon abbreviated as BDS. The components and weight ratios of the self-healing epoxy found in **Table 4.1** correspond to [39]. The reference epoxy consists of epoxy resin and amine hardener mixed in stoichiometric ratio.

Table 4.1 *Weight ratio of components in self-healing epoxy and non-healing epoxy*

		SH epoxy	NH epoxy
Ingredient	*Abbreviation*	*Weight ratio*	*Weight ratio*
Epikote™828	Epoxy	1	1
Ancamine®2500	Hardener	0.579	0.7
(3-aminopropyl)trimethoxysilane	APTS	0.076	0
Pentaerythritol tetrakis (3-mercaptopropionate)	Tetra-thiol	0.566	0
Bis(3-(triethoxysilyl)propyl)disulfide	BDS	0.646	0
Triethylamine	TEA	0.014	0

4.2. Polymer preparation

Epikote™828 is pre-heated in an oven at 65°C for 15 minutes to lower its viscosity. Epikote™828, APTS and BDS are weighed, poured, and then hand-stirred for 1 minute until the mixture becomes consistent. Using a magnetic stirring bar, the mixture is stirred for 3 hours at 625 RPM at room temperature. This length of time is required to allow the inorganic network to develop. Next, TEA, tetra-thiol and Ancamine®2500 are added, after which the mixture is once more hand-stirred for 1 minute and magnetically stirred for 3 minutes. The magnetic stirring bar is then removed and the mixture transferred to a vacuum chamber for 3 minutes to remove air bubbles introduced during mixing.

The mixture is poured into a PTFE mold and spread to an even thickness using a clean, 8 mm diameter steel rod (**Figure 4.1d**). The mold's external dimensions are 300x300x10 mm (length x width x thickness) with a 220x220x0.2 mm recession in the top face to pour the polymer mixture in to (**Figure 4.1a**). The mold is CNC milled and backed by a 5 mm thick aluminum plate to ensure maximum flatness (**Figure 4.1b**). It is situated on a 'balancing board', a 10mm plywood plate that can be leveled with 3 adjustment screws (**Figure 4.1c**). This way the obtained polymer film has an even thickness throughout.

After pouring, the mixture is allowed to cure at room temperature (22°C) for 24 hours. A smooth, white elastomeric film is obtained. The edges are trimmed off as they may have a different thickness than the bulk. Dogbone samples are punched from the film using a Gibitre Manual Die Cutting machine with a ASTM D1708 standard cutter (**Figure 4.1e**). The dogbone samples are placed on a PTFE tray, which is then placed in an oven pre-heated to 100°C for 48 hours. After this post-curing treatment, the dogbone samples are allowed to cool down to room temperature. The samples have a remarkably smooth and consistent appearance, with a thickness varying between 0.14 – 0.16 mm as measured by a micrometer (**Figure 4.1f**). The thickness reduction compared to the initial pouring (0.20 mm) can be attributed to polymerization and crosslinking. After reaching room temperature the samples are stacked flat and vertically in a PE cup with lid and placed in a fridge at 4°C. This way, ageing and humidity effects are suppressed as much as possible.

Figure 4.1 *Preparation of polymer samples.* ***(a)*** *Milled PTFE mold with recession to facilitate a thin film of polymer* ***(b)*** *5mm thick aluminum support attached with screws to back of PTFE mold* ***(c)*** *Plywood balance board with adjustment screws* ***(d)*** *Poured polymer in PTFE mold, situated on top of balance board* ***(e)*** *ASTM D1708-18 dogbone sketch with dimensions. Image retrieved from [41]* ***(f)*** *Dogbone samples after curing*

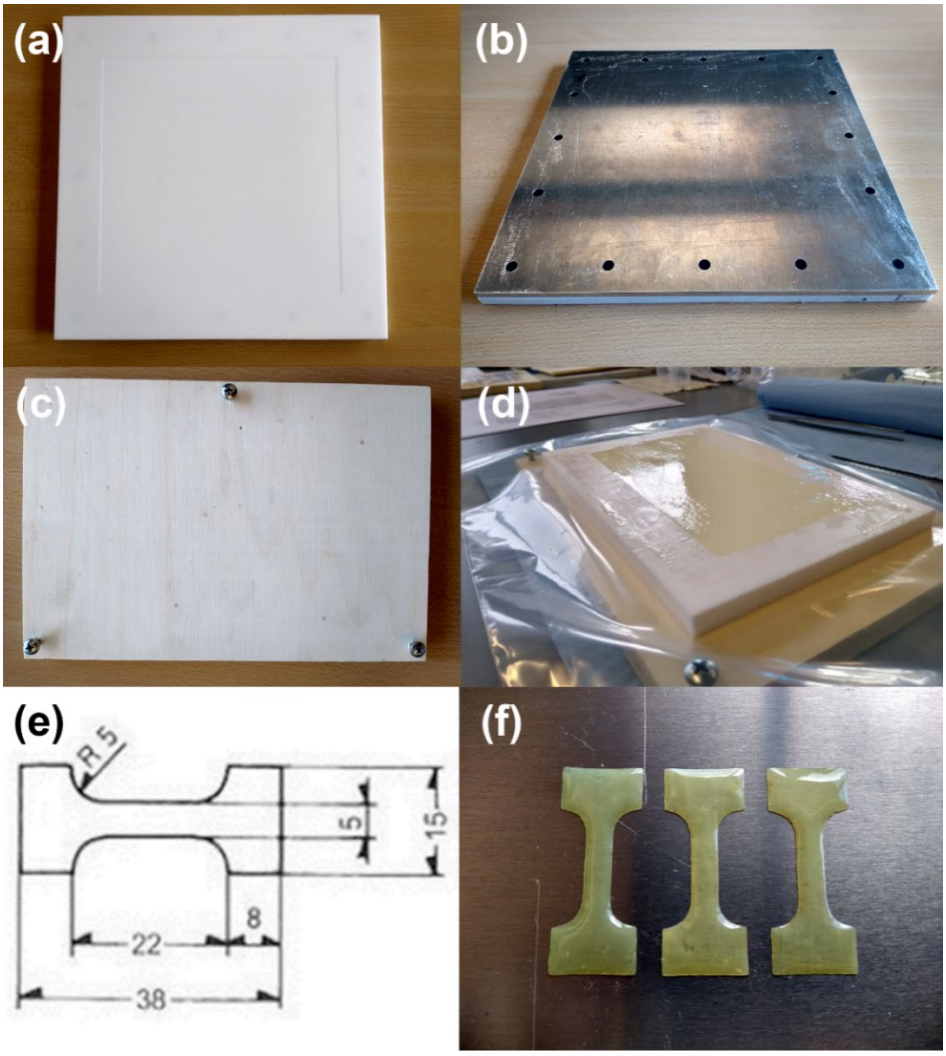

4.3. Temperature sweeps

Temperature sweeps are conducted on both a TA Instruments DSC 2500 and a TA Instruments RSA-G2 DMA under nitrogen. In the DSC approximately 10 mg of polymer is placed in a hermetically sealed aluminum container and heated twice from 0°C to 200°C at 10°C/min with in-between cooling at 5°C/min. The calorimetric T_g is taken from the 2nd heating run as the inflection point of the endothermic event. In the DMA samples are heated from 0°C to 150°C at a heating rate of 10°C/min, a frequency of 1 Hz, and 0.1% strain. The mechanical T_g is taken as the peak of the loss modulus [23].

4.4. Raman spectroscopy

Raman spectroscopy is conducted at room temperature on a Renishaw inVia^{TM} confocal Raman microscope in single spot mode using a 785nm laser. A spectrum is collected between 200 – 1400 cm^{-1} at 50x magnification using a 1% laser power, 10s exposure time, 100 accumulations, and 1200 l/mm grating. Raman spectroscopy is used to observe stretching of symmetric S-S bonds, which manifest themselves around 510 cm^{-1} [29].

4.5. Tensile straining (DMA)

Two hours before straining, samples are removed from the fridge and allowed to acclimatize to laboratory conditions at room temperature. The tensile fixtures of a TA Instruments RSA-G2 DMA are zeroed and the loading gap is set to 10 mm. A sample is then placed between the fixtures while wearing nitrile gloves to prevent contamination. Vertical alignment (centered and parallel to fixtures) is confirmed visually, and the sample is clamped between the fixtures to 25 cNm torque at each bolt using a torque wrench. A temperature chamber is placed around the fixtures and set to 20°C under nitrogen. A 0.1 N tensile pre-load is set, and after a 2 minute acclimatization period the sample is loaded to the specified strain at a 2%/min strain rate. After reaching the specified strain the sample is rapidly unloaded back to a 0.1 N tensile pre-load. Between straining and subsequent TF sweeping, the sample remains unaltered in the fixtures.

4.6. Temperature-frequency sweep (DMA)

Temperature-frequency sweeps are performed in a climate chamber under nitrogen from 0°C to 100°C in 5°C steps. For acclimatization purposes, samples are kept at the starting temperature (0°C) for 5 minutes and then 2 minutes at each consecutive temperature before starting measurements. At each temperature, the sample is loaded to 0.1% strain at frequencies from 0.1 to 10 Hz in 10 logarithmic steps per decade. Amplitude sweeps at the extremes of the temperature range confirm that samples remained within their linear viscoelastic range (LVR) at all temperatures (**Figure A 1**).

4.7. Time-temperature Superposition (TTS) and conversion to relaxation spectra

Time-temperature Superposition (TTS) is performed using TA Instruments TRIOS software. Storage and loss modulus data is frequency shifted using a WLF shifting protocol and a 70°C reference temperature, which is the temperature where the loss modulus peaks on a DMA temperature sweep (**Figure 5.3b**). The validity of the resulting frequency master curves is confirmed by observing that the horizontal shift factors a_T form a descending line when plotted logarithmically against the temperature (**APPENDIX B**). A control experiment conducted on a separate DMA device validates the resulting TTS master curves (**Figure B 22**). Continuous relaxation spectra are generated automatically from the frequency master curves using a built-in functionality of the TRIOS software. Experimental data is mathematically approximated with a high goodness-of-fit (**APPENDIX B**).

4.8. Hysteresis measurements

Hysteresis measurements are performed on an Instron 3365 tensile bench with a 1 kN load cell. At room temperature, samples are loaded to and from the specified strain at strain rates of 2%/min and 6%/min, respectively.

5. RESULTS

5.1. Establishment of a characterization protocol

A recurrent problem encountered when using TRIOS software for converting TTS master data into relaxation spectra is that the resulting approximation of experimental data has a high global, but not always local, goodness-of-fit. TTS master curves can span a very wide frequency range, up to 20 decades in this thesis, and as a result R^2 values > 0.95 can easily be reached while not well capturing experimental data in certain 'problematic regions'. This can be quite misleading when drawing conclusions based upon small differences in relaxation behavior, especially if problematic regions lay within the region of interest, e.g. the main relaxation peak (**Figure 5.1**).

Figure 5.1 TRIOS regression with high overall goodness-of-fit (> 0.95), but local underestimation of loss modulus peak (at black arrow). This leads to a lower stress relaxation peak when converting to a continuous relaxation spectrum.

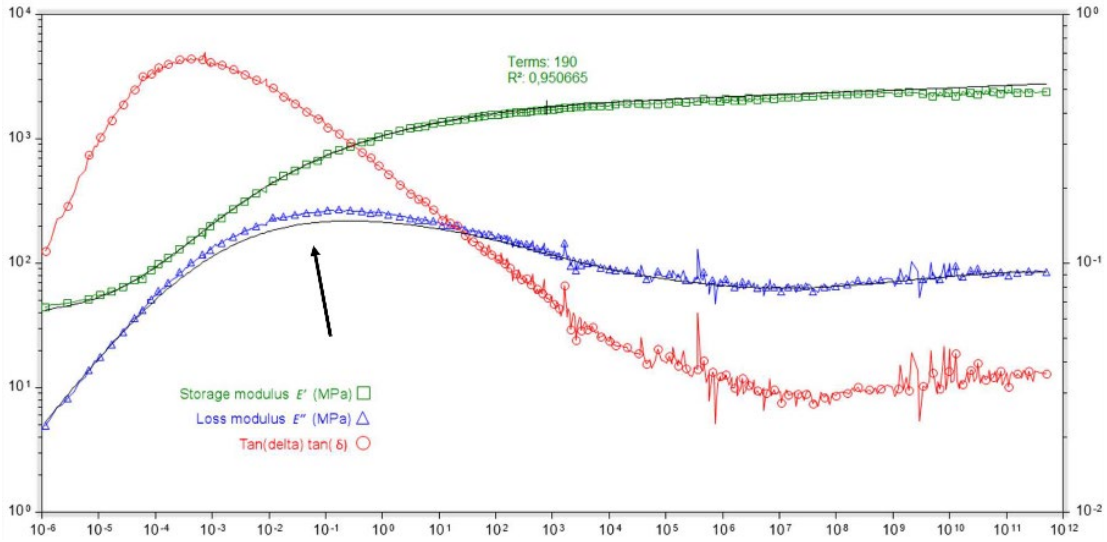

A second problem is specifically linked to data originating from measurements well below T_g. These noisy results are then converted in the relaxation spectrum into 'bumpiness' at short relaxation times (**Figure 2.3b**).

Figure 5.2a shows the storage modulus measurements at all 21 ($= 100°C/5°C] + 1$) probed temperatures. Well below T_g the modulus does not change significantly with temperature, so data sets of 0°C to 40°C mostly overlap. When shifting this data to generate a TTS master curve there are virtually infinitely many solutions. That is, an almost identical result is reached by shifting 0°C data as by shifting 40°C data. Moreover, low temperature loss modulus data tends to be quite noisy, because at these temperatures the material response is very dominantly elastic and thus the viscous signal is very weak (**Figure 5.2b**). This noise further complicates the shifting process. As a result, TTS master curves tend to generate somewhat noisy and unreliable results at very high frequencies.

Figure 5.2 (a) *DMA storage modulus data obtained at 0°C to 100°C in 5°C steps. Below T_g data clusters at high modulus values. Data obtained at 100°C has the lowest storage modulus.* ***(b)*** *DMA loss modulus data obtained at 30°C (triangles) and 100°C (squares). 30°C data is clearly noisier, especially at low frequencies.*

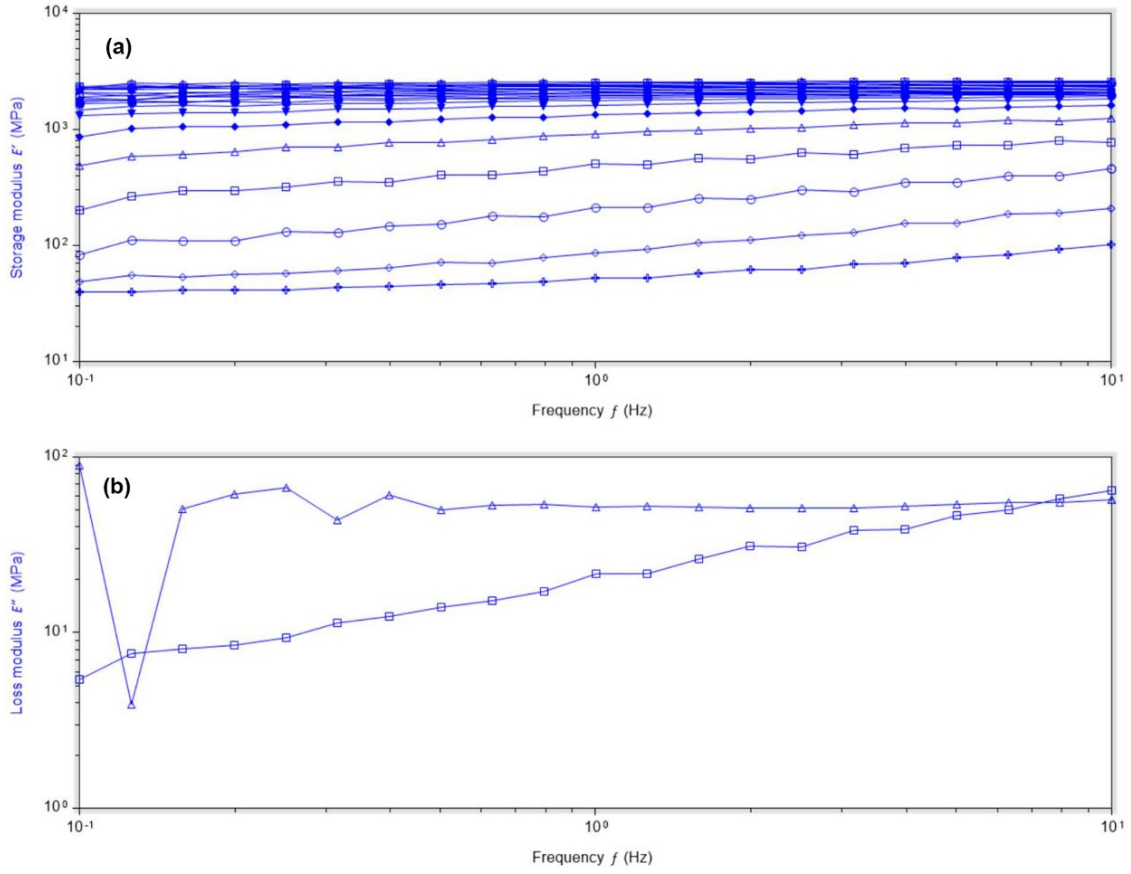

An elegant solution to these problems is to eliminate data below T_g from TTS shifting. Not only does this discard the less reliable low temperature data, it also strongly reduces the frequency bandwidth that needs to be fitted in subsequent regression, leading to more accurate relaxation spectrum results. The data that is left (70°C to 100°C), hereby dubbed the 'reduced relaxation spectrum', includes the main relaxation peak, where most effects of damaging are expected to be seen since most energy is dissipated there.

5.2. Pristine state experiments

5.2.1. DSC and DMA temperature sweeps

DSC temperature sweep results are shown in **Figure 5.3a**. A single endothermic event related to glass transition is observed between 50°C and 70°C. Taking the infliction point as reference, the calorimetric T_g is 65°C.

DMA temperature sweep results are shown in **Figure 5.3b**. The storage modulus E' is relatively constant at low temperatures, but drops almost two decades between 60°C and 105°C. At higher temperatures an elastic plateau is reached, corresponding to the crosslinked nature of the polymer. The loss modulus E" is also relatively constant at low temperatures. It increases from 30°C until it reaches a maximum at 70°C. It then significantly decreases to a value over two decades lower than at cold temperatures, flattening off at 140°C. The tanδ peak is very broad, ranging from 30°C to 140°C, indicating heterogeneity and/or polydispersity. This makes sense given the dual network structure of the SH epoxy. Moreover, the absence of distinguishable tanδ peaks suggests that no significant phase separation is present. Taking the temperature at loss modulus peak, the mechanical T_g is 70°C.

5.2.2. Raman spectroscopy

Figure 5.3c shows a normalized Raman spectrum of the self-healing epoxy. The presence of a strong, broad peak around 510 cm^{-1} Raman shift confirms the presence of dynamic S-S bonds in the self-healing epoxy.

5.2.3. Tensile stress-strain curves

Figure 5.4a shows the tensile stress-strain curves of the self-healing and non-healing epoxy. The self-healing network is less stiff and elongates more before failure. This agrees with the presence of S-S bonds which have a lower bond energy than C-C bonds (65 vs. 80 kcal mol^{-1} [42]), making the self-healing network softer than the non-healing reference.

5.2.4. Full CRS comparison: SH vs. NH epoxy

Figure 5.4b shows the full stress relaxation response of the pristine self-healing and non-healing epoxy. The full, non-reduced spectrum is shown for qualitative comparison. In all consecutive experiments, only reduced spectra are used. The main relaxation peak of the self-healing epoxy occurs at an approximately one logarithmic decade lower relaxation time that that of the non-healing epoxy. The peak height of the self-healing epoxy is significantly lower than that of the non-healing epoxy (176 MPa vs. 220 MPa). Between 10^{-3} - 10^{-5} seconds the non-healing epoxy displays an energy plateau that is absent in the self-healing epoxy. Finally, towards very short relaxation times (< 10^{-5} s) the self-healing epoxy dissipates increasingly more energy, while the non-healing epoxy dissipated incrementally less energy.

Figure 5.3 (a) *Temperature sweep performed on DSC. Taken at the infliction point, the T_g is 65°C.* ***(b)*** *Temperature sweep performed on DMA. The loss modulus peaks at 70°C.* ***(c)*** *Raman spectrum of the pristine SH epoxy. The presence of S-S bonds is confirmed by the S-S stretching peak at 510 cm^{-1}.*

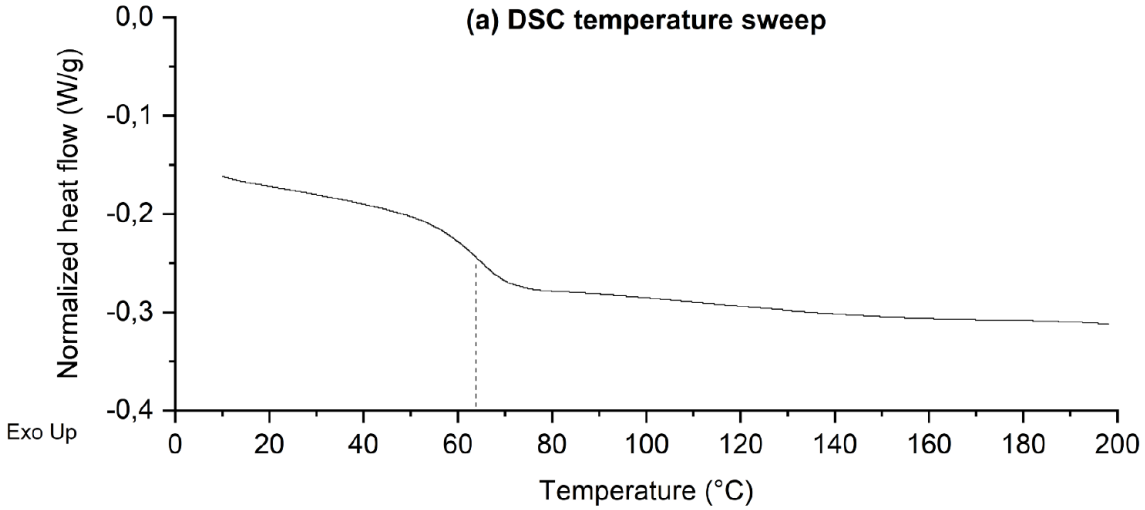

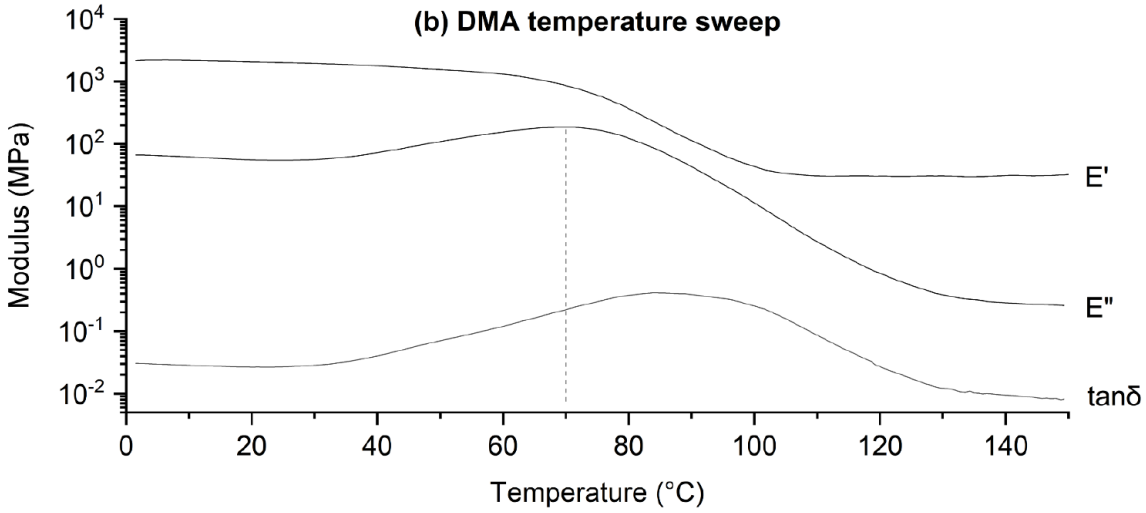

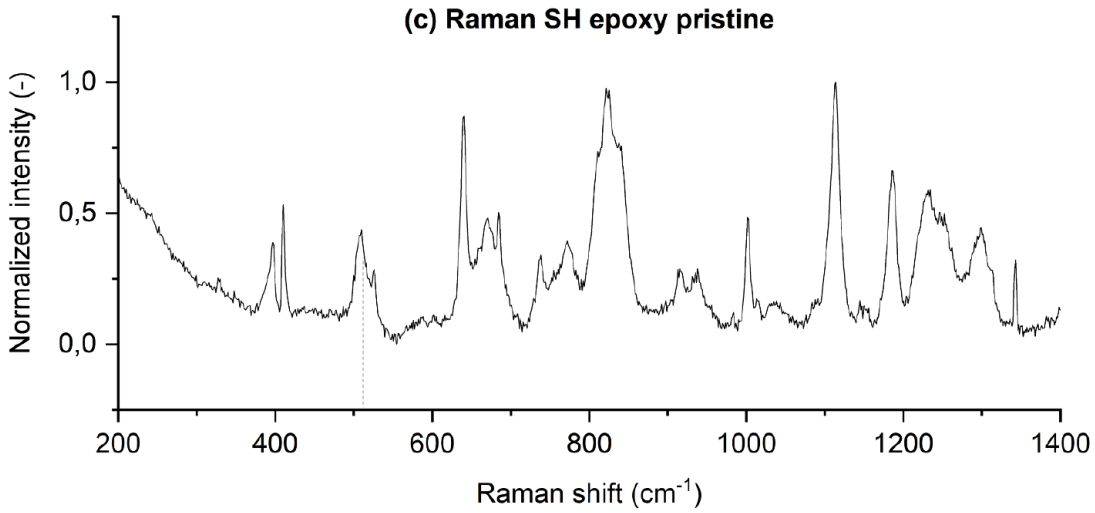

Figure 5.4 (a) *Tensile stress-strain curves of the self-healing (SH) and non-healing (NH) epoxy.* ***(b)*** *Comparison of the full relaxation spectra of the pristine SH versus NH epoxy.* T_{ref} *= 70°C.*

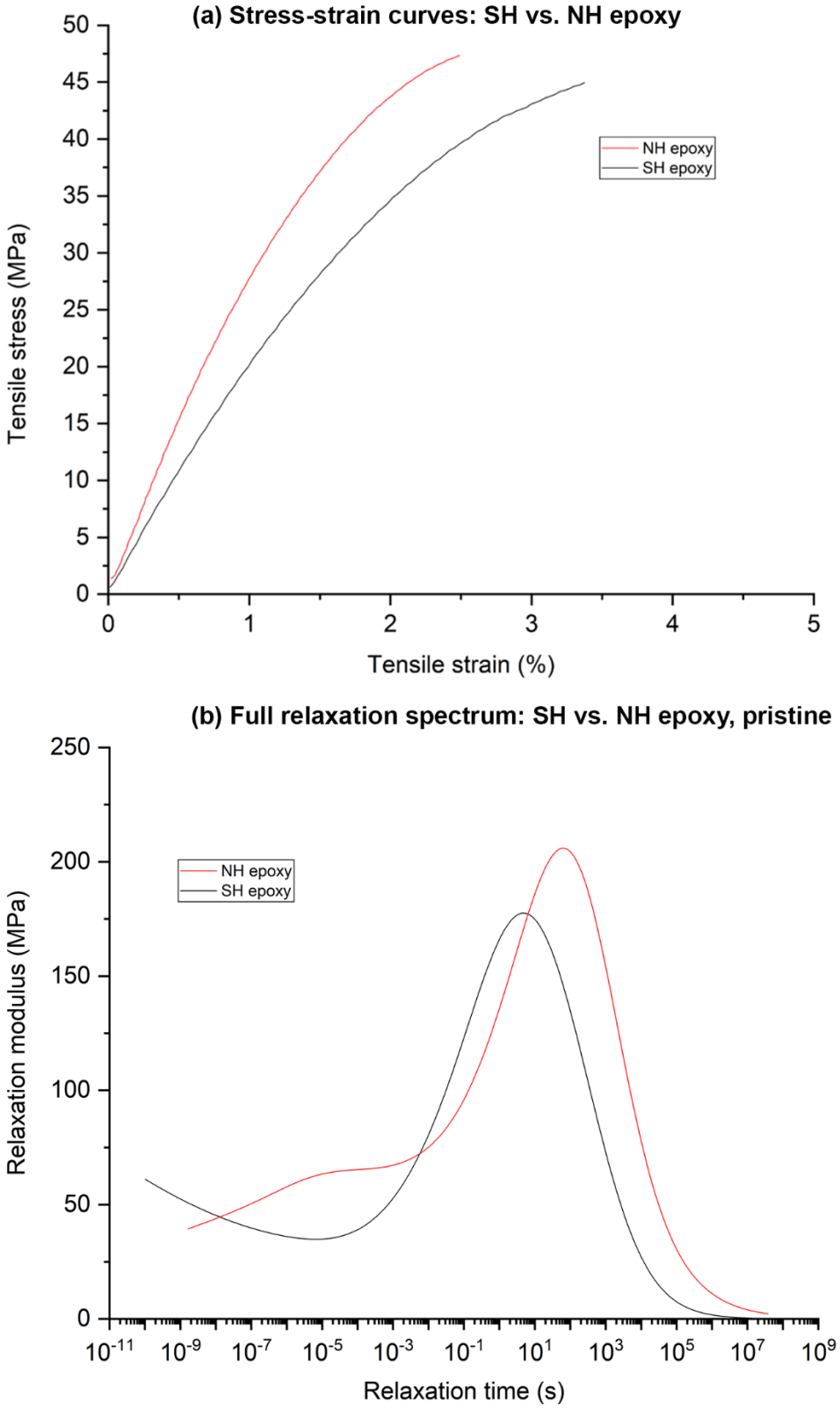

5.3. Straining experiments

5.3.1. CRS comparison: pristine vs. partial PD vs. full PD SH epoxy

Figure 5.5 shows the stress relaxation response of the self-healing epoxy after different levels of plastic deformation (PD). The overall shape of the stress relaxation response is quite consistent in all cases, so the PD levels probed do not seem to cause drastic changes to the relaxation behavior. Pristine samples have a very consistent peak height (0.5 MPa spread) and small variation in half peak width (± 0.7 log decades spread) and peak time (0.6 log decades spread) (**Figure 5.5a**). In partially PD samples the peak height is also consistent (1 MPa spread), ignoring one outlier that is further discussed in **Chapter 6**. The half peak width spreads 0.6 log decades and the peak time 0.65 log decades (**Figure 5.5b**). Fully PD samples have a 5.6 MPa peak height spread and a 0.55 and 0.35 log decades half peak width and peak time spread, respectively (**Figure 5.5c**). Peak parameters are summarized in **Figure 5.6d**. **Figure 5.6a** shows that both partially PD and fully PD samples have an average peak height approximately 5% lower than pristine samples. Between the deformed samples (partial, full) no further peak height difference is detected. The average peak time (**Figure 5.6b**) and half peak width (**Figure 5.6c**) vary marginally between levels of deformation, but no trend was found here.

5.3.2. Effect sample stiffness on peak parameters

All partially PD samples were stiffer than the fully PD samples (**Figure 5.7a**). Overall, these relative differences in stiffness are not reflected in appreciable changes to the investigated peak parameters (height, width, time). However, the peak height outlier in the partially PD sample set has by far the greatest stiffness, suggesting a possible relationship between peak height and sample stiffness.

5.3.3. Hysteresis measurements

Hysteresis and plastic strain are observed in both partially and fully PD samples (**Figure 5.7b**). However, both are significantly greater in fully PD samples, indicating that more damage is present there, as is to be expected. Both levels of deformation show good consistency between three individual samples.

Figure 5.5 *Reduced relaxation spectra, T_{ref} = 70°C.* ***(a)*** *Pristine state,* ***(b)*** *Partial plastic deformation,* ***(c)*** *Full plastic deformation.*

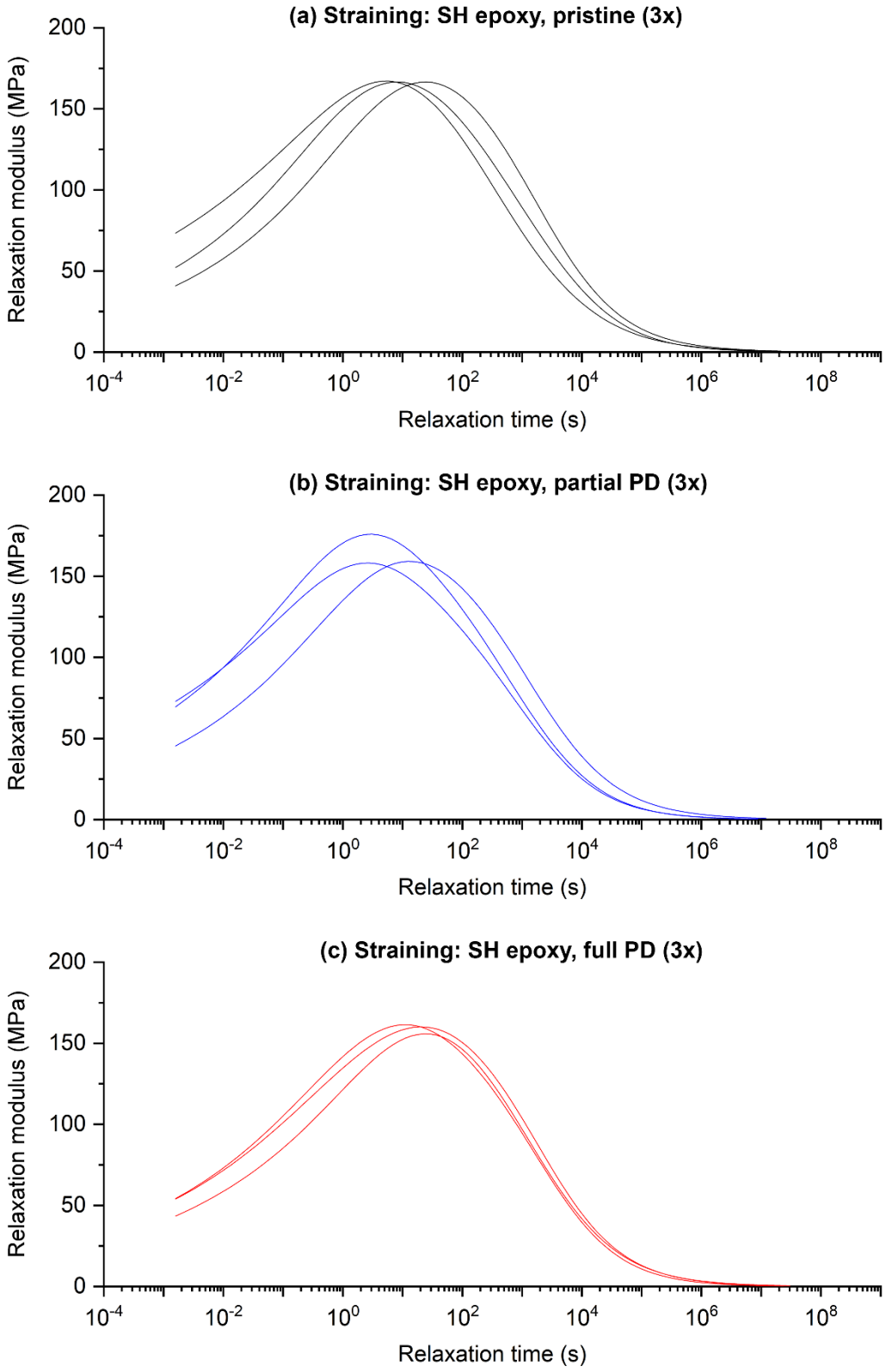

Figure 5.6 *Comparison of SH epoxy main relaxation peak properties for different levels of strain damage. Black dashed lines indicate the average value. Note: for partial PD the average is taken from the first two samples only due to the peak height outlier. Numbers #1-3 denote sample numbers.* ***(a)*** *Relaxation peak height.* ***(b)*** *Half relaxation peak width.* ***(c)*** *Relaxation peak time.* ***(d)*** *Table summarizing peak parameters.*

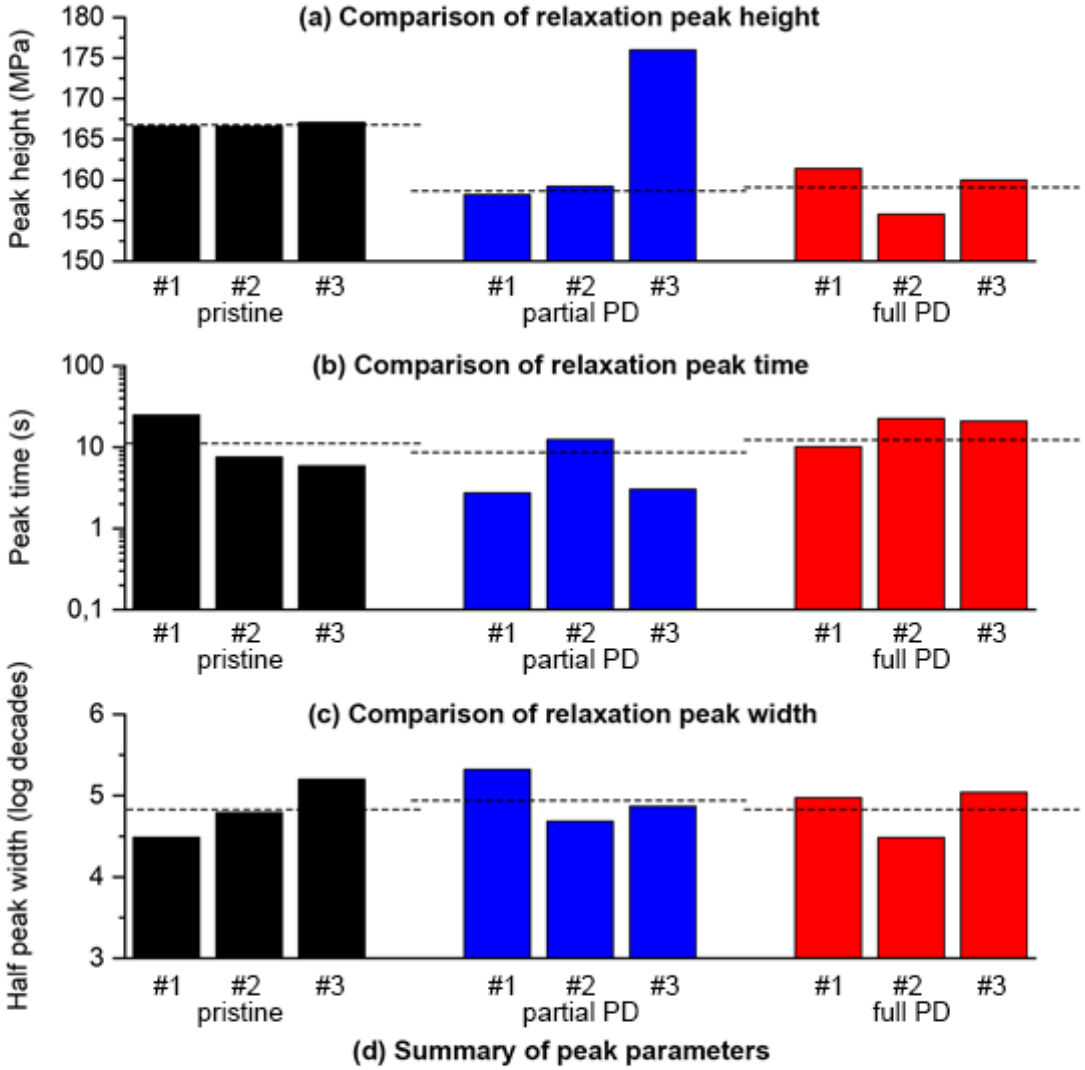

(d) Summary of peak parameters

	Pristine				*40%*				*80%*			
	S1	*S2*	*S3*	***Avg***	*S1*	*S2*	*S3*	***Avg***	*S1*	*S2*	*S3*	***Avg***
Height (MPa)	166.6	166.6	167.1	**166.8**	158.2	159.2	176.0	**158.7**	161.4	155.8	160.0	**159.1**
Time (s)	$10^{1.40}$	$10^{0.88}$	$10^{0.77}$	$\mathbf{10^{1.11}}$	$10^{0.44}$	$10^{1.10}$	$10^{0.49}$	$\mathbf{10^{0.88}}$	$10^{1.00}$	$10^{1.35}$	$10^{1.32}$	$\mathbf{10^{1.25}}$
Width (decs)	4.49	4.79	5.20	**4.83**	5.32	4.69	4.87	**4.96**	4.98	4.49	5.04	**4.84**

Figure 5.7 (a) *Variation in tensile stress-strain curves of deformed samples. The stiffest curve (partial PD #3) corresponds to the peak height outlier.* ***(b)*** *Hysteresis curves of deformed samples. More deformation leads to more dissipated energy and more plastic strain.*

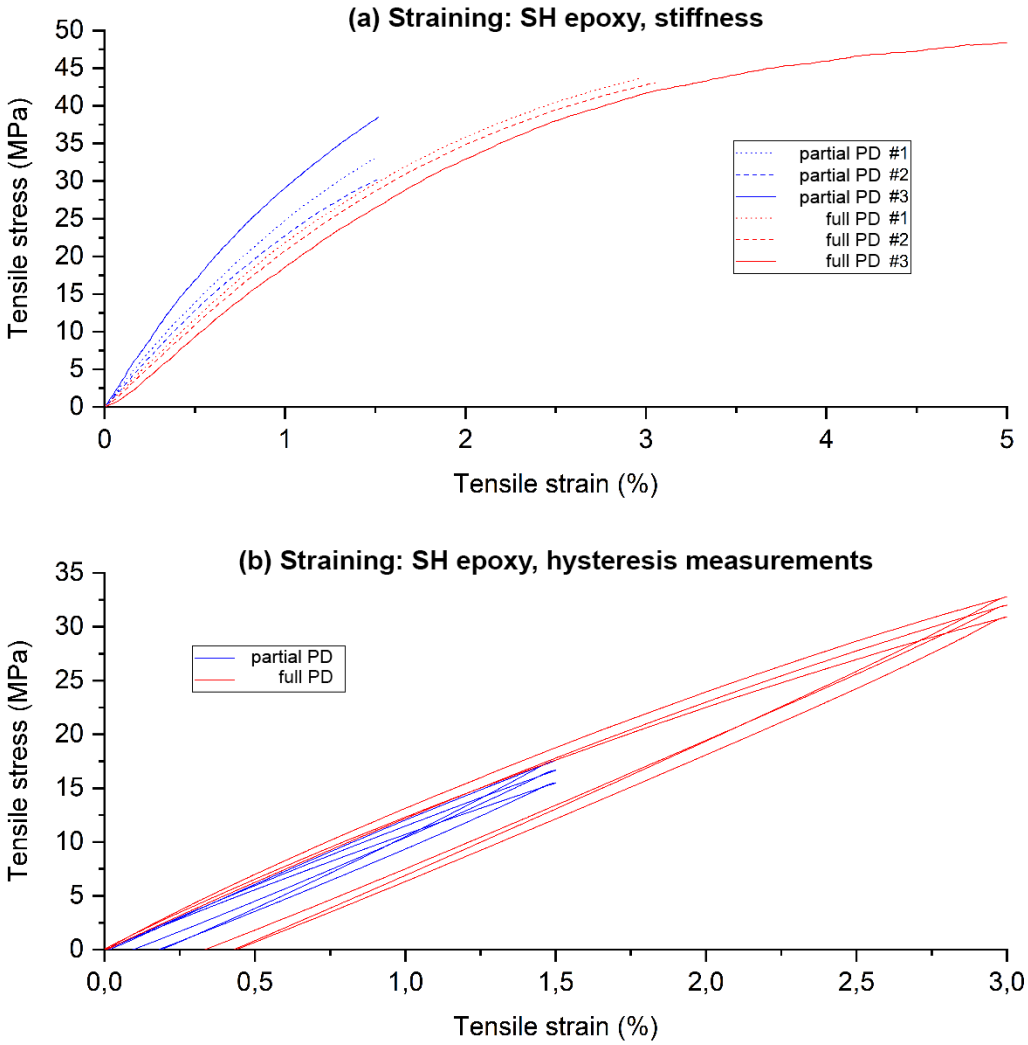

5.4. Healing experiments

5.4.1. CRS comparison: pre-oven vs. post-oven

Figure 5.8 shows the stress relaxation response before and after a 2 hour 70°C oven treatment for a pristine and fully PD self-healing epoxy, as well as a pristine non-healing epoxy. The stress relaxation response of the self-healing epoxy shifts by approximately two decades to longer relaxation times, regardless of the state of deformation (pristine and fully PD). This shift is not seen in the non-healing system. In all cases the peak height and half peak width remain unchanged, with one exception: the peak height of the pristine non-healing epoxy reduces slightly (195 MPa -> 185 MPa) after the oven treatment, which could be attributed to relaxation of cure stress.

5.4.2. Effect of removing oven step

Eliminating the oven step for a fully PD self-healing epoxy sample results in negligible differences between the stress responses obtained after the 1st and 2nd TF sweep (**Figure 5.9a)**.

5.4.3. Calorimetric T_g measurements pre-oven vs. post-oven

The calorimetric heat flow profile of a pristine self-healing epoxy sample remains almost identical throughout the oven treatment (**Figure 5.9b**). However, data shown is obtained during the second heating run, which means that oven induced changes to the calorimetric heat profile could have presented themselves during the first heating run and not show up in the second run.

5.4.4. Effect of one week recovery period between oven and 2nd TF sweep

Allowing a fully PD self-healing epoxy sample to gradually cool down and recover for 1 week after the oven treatment changes the stress response strongly. Contrary to the two decade shift to longer relaxation times observed without recovery step, a small shift (0.5 log decades) to lower relaxation times is seen (**Figure 5.9c**). Moreover, a stark reduction in peak height (168 MPa -> 136 MPa) is detected.

Figure 5.8 *Effect of a 2h 70°C oven healing treatment. Reduced relaxation spectra, T_{ref} = 70°C.* ***(a)*** *Fully PD sample CRS pre-oven and post-oven* ***(b)*** *Pristine sample CRS pre-oven and post-oven* ***(c)*** *Pristine NH epoxy CRS pre-oven and post-oven.*

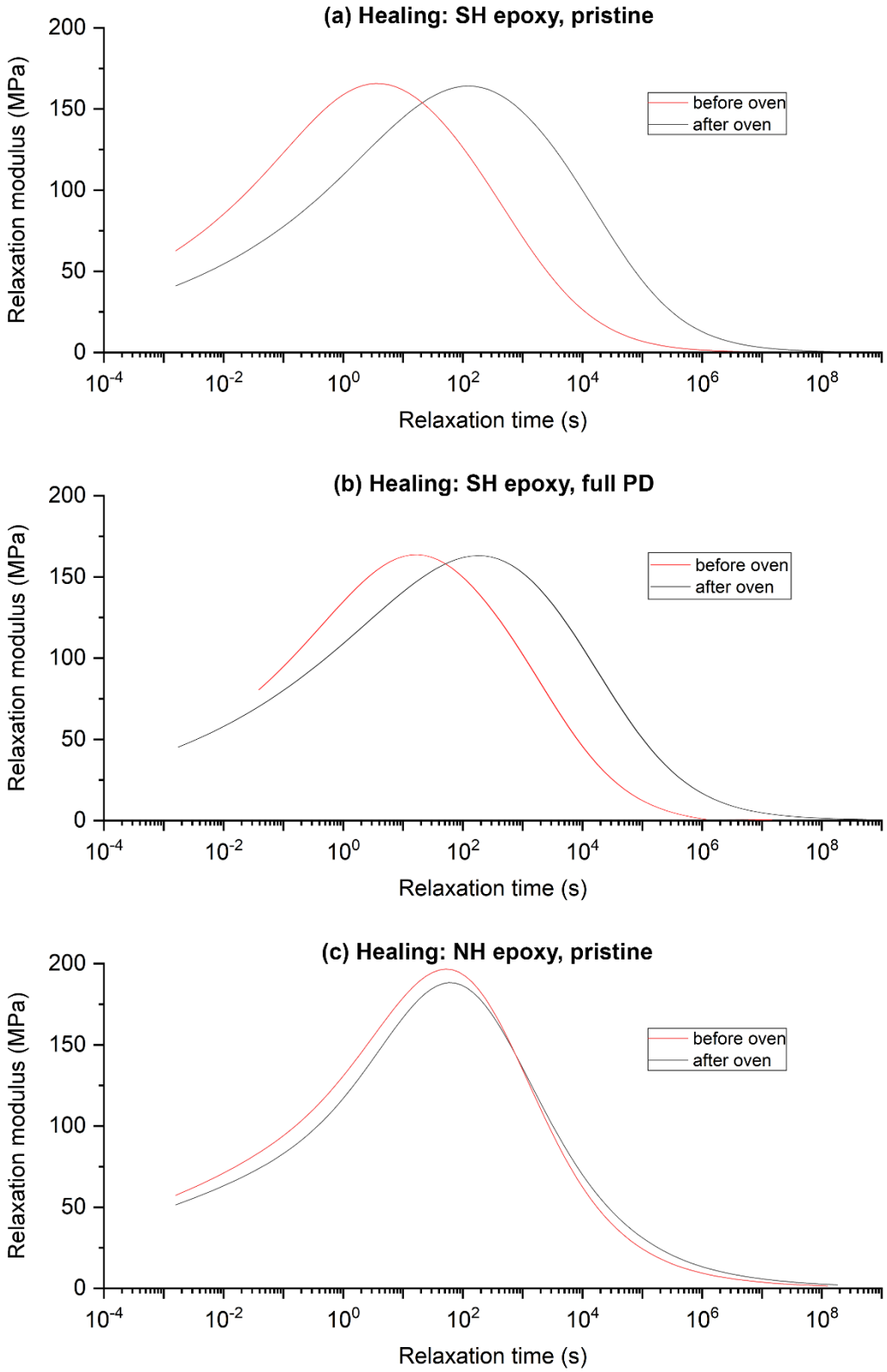

Figure 5.9 (a) *Reduced relaxation spectrum, T_{ref} = 70°C. CRS of fully PD SH epoxy taken from two consecutive TF sweeps without intermediate oven cycle* ***(b)*** *Calorimetric scan pre-oven and post-oven* ***(c)*** *Reduced relaxation spectrum, T_{ref} = 70°C. CRS of fully PD SH epoxy taken pre-oven and post-oven + one week.*

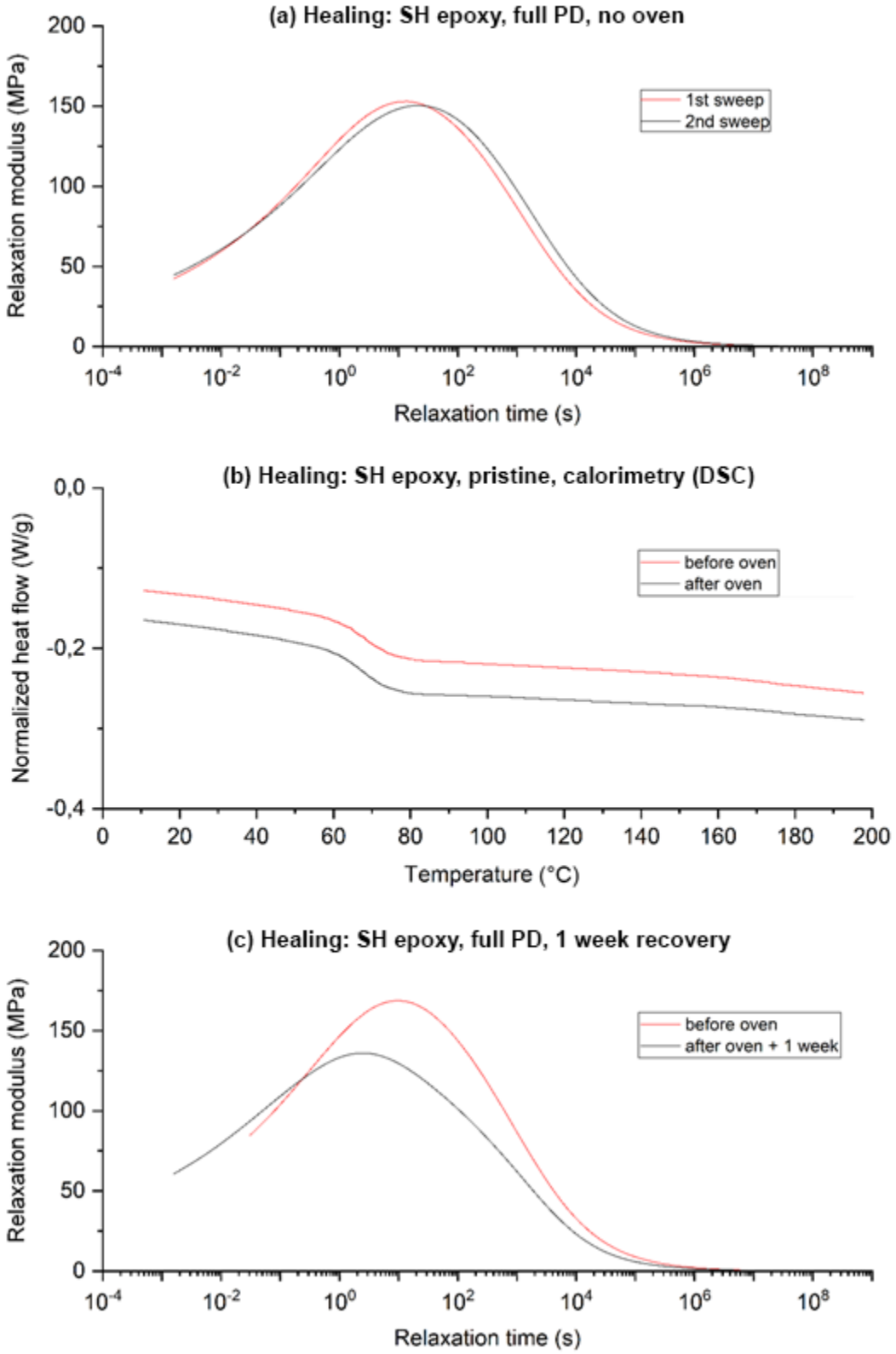

6. DISCUSSION

6.1. Stress relaxation response of as-produced self-healing and non-healing samples

The self-healing epoxy relaxes faster than the non-healing epoxy, as measured by the peak relaxation time (**Figure 5.4b**). This is a somewhat surprising result; one would expect the non-healing epoxy to relax faster due to its elastic and highly crosslinked nature, as opposed to the self-healing epoxy which has viscous contributions from the dynamic S-S bonds and has a comparable strength but lower stiffness (**Figure 5.4a**). Possibly, however, these same dynamic S-S bonds that provide a viscous component to the stress relaxation response also allow the self-healing epoxy to relax in more different ways, with less hindrance by 'traditional' crosslinks. This could then result in a faster overall relaxation. Inversely, this could also explain the greater peak height of the non-healing epoxy. In the absence of dynamic crosslinks, epoxies tend to build up internal stresses as a consequence of curing [43, 44]. These internal stresses could lead to a larger instantaneous relaxation energy, which is reflected in a higher stress relaxation peak. **Figure 5.8c** lends some credibility to this theory, as the oven treatment causes lowering of the stress relaxation peak in the non-healing epoxy. Since the oven temperature is below the suspected T_g of the non-healing epoxy, this could be a manifestation of annealing [45].

Noteworthy is the behavioral difference at very low (< 10^{-5} s) relaxation times: increasing energy is dissipated in the self-healing epoxy, while decreasing energy is dissipated in the non-healing epoxy. Logically, this should be attributed to disulfide exchange in the healing polymer. At the reference temperature these exchange reactions can be extremely rapid, especially in the vicinity of thiols [46, 47] or nucleophiles such as triethylamine [48], both of which are present in the self-healing epoxy.

The frequency independent energy plateau between 10^{-3} - 10^{-5} seconds found exclusively in the non-healing epoxy is not so readily explained. It could be related to the elastic network, or alternatively it could be a secondary manifestation of residual curing stress, a display of incomplete curing, or something else altogether, and its explanation is left to future work. However, as explained in **Chapter 5.1**, data below T_g is less reliable due to shifting problems and care must be taken when interpreting results.

6.2. Stress relaxation response of plastically deformed samples

The peak height lowering observed across both partially and fully PD self-healing samples (**Figure 5.6a**) is in line with expectations. Assuming the area under a segment dτ of the relaxation curve represents the energy dissipated in the relaxation process at that instant (**Figure 1.5**), the reduced number of (permanent) bonds in plastically deformed samples should be reflected in a lower instantaneous energy dissipation, i.e. a lower relaxation peak. However, if this assumption holds *and* if the measuring method is sensitive enough, it should also be expected that full PD results in a lower peak than partial PD, which is not the

case. Moreover, the peak height difference between pristine and deformed samples is so small (± 5%) that it cannot reasonably be separated from experimental error such as experimental noise, manufacturing inaccuracies, etc.

Plastic deformation could also be expected to change the half peak width and / or peak time, because broken permanent bonds form free chain ends that should have less incentive to relax than 'fully bound' chains. This is readily understood through the mechanical model analogy: free chain ends are affected by the polymer network 'spring force' from only one end, reducing the relaxation incentive. Therefore, under plastic deformation the stress response can be expected to shift to longer relaxation times, or for the relaxation peak to 'broaden' towards longer relaxation times, or both. However, neither seems to be the case.

A number of potential explanations are sought for the observed behavior:

1. Stiffness variations are a major contributor to differences in peak height
2. Partially and fully PD samples have approximately the same number of broken bonds
3. Time-dependent effects are a major contributor to differences in peak height
4. Damage dominantly manifests itself away from the main relaxation peak
5. Damage can better be monitored via other parameters than used here, e.g. total energy under curve [23] or slope of peak walls

All self-healing epoxy samples come from a single batch, where special care was taken to attain homogeneity, a constant thickness, and mitigate ageing and humidity effects. Nonetheless, significant variation is observed between sample stiffnesses (**Table 6.1**). In part, this could have been caused by inaccurate measurements of sample thickness and width. The DMA measures the force required for deformation which is dictated by the weakest location on the sample, which in turn is usually the thinnest location. If due to thickness or width variations a thicker location is measured in some samples while the thinnest location is measured in others, the calculated stress and stiffness will be accurate in some cases while being underestimated in others, leading to dispersion in the stress-strain curves. However, this effect is deemed minimal as thickness measurements were taken at multiple locations along each sample's length using a micrometer. If stiffness measurements are indeed quite accurate, then *stiffness variations are an unlikely cause of the observed peak height differences*, because no strong correlation is found between stiffness and peak height. This can easily be seen by comparing **Figure 5.6a** to **Table 6.1** / **Figure 5.7a**. Nonetheless, is seems probable that there is some relationship between the extremely high stiffness (i.e. 26% stiffer than average for partially PD samples) and the outlying peak height of the outlier in the partial PD sample set. No correlation is found between stiffness and peak time or peak width.

Table 6.1 *Stiffness of plastically deformed samples, taken at ε = 0.5%. Note: for partially PD samples the average is taken from the first two samples only. Note: 'P. PD' and 'F. PD' signify 'partial plastic deformation' and 'full plastic deformation', respectively.*

	P. PD				F. PD			
	S1	*S2*	*S3*	***Avg***	*S1*	*S2*	*S3*	***Avg***
Stiffness (MPa)	2777	2555	3369	**2666**	1853	2327	2170	**2117**

A hint towards the origins of the peak height differences is offered by the results of the hysteresis experiment (**Figure 5.7b**). Two immediate observations are made:

1. The polymer follows distinct paths for loading and unloading
2. The unloading path does not pass back through the origin

The hysteresis between the loading and unloading paths shows that energy is dissipated between the loading and unloading cycle. This type of behavior is typically observed in elastomers (**Figure 6.1a**), but can also be caused by plastic deformation (**Figure 6.1b**). In this case it is a combination of these two factors. Weak S-S bonds are first to break under load, dissipating energy and altering the unloading path. Broken S-S bonds then quickly reform because the resulting thiyl (-S•) radicals are unstable and at room temperature the associated S-S state is energetically favorable. This makes S-S bonds a reversible viscous energy dissipator, somewhat analogous to a mechanical dashpot, and a contributor to hysteresis. It also means that as S-S bonds break under load, the equilibrium length where zero stress is experienced shifts to a slightly stretched state. At some level of strain permanent bonds begin to break irreversibly, dissipating additional energy and contributing to hysteresis. Now, the equilibrium length shifts to an even more stretched state because there is a reduced elastic force pulling the network back to its original shape.

With this knowledge, the presence of hysteresis and plastic strain can be explained. Now, observing that fully PD samples display both significantly more hysteresis as plastic strain, it can be stated that *partially and fully PD samples probably do not have the approximate same number of broken bonds*. Rather, the number of broken bonds will be greater in the fully PD samples.

A second conclusion can be derived from the presence of hysteresis in the self-healing epoxy. Namely, that *if viscous energy dissipation is observed then a time-dependent component must be present in the stress relaxation response*. This time-dependency means that the time between damaging and testing might be a crucial parameter. During the damaging experiments this recovery time was not controlled, but an estimated average of 5 minutes passed between unloading and rapid cooling to 0°C in the DMA temperature-frequency sweep. 0°C is far below T_g (65°C, **Figure 5.3a**), largely inhibiting polymer motion and thereby relaxation. It is possible that this unintentional 'capturing' different states of relaxation, even within a single state of damage, could have greatly affected the observed relaxation response. The discussion of this temporal aspect of relaxation is continued in **Chapter 6.3**.

Figure 6.1 (a) *Hysteresis in elastically deformed materials. Arrows indicate loading (up) and unloading (down). Area between curves represents dissipated energy.* ***(b)*** *Hysteresis in plastically deformed materials. Note the residual strain ($\varepsilon_{plastic}$) at zero stress, indicating plastic deformation.*

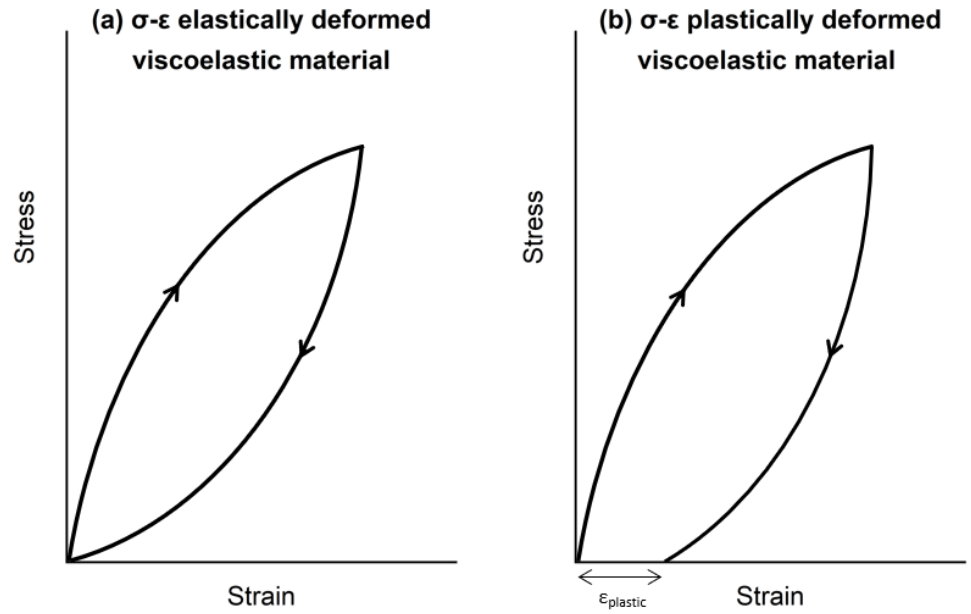

On a final note, since this thesis mostly focuses on the behavior of the main relaxation peak there exists a possibility that effects of plastic deformation manifest themselves more clearly outside the probed relaxation time window. This possibility is briefly discussed in **Chapter 6.3**. Also, it remains possible that the peak parameters of interest (height, width, time) are not suitable for capturing plastic deformation damage, or that they do not capture it individually as well as they do together (energy under curve). This premise is left mostly to future work. However, as **Chapter 6.3** will further illustrate, it is likely that recovery time plays a more pivotal role in the observed stress relaxation behavior.

6.3. Stress relaxation response of healed samples

An oven treatment causes a two decade increase in relaxation time of the main peak. This increase is consistent across pristine (**Figure 5.8a**) and fully PD (**Figure 5.8b**) self-healing samples, but is not found in non-healing samples (**Figure 5.8c**), nor when the oven treatment is removed (**Figure 5.9a**). Finally, a one week recovery period between the oven treatment and the second temperature-frequency sweep undoes the relaxation time shift, and reveals a sharp drop in relaxation peak height (**Figure 5.9c**). This suggests that:

1. the time shift must be related to the network structure and / or dynamic S-S bonds of the self-healing epoxy, and
2. the time shift is specifically related to the 2h 70°C oven treatment, not to the DMA temperature-frequency sweep where samples spend approximately 40 minutes between 70°C and 100°C (**Chapter 4.6**), and
3. the recovery time between the oven treatment and DMA temperature-frequency sweep has a strong influence on the stress relaxation response of SH samples

Again, a number of explanations are sought for the observed behavior:

1. Post-curing of epoxy network causes relaxation time shift after oven
2. Post-curing of siloxane network causes relaxation time shift after oven
3. Oxidation of S-S bonds causes relaxation time shift after oven
4. Relaxation time shift after oven is a quenching effect

Post-curing is an immediate though, since the time shift is related to the oven treatment. No time shift is observed in the non-healing epoxy, so *post-curing of the organic epoxy-amine structure within the self-healing network is an unlikely cause for the time shift*. Post-curing of the inorganic siloxane structure through continued hydrolysis and condensation is still a possibility. However, previous work has shown that for the temperature and oven time at hand *no significant post-curing of the siloxane network* should occur in the time frame studied [39]. Side reactions of free epoxy groups with tetra-thiol groups could underlie the time shift, but *post-curing should be reflected in an increased* T_g as a consequence of reduced mobility caused by the formation of additional crosslinks, which is not the case (**Figure 5.9b**). Oxidation of S-S bonds is another possibility, since time shifting is only observed in the self-healing epoxy. However, again previous work has shown that at the oven temperature and time used in this study *no significant oxidation of S-S bonds* should occur [29]. Moreover, the time shift appears to be reversible (**Figure 5.9c**), which rules oxidation unlikely.

It is proposed that quenching of relaxation processes induced by the presence of dynamic S-S bonds is the most likely explanation for the observed behavior. During the oven treatment the self-healing network gains extraordinary mobility from simultaneously passing through T_g and active 'shuffling' of dynamic S-S bonds. This mobility allows the network to partially relax internal stresses and, importantly, *establish an equilibrium network shape different from the equilibrium network shape at room temperature*. When the sample is removed from the oven, it slowly cools back down to room temperature from the outside inwards. As this process takes place, it gradually becomes energetically favorable for S-S bonds stop 'shuffling', and they start behaving mostly like permanent bonds. At the same time the network loses mobility as it cools through T_g.

If left undisturbed, the network approaches its room temperature equilibrium shape asymptotically at a decreasing exponential rate (**Figure 6.2**). Initially there is plenty of mobility, especially in the sample core which cools at a slower rate. Then, as mobility is lost, it takes incrementally more time for the network to relax to its room temperature equilibrium. Reformed S-S bonds become obstructions for relaxation, that under continuous internal stress may break over time and reform in energetically more favorable positions.

Figure 6.2 *Hypothetical re-equilibration of self-healing epoxy as function of time.*

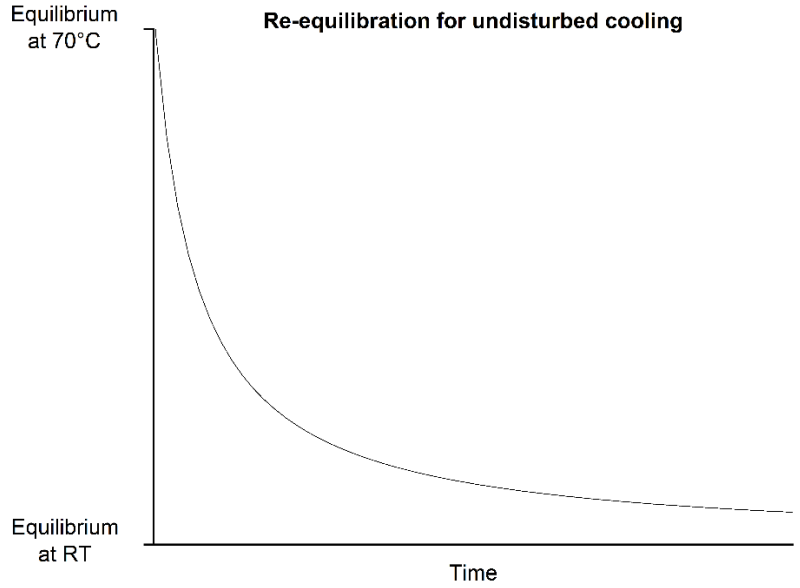

However, in reality the cooling process is accelerated in the tests performed in this work. After the oven treatment, the heated sample is clamped in the DMA and rapidly cooled to 0°C to start the temperature-frequency sweep. Between taking the sample out of the oven and this DMA induced quenching action there is about 5 minutes time. This means that a significant part of the internal equilibration has not yet completed. Only as the sample is heated back through T_g the relaxation process continues. Consequently, relaxation takes more time, which reveals itself as a shift to longer relaxation times.

The proposal postulated above, from now on referred to as the 'quenching hypothesis' at an out of equilibrium state, explains many of the results obtained. For example, it explains why the time shift occurs independent of the degree of damage. It also explains why the non-healing epoxy does not display a time shift, and why removing the oven step eliminates the time shift in self-healing samples. However, the question remains why in a damaged self-healing epoxy the peak height drops so dramatically after one week of recovery (**Figure 5.9c**) compared to the equal peak height obtained without recovery (**Figure 5.8b**).

An interesting explanation is possible *within* the quenching hypothesis, namely that quenching not only shifts the relaxation time but also increases the relaxation peak height compared to the room temperature equilibrium (**Figure 6.3**). Physically, this can be explained by the quenched network having to relax from a more strained state, which both requires more energy (higher peak) and takes more time (longer time). Under this argument, it can be argued that the marginal decrease in peak height observed in the damaging experiments (**Figure 5.6a**) was only a fraction of the actual decrease in peak height that would be observed if the system were given sufficient time to relax to its (damaged) room temperature equilibrium.

Figure 6.3 *Quenching hypothesis. System tends towards longer relaxation times and greater dissipated relaxation energy.*

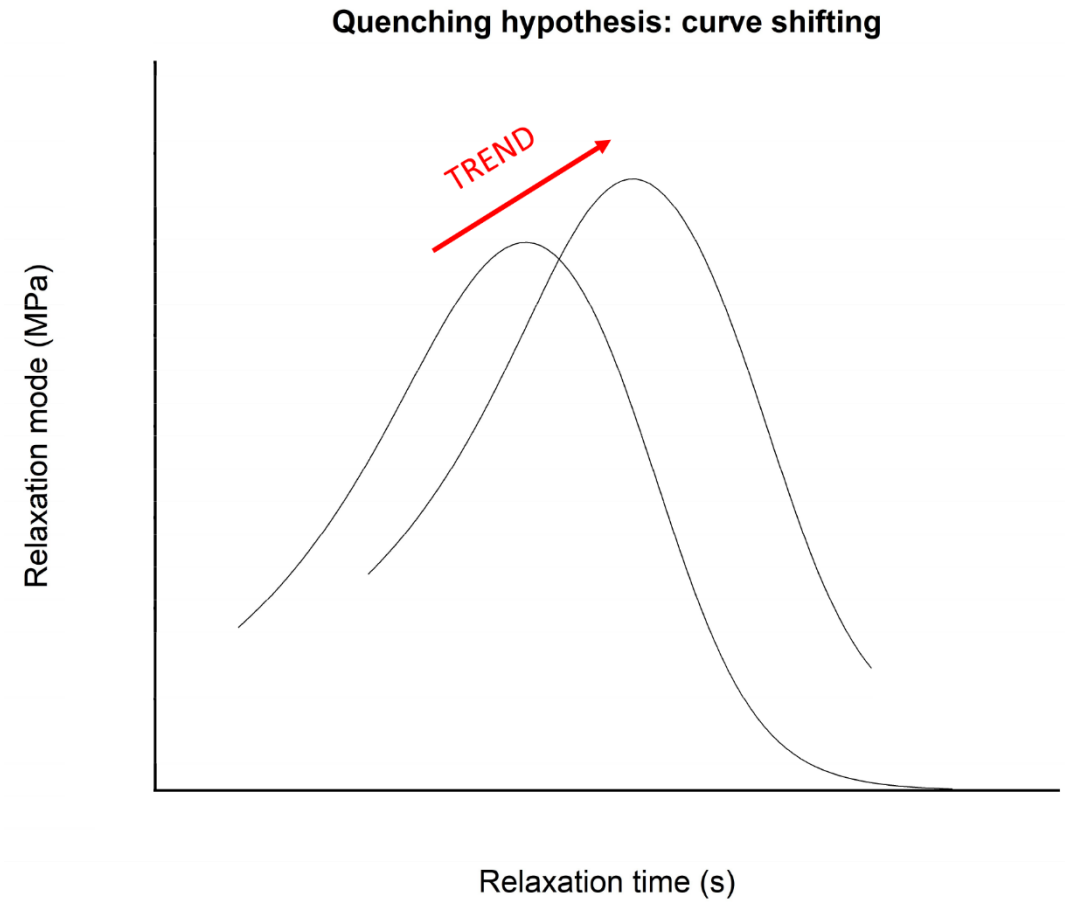

7. CONCLUSIONS

This work investigated whether damage degree and damage restoration after plastic deformation in self-healing polymer networks can be identified via continuous relaxation spectra. Specifically, it aimed to address three research questions:

1. Can plastic deformation in self-healing polymers be identified using continuous relaxation spectra?
2. Can the effect of a healing treatment be identified using continuous relaxation spectra?
3. Can continuous relaxation spectra be used as a quantification method for measuring plastic deformation and healing in polymers?

7.1. Identification of plastic deformation effects using continuous relaxation spectra

For self-healing epoxy samples, both partial and full plastic deformation led to lowering of the main stress relaxation peak compared to the pristine state. This trend was consistent across a batch size of 3 samples per deformation state, and is in line with the reduced relaxation energy available in damaged polymers due to breaking of permanent bonds. Contrary to expectation, no further distinction in peak height was found between partially and fully plastically deformed samples, although they were shown to house distinctly different amounts of plastic strain. A priori, plastic deformation was expected to increase the relaxation peak width and/or time since breaking of permanent bonds creates free chain ends with reduced incentive to relax. However, no significant alteration of either parameter with deformation was observed. Differences in peak height could not be correlated to variation in sample stiffness, although an outlier sample with a greater relaxation peak height also was much stiffer than other samples.

7.2. Identification of healing treatment effects using continuous relaxation spectra

A 2 hour 70°C oven treatment, intended to repair any induced damage by stimulating network mobility through sulfur-sulfur bond reshuffling above T_g, was found to induce a two decade increase in relaxation peak time for a fully plastically deformed self-healing epoxy sample. This time shift was also present in a pristine self-healing sample, but not in a fully plastically deformed non-healing sample, nor when performing two consecutive temperature-frequency sweeps without intermediate oven treatment. Finally, a one week recovery period after the oven treatment eliminated the time shift for a fully plastically deformed self-healing sample, as well as drastically lowering the peak height.

Post-curing and oxidation of S-S bonds were dismissed as probable reason for the time shift because of (i) the apparent reversibility of the time shift, (ii) the unchanged calorimetric T_g

after the oven treatment, and (iii) the fact that previous work that showed no significant post-curing or oxidation should occur under the oven treatment conditions.

Quenching of a non-equilibrium polymer state is proposed as the most likely mechanism underlying the observed relaxation behavior. This 'quenching hypothesis' can satisfactorily explain most results from the plastic deformation and healing experiments. The oven treatment brings the polymer above T_g and at its optimal disulfide shuffling temperature, providing extraordinary mobility to the polymer network. This allows it to attain a new internal equilibrium structure, different from that at room temperature. When immediately after the oven treatment a temperature-frequency sweep is performed in the DMA, this new equilibrium structure is trapped by fast cooling to 0°C. This results in a longer stress relaxation time. Similarly, an insufficient time window between plastic deformation and temperature-frequency sweeping can cause an increased relaxation peak height without accompanying time shift. Here, 'trapping' a damaged and somewhat stretched state causes increased energy release upon heating through T_g, effectively increasing the relaxation peak height and thereby 'hiding' the true effect of damage on the peak height. This would explain both the minor reduction in peak height observed in the damaging experiments, as well as the large reduction in peak height observed when allowing a one week recovery period.

7.3. Continuous relaxation spectra as quantification method

Continuous relaxation spectra were found to be sensitive to changes induced by plastic deformation. In this sense, they hold potential as a quantification method for plastic deformation and/or healing. However, due to the viscoelastic nature of self-healing epoxy samples their relaxation spectra were also sensitive to the testing conditions, e.g. time between plastic deformation or oven treatment and generation of relaxation spectra. Moreover, the complexity and dynamic nature of the polymer used in this work do not match the traditional requirement of thermorheological simplicity, meaning that results must be carefully interpreted and further validated. At this point, it is difficult to evaluate the true potential of continuous relaxation spectra as quantification method for plastic deformation and healing. However, it is clear that its use requires a custom approach, where extensive knowledge of the investigated materials system and viscoelasticity, as well as experience with rheological test methods are key.

8. RECOMMENDATIONS

The quenching hypothesis proposed in this thesis must be tested to prove or disprove its premises. To this end, the following is proposed:

Prepare 18 dogbone samples, 9 self-healing and 9 non-healing epoxy. For each set, obtain a reliable baseline stress relaxation response of the pristine state using 3 samples. Strain the remaining 6 samples to full plastic deformation, where 3 samples are left to rest for a week at room temperature and 3 samples are immediately quenched for a DMA temperature-frequency sweep. Compare results, and see if:

1. Rapid quenching indeed leads to a higher relaxation peak, and
2. Rapid quenching does not shift the relaxation time, and
3. There is a difference between self-healing and non-healing samples

A similar experiment could be conducted with an oven treatment, with and without a one week recovery period for both healing and non-healing samples.

A lack of reference material about the stress relaxation response of crosslinked polymers has hampered understanding of the results of this thesis. If continuous relaxation spectra should be further investigated as a tool for quantifying damage in self-healing network polymers, it is advisable that a separate study be conducted into the stress relaxation response of a very simple, non-healing crosslinked polymer, e.g. a simple epoxy-amine system. From there, steps can be taken to understand the relaxation response of more complicated self-healing crosslinked systems.

For further studies it is recommended that a polymer system is used where the difference in polymer structure between the self-healing material and non-healing reference is minimal. The bis(3-(triethoxysilyl)propyl)disulfide organically modified silicone alkoxide used in this study happens to be available with either a S-S or substituent C-C link. In other words, it is advised that future studies change the non-healing epoxy used in this thesis for the exact same network polymer as the self-healing epoxy, but with a C-C link instead of a S-S link to minimize experimental variables.

Polymer samples were manufactured with great care, but nevertheless had minor variations in thickness. Because the dogbone samples are very thin (0.2 mm) these variations lead to significant spread in sample stiffness. Although this spread could not be linked to trends in the relaxation spectra, it emphasized the importance of performing more test repetitions to average out effects of variability in manufacturing, testing conditions, etc., in individual results.

REFERENCES

[1] S. C. G. Leeuwenburgh, N. De Belie, and S. van der Zwaag, "Self-Healing Materials are Coming of Age," *Advanced Materials Interfaces,* vol. 5, no. 17, 2018, doi: 10.1002/admi.201800736.

[2] S. R. White *et al.*, "Autonomic healing of polymer composites," *Nature,* vol. 409, no. 15, 2001, doi: 10.1038/35057232.

[3] S. van der Zwaag, *Self healing materials: an approach to 20 centuries of materials science*. Springer, 2007.

[4] A. Kawasumi, N. Sagawa, S. Hayashi, H. Yokoyama, and K. Tamura, "Wound healing in mammals and amphibians: toward limb regeneration in mammals," *Curr Top Microbiol Immunol,* vol. 367, pp. 33-49, 2013, doi: 10.1007/82_2012_305.

[5] M. D. Hager, P. Greil, C. Leyens, S. van der Zwaag, and U. S. Schubert, "Self-healing materials," *Advanced Materials,* vol. 22, 2010, doi: 10.1002/ adma201003036.

[6] I. L. Hia, V. Vahedi, and P. Pasbakhsh, "Self-Healing Polymer Composites: Prospects, Challenges, and Applications," *Polymer Reviews,* vol. 56, no. 2, pp. 225-261, 2016, doi: 10.1080/15583724.2015.1106555.

[7] S. J. García, H. R. Fischer, and S. van der Zwaag, "A critical appraisal of the potential of self healing polymeric coatings," *Progress in Organic Coatings,* vol. 72, no. 3, pp. 211-221, 2011, doi: 10.1016/j.porgcoat.2011.06.016.

[8] C. J. Kloxin and C. N. Bowman, "Covalent adaptable networks: smart, reconfigurable and responsive network systems," *Chem Soc Rev,* vol. 42, no. 17, pp. 7161-73, Sep 7 2013, doi: 10.1039/c3cs60046g.

[9] J. Kang, J. B. H. Tok, and Z. Bao, "Self-healing soft electronics," *Nature Electronics,* vol. 2, no. 4, pp. 144-150, 2019, doi: 10.1038/s41928-019-0235-0.

[10] A. Lutz *et al.*, "A shape-recovery polymer coating for the corrosion protection of metallic surfaces," *ACS Appl Mater Interfaces,* vol. 7, no. 1, pp. 175-83, Jan 14 2015, doi: 10.1021/am505621x.

[11] G. Rivero, L.-T. T. Nguyen, X. K. D. Hillewaere, and F. E. Du Prez, "One-Pot Thermo-Remendable Shape Memory Polyurethanes," *Macromolecules,* vol. 47, no. 6, pp. 2010-2018, 2014, doi: 10.1021/ma402471c.

[12] M. Samadzadeh, S. H. Boura, M. Peikari, A. Ashrafi, and M. Kasiriha, "Tung oil: An autonomous repairing agent for self-healing epoxy coatings," *Progress in Organic Coatings,* vol. 70, no. 4, pp. 383-387, 2011, doi: 10.1016/j.porgcoat.2010.08.017.

[13] V. Montano, W. Vogel, A. Smits, S. van der Zwaag, and S. J. Garcia, "From Scratch Closure to Electrolyte Barrier Restoration in Self-Healing Polyurethane Coatings," *ACS Appl Polym Mater,* vol. 3, no. 5, pp. 2802-2812, May 14 2021, doi: 10.1021/acsapm.1c00323.

[14] E. D. Rodriguez, X. Luo, and P. T. Mather, "Linear/network poly(epsilon-caprolactone) blends exhibiting shape memory assisted self-healing (SMASH)," *ACS Appl Mater Interfaces,* vol. 3, no. 2, pp. 152-61, Feb 2011, doi: 10.1021/am101012c.

[15] S. M. Kim *et al.*, "Superior Toughness and Fast Self-Healing at Room Temperature Engineered by Transparent Elastomers," *Adv Mater,* vol. 30, no. 1, Jan 2018, doi: 10.1002/adma.201705145.

[16] Y. Lai, X. Kuang, P. Zhu, M. Huang, X. Dong, and D. Wang, "Colorless, Transparent, Robust, and Fast Scratch-Self-Healing Elastomers via a Phase-Locked Dynamic Bonds Design," *Adv Mater,* vol. 30, no. 38, p. e1802556, Sep 2018, doi: 10.1002/adma.201802556.

[17] Z. Wang, Y. Gu, M. Ma, and M. Chen, "Strong, Reconfigurable, and Recyclable Thermosets Cross-Linked by Polymer–Polymer Dynamic Interaction Based on Commodity Thermoplastics," *Macromolecules,* vol. 53, no. 3, pp. 956-964, 2020, doi: 10.1021/acs.macromol.9b02325.

[18] W. Post, R. K. Bose, S. J. Garcia, and S. Van der Zwaag, "Healing of Early Stage Fatigue Damage in Ionomer/Fe(3)O(4) Nanoparticle Composites," *Polymers (Basel),* vol. 8, no. 12, Dec 15 2016, doi: 10.3390/polym8120436.

[19] M. Hernandez, A. M. Grande, S. van der Zwaag, and S. J. Garcia, "Monitoring Network and Interfacial Healing Processes by Broadband Dielectric Spectroscopy: A Case Study on Natural Rubber," *ACS Appl Mater Interfaces,* vol. 8, no. 16, pp. 10647-56, Apr 27 2016, doi: 10.1021/acsami.6b02259.

[20] S. Bode *et al.*, "Characterization of Self-Healing Polymers: From Macroscopic Healing Tests to the Molecular Mechanism," in *Self-healing Materials*, (Advances in Polymer Science, 2015, ch. Chapter 341, pp. 113-142.

[21] F. Zhang, L. Wang, C. Li, and Y. Xing, "The Discrete and Continuous Retardation and Relaxation Spectrum Method for Viscoelastic Characterization of Warm Mix Crumb Rubber-Modified Asphalt Mixtures," *Materials,* vol. 13, no. 3723, 2020, doi: 10.3390/ma13173723.

[22] D. D. Fox, O. C. Zienkiewicz, and R. L. Taylor, *The finite element method for solid and structural mechanics*, 7th ed. Butterworth-Heinemann (Elsevier), 2014.

[23] V. Montano, S. J. Picken, S. van der Zwaag, and S. J. Garcia, "A deconvolution protocol of the mechanical relaxation spectrum to identify and quantify individual polymer feature contributions to self-healing," *Phys Chem Chem Phys,* vol. 21, no. 19, pp. 10171-10184, 2019, doi: 10.1039/c9cp00417c.

[24] G. M. Scheutz, J. J. Lessard, M. B. Sims, and B. S. Sumerlin, "Adaptable Crosslinks in Polymeric Materials: Resolving the Intersection of Thermoplastics and Thermosets," *J Am Chem Soc,* vol. 141, no. 41, pp. 16181-16196, Oct 16 2019, doi: 10.1021/jacs.9b07922.

[25] C. J. Kloxin, T. F. Scott, B. J. Adzima, and C. N. Bowman, "Covalent Adaptable Networks (CANs): A Unique Paradigm in Crosslinked Polymers," *Macromolecules,* vol. 43, no. 6, pp. 2643-2653, Mar 23 2010, doi: 10.1021/ma902596s.

[26] D. Montarnal, M. Capelot, F. Tournilhac, and L. Leibler, "Silica-Like Malleable Materials from Permanent Organic Networks," *Science,* vol. 334, no. 6058, 2011, doi: 0.1126/science.1212648.

[27] M. Capelot, M. M. Unterlass, F. Tournilhac, and L. Leibler, "Catalytic Control of the Vitrimer Glass Transition," *ACS Macro Letters,* vol. 1, no. 7, pp. 789-792, 2012, doi: 10.1021/mz300239f.

[28] J. Canadell, H. Goossens, and B. Klumperman, "Self-Healing Materials Based on Disulfide Links," *Macromolecules,* vol. 44, no. 8, pp. 2536-2541, 2011, doi: 10.1021/ma2001492.

[29] M. AbdolahZadeh, A. C. C. Esteves, S. van der Zwaag, and S. J. Garcia, "Healable dual organic-inorganic crosslinked sol-gel based polymers: Crosslinking density and tetrasulfide content effect," *Journal of Polymer Science Part A: Polymer Chemistry,* vol. 52, no. 14, pp. 1953-1961, 2014, doi: 10.1002/pola.27200.

[30] S. Y. An, S. M. Noh, J. H. Nam, and J. K. Oh, "Dual Sulfide-Disulfide Crosslinked Networks with Rapid and Room Temperature Self-Healability," *Macromol Rapid Commun,* vol. 36, no. 13, pp. 1255-60, Jul 2015, doi: 10.1002/marc.201500123.

[31] C. D. Han and J. K. Kim, "On the use of time-temperature superposition in multicomponent/multiphase polymer systems," *Polymer,* vol. 34, no. 12, 1993, doi: 10.1016/0032-3861(93)90585-X.

[32] L. Palade, H. J. Lehermeier, and J. R. Dorgan, "Melt Rheology of High L-Content Poly(lactic acid)," *Macromolecules,* vol. 34, 2001.

[33] W. P. Hernández, D. A. Castello, N. Roitman, and C. Magluta, "Thermorheologically simple materials: A bayesian framework for model calibration and validation," *Journal of Sound and Vibration,* vol. 402, pp. 14-30, 2017, doi: 10.1016/j.jsv.2017.05.005.

[34] M. L. Williams, R. F. Landel, and J. D. Ferry, "The temperature dependence of relaxation mechanisms in amorphous polymers and other glass-forming liquids," *Journal of the American Chemical Society,* vol. 77, no. 14, 1955, doi: 10.1021/ja01619a008.

[35] K. M. Kirkwood, L. G. Leal, D. Vlassopoulos, P. Driva, and N. Hadjichristidis, "Stress Relaxation of Comb Polymers with Short Branches," *Macromolecules,* vol. 42, no. 24, pp. 9592-9608, 2009, doi: 10.1021/ma900950s.

[36] R. K. Bose, N. Hohlbein, S. J. Garcia, A. M. Schmidt, and S. van der Zwaag, "Relationship between the network dynamics, supramolecular relaxation time and healing kinetics of cobalt poly(butyl acrylate) ionomers," *Polymer,* vol. 69, pp. 228-232, 2015, doi: 10.1016/j.polymer.2015.03.049.

[37] J. Ferry, *Viscoelastic properties of polymers*, 3rd ed. John Wiley & Sons, 1980.

[38] J. Honerkamp and J. Weese, "A nonlinear regularization method for the calculation of relaxation spectra," *Rheologica Acta,* vol. 32, 1, pp. 65-73, 1993, doi: 10.1007/BF00396678.

[39] N. Zhong, "Self-healing thermal interface materials," PhD dissertation, Faculty of Aerospace Engineering, Delft University of Technology, 2020.

[40] W. Post, A. Cohades, V. Michaud, S. van der Zwaag, and S. J. Garcia, "Healing of a glass fibre reinforced composite with a disulphide containing organic-inorganic epoxy matrix," *Composites Science and Technology,* vol. 152, pp. 85-93, 2017, doi: 10.1016/j.compscitech.2017.09.017.

[41] *ASTM D1708-18 Standard Test Method for Tensile Properties of Plastics by Use of Microtensile Specimens*, 2018. [Online]. Available: www.astm.org

[42] F. Denes, M. Pichowicz, G. Povie, and P. Renaud, "Thiyl radicals in organic synthesis," *Chemical Reviews,* vol. 114, no. 5, pp. 2587-693, 2014, doi: 10.1021/cr400441m.

[43] C. Brahatheeswaran and V. B. Gupta, "Internal stresses in a cured epoxy resin system," *Polymer,* vol. 34, no. 2, 1993, doi: 10.1016/0032-3861(93)90079-P.

[44] Y. K. Kim and S. R. White, "Stress relaxation behavior of 3501-6 epoxy resin," *Polymer Engineering and Science,* vol. 36, no. 23, 1996, doi: 10.1002/pen.10686.

[45] R. J. C. Carbas, L. F. M. da Silva, E. A. S. Marques, and A. M. Lopes, "Effect of post-cure on the glass transition temperature and mechanical properties of epoxy adhesives," *Journal of Adhesion Science and Technology,* vol. 27, no. 23, pp. 2542-2557, 2013, doi: 10.1080/01694243.2013.790294.

[46] P. Nagy, "Kinetics and mechanisms of thiol-disulfide exchange covering direct substitution and thiol oxidation-mediated pathways," *Antioxid Redox Signal,* vol. 18, no. 13, pp. 1623-41, May 1 2013, doi: 10.1089/ars.2012.4973.

[47] R. P. Szajewski and G. M. Whitesides, "Rate constants and equilibrium constants for thiol-disulfide interchange reactions involving oxidized glutathione," *Journal of the American Chemical Society,* vol. 102, no. 6, 1978, doi: 10.1021/ja00526a042.

[48] S. Nevejans, N. Ballard, J. I. Miranda, B. Reck, and J. M. Asua, "The underlying mechanisms for self-healing of poly(disulfide)s," *Phys Chem Chem Phys,* vol. 18, no. 39, pp. 27577-27583, Oct 5 2016, doi: 10.1039/c6cp04028d.

APPENDIX A
Amplitude sweeps

Figure A 1 *Amplitude sweeps of pristine and fully PD samples at 0°C and 100°C.*

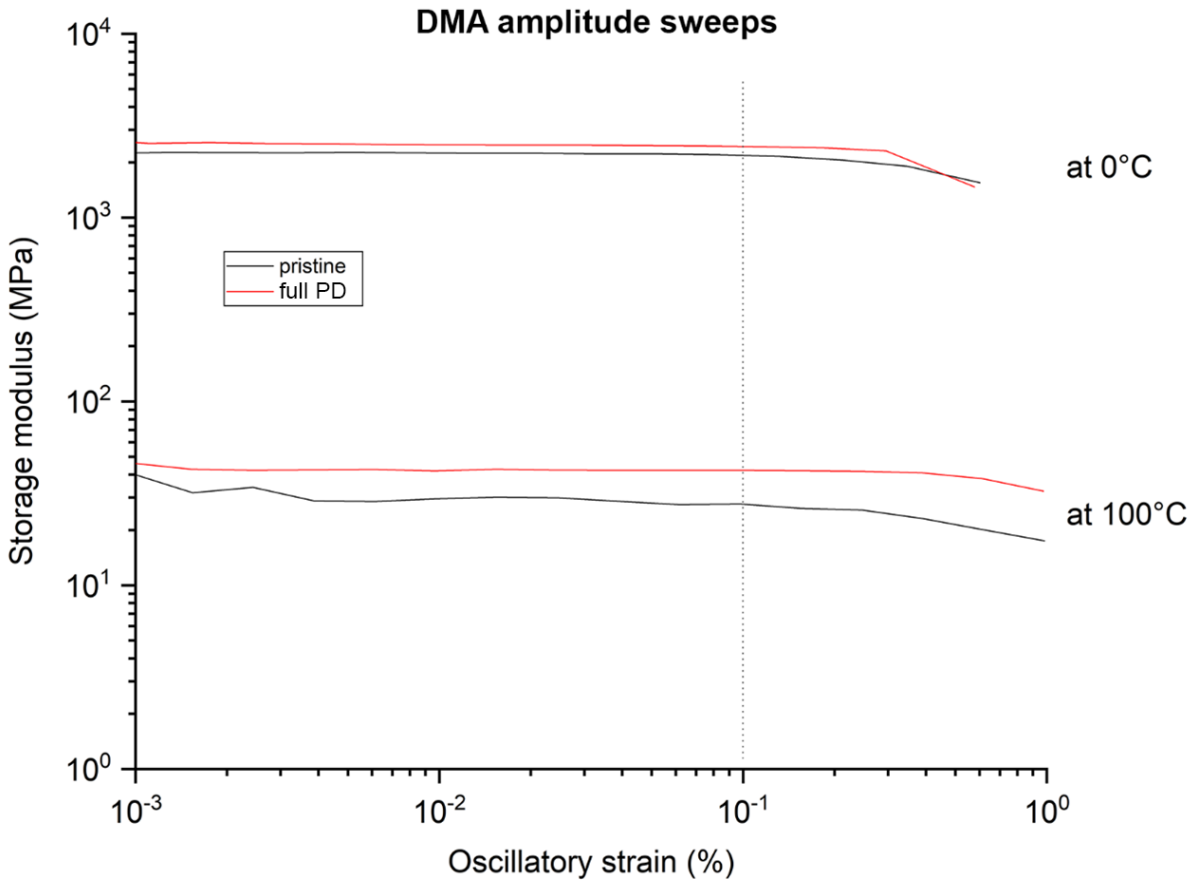

APPENDIX B
TTS master curve data

Figure B 1 *Reduced TTS master curve and horizontal shift factors a_T for: pristine SH epoxy #1. T_{ref} = 70°C.*

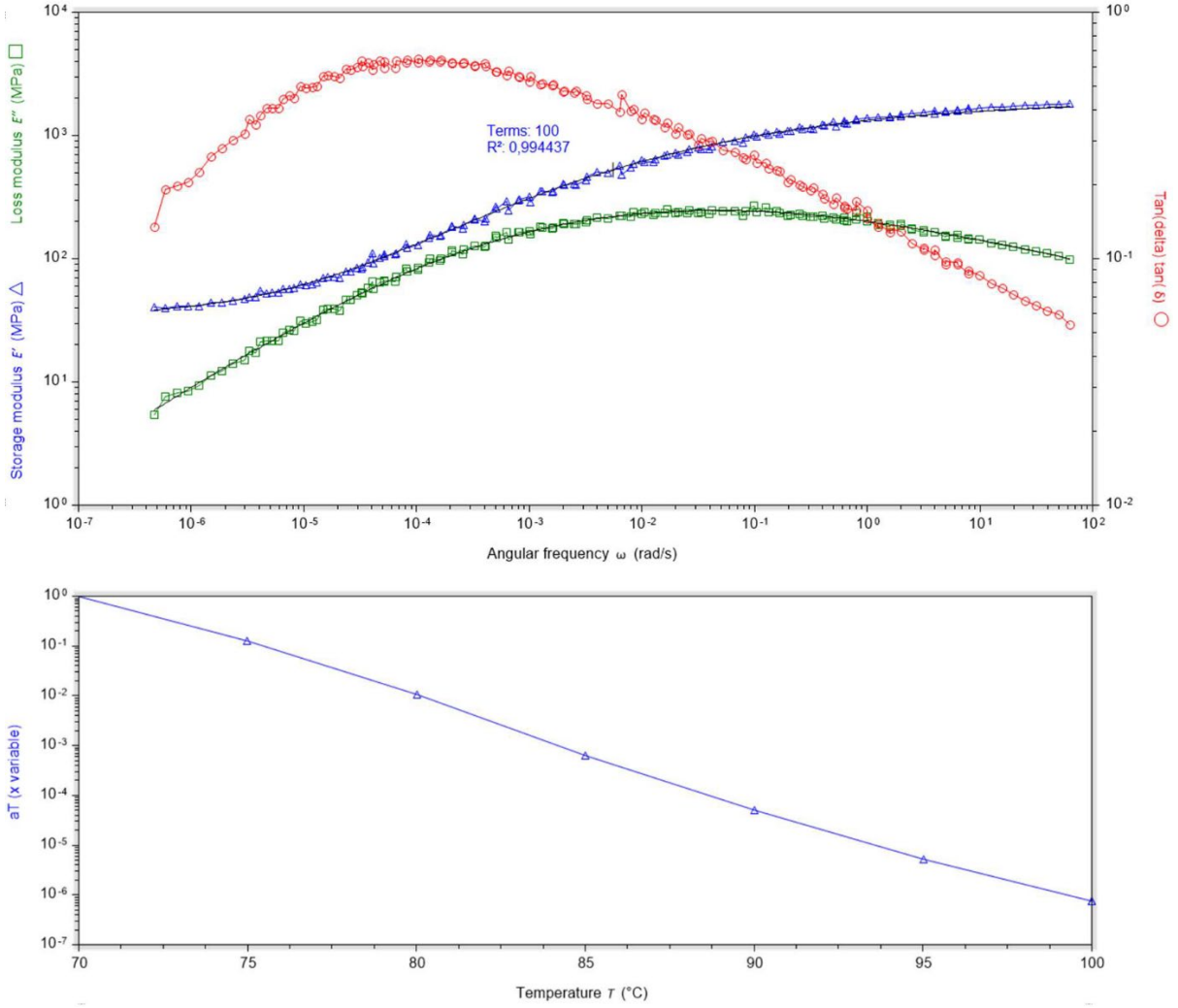

Figure B 2 *Reduced TTS master curve and horizontal shift factors a_T for: pristine SH epoxy #2. T_{ref} = 70°C.*

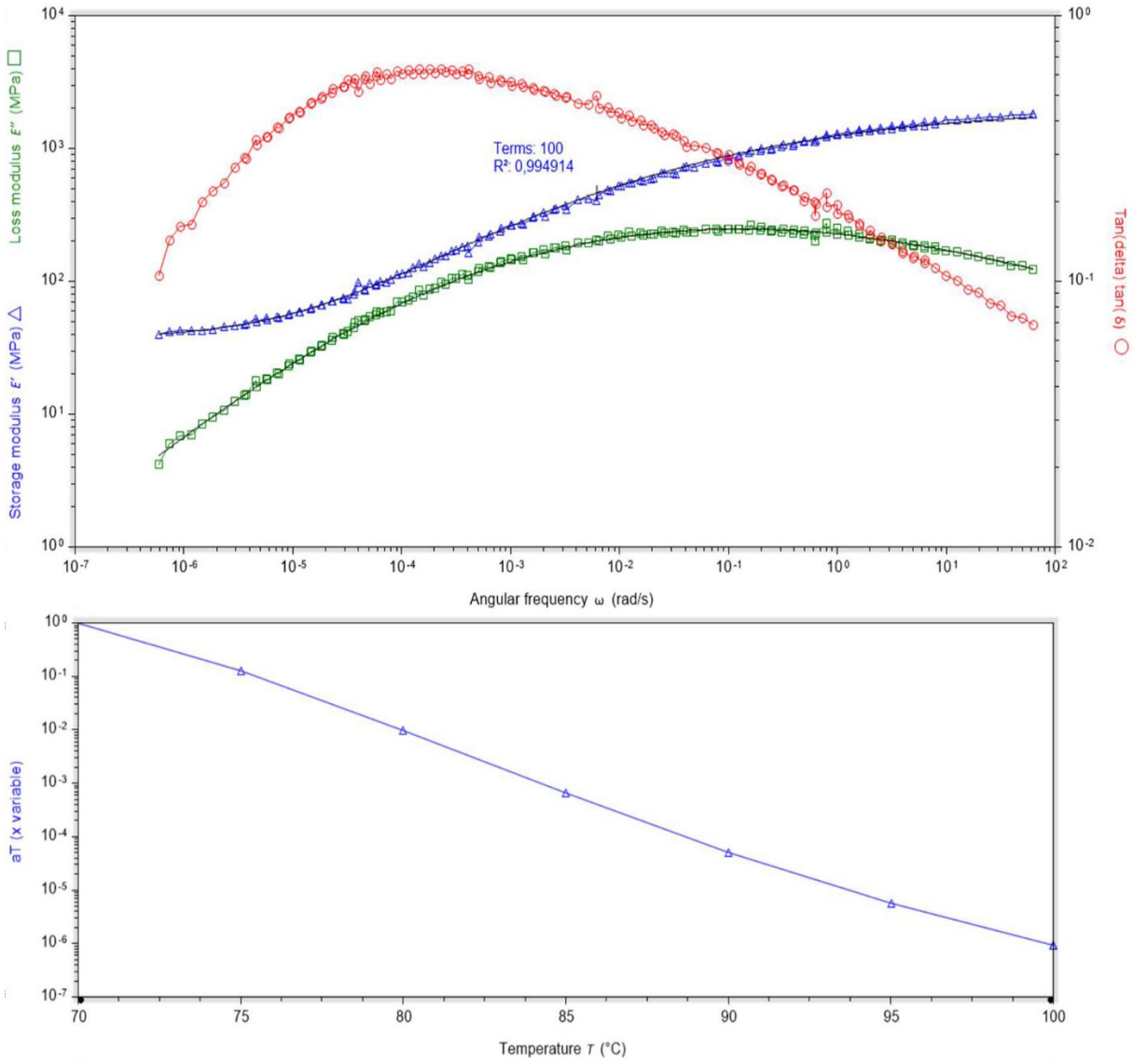

Figure B 3 *Reduced TTS master curve and horizontal shift factors a_T for: pristine SH epoxy #3. T_{ref} = 70°C.*

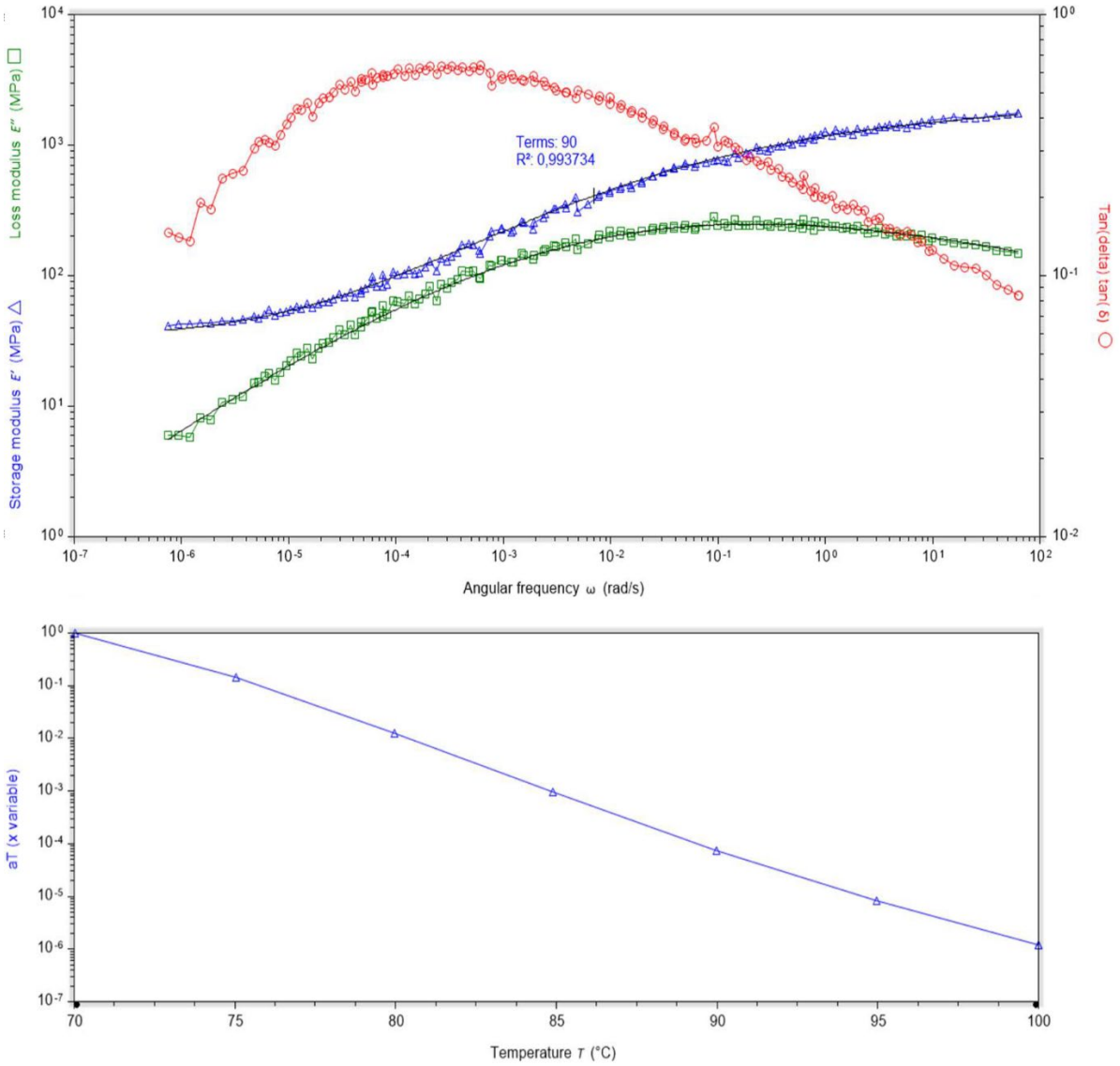

Figure B 4 *Reduced TTS master curve and horizontal shift factors a_T for: partially PD SH epoxy #1. T_{ref} = 70°C.*

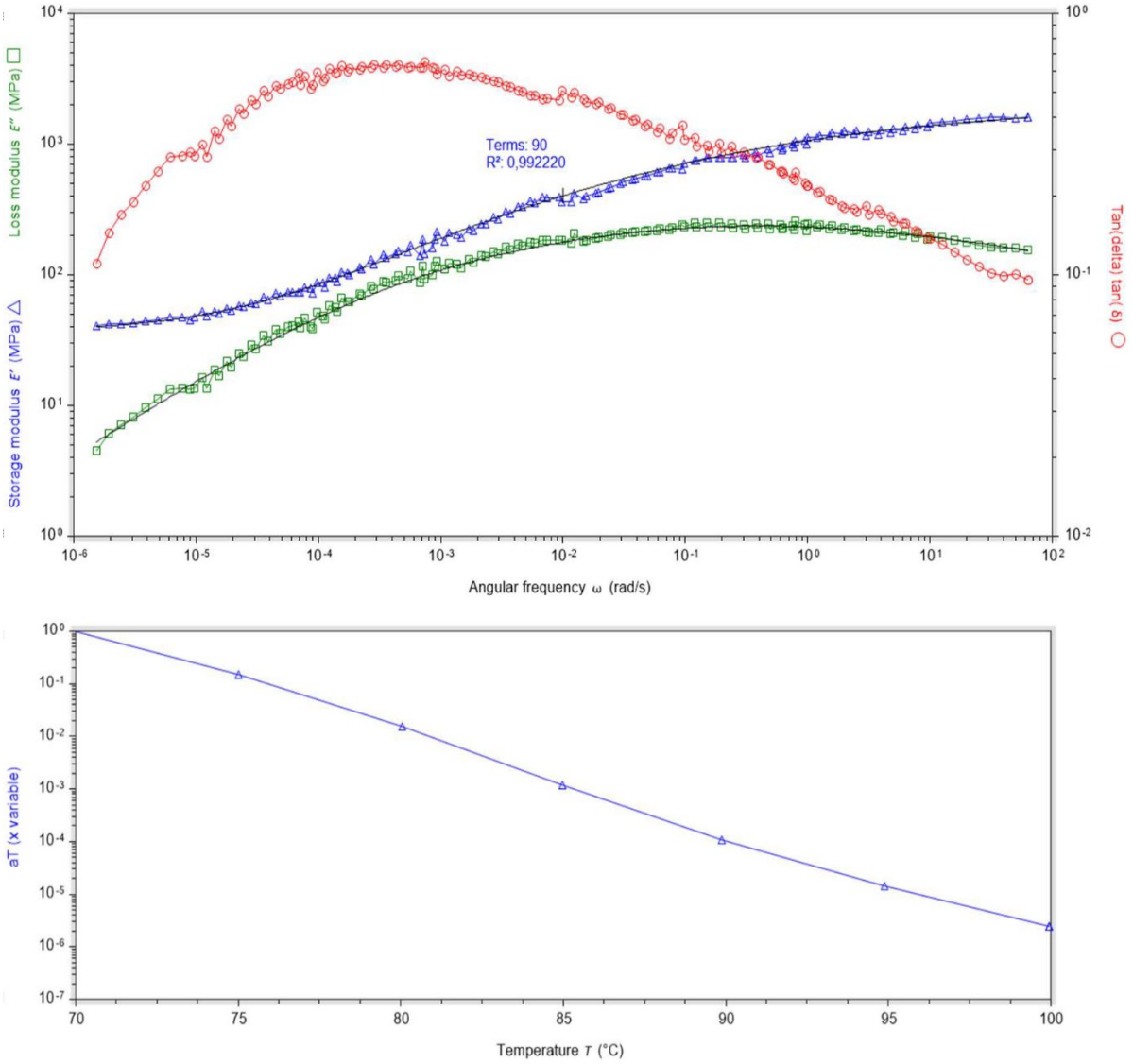

Figure B 5 *Reduced TTS master curve and horizontal shift factors a_T for: partially PD SH epoxy #2. T_{ref} = 70°C.*

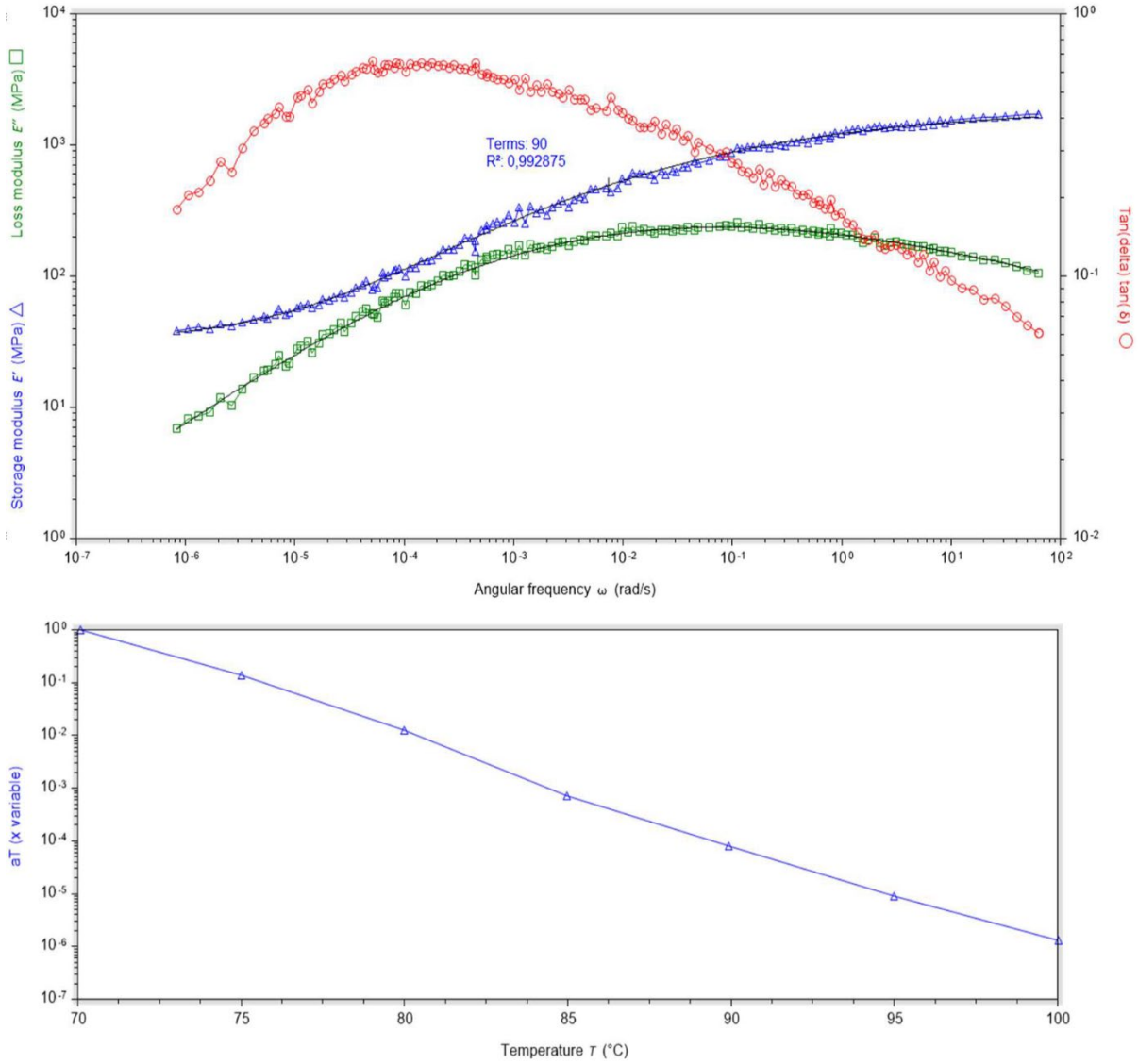

Figure B 6 *Reduced TTS master curve and horizontal shift factors a_T for: partially PD SH epoxy #3. T_{ref} = 70°C.*

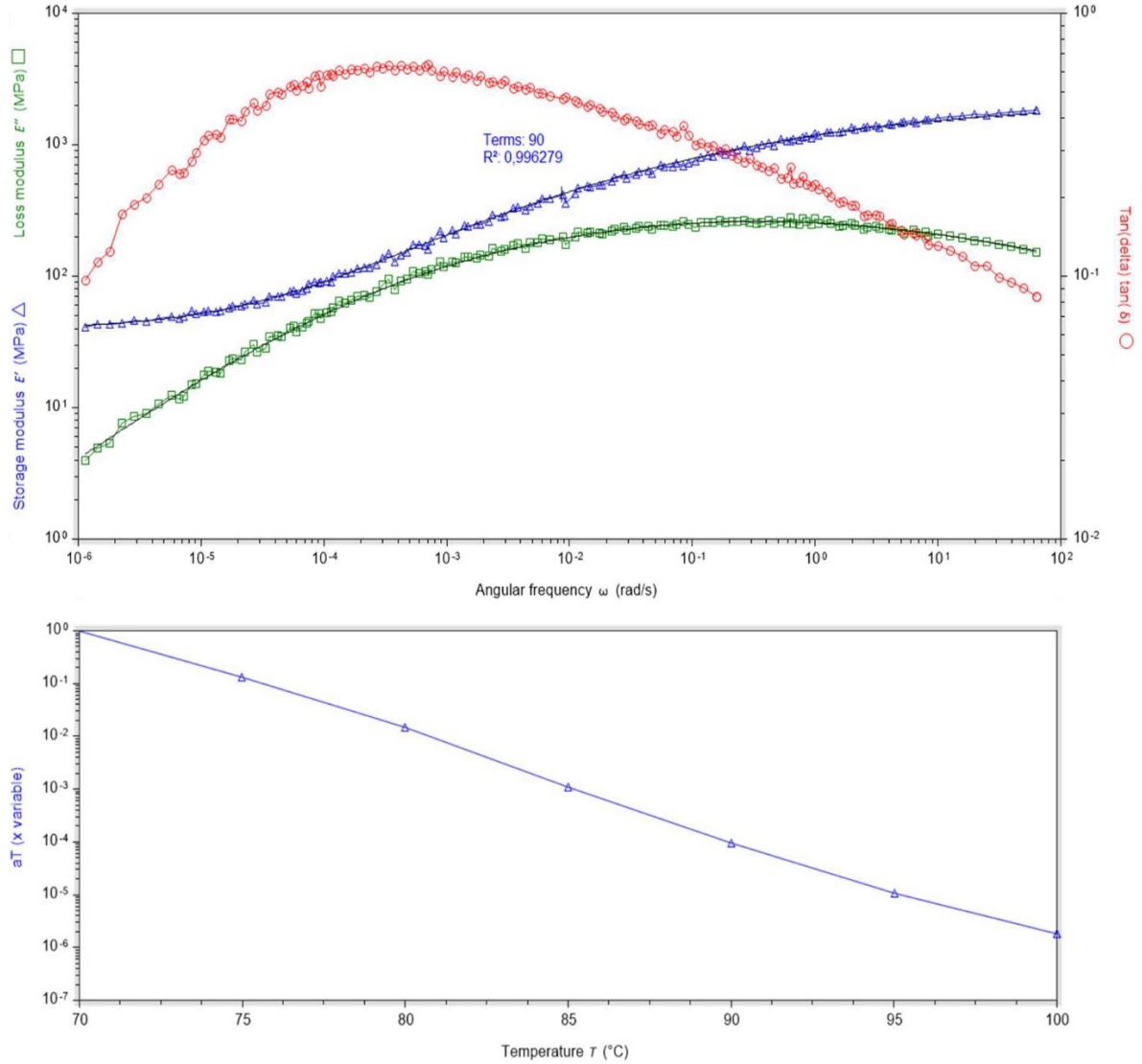

Figure B 7 *Reduced TTS master curve and horizontal shift factors a_T for: fully PD SH epoxy #1. T_{ref} = 70°C.*

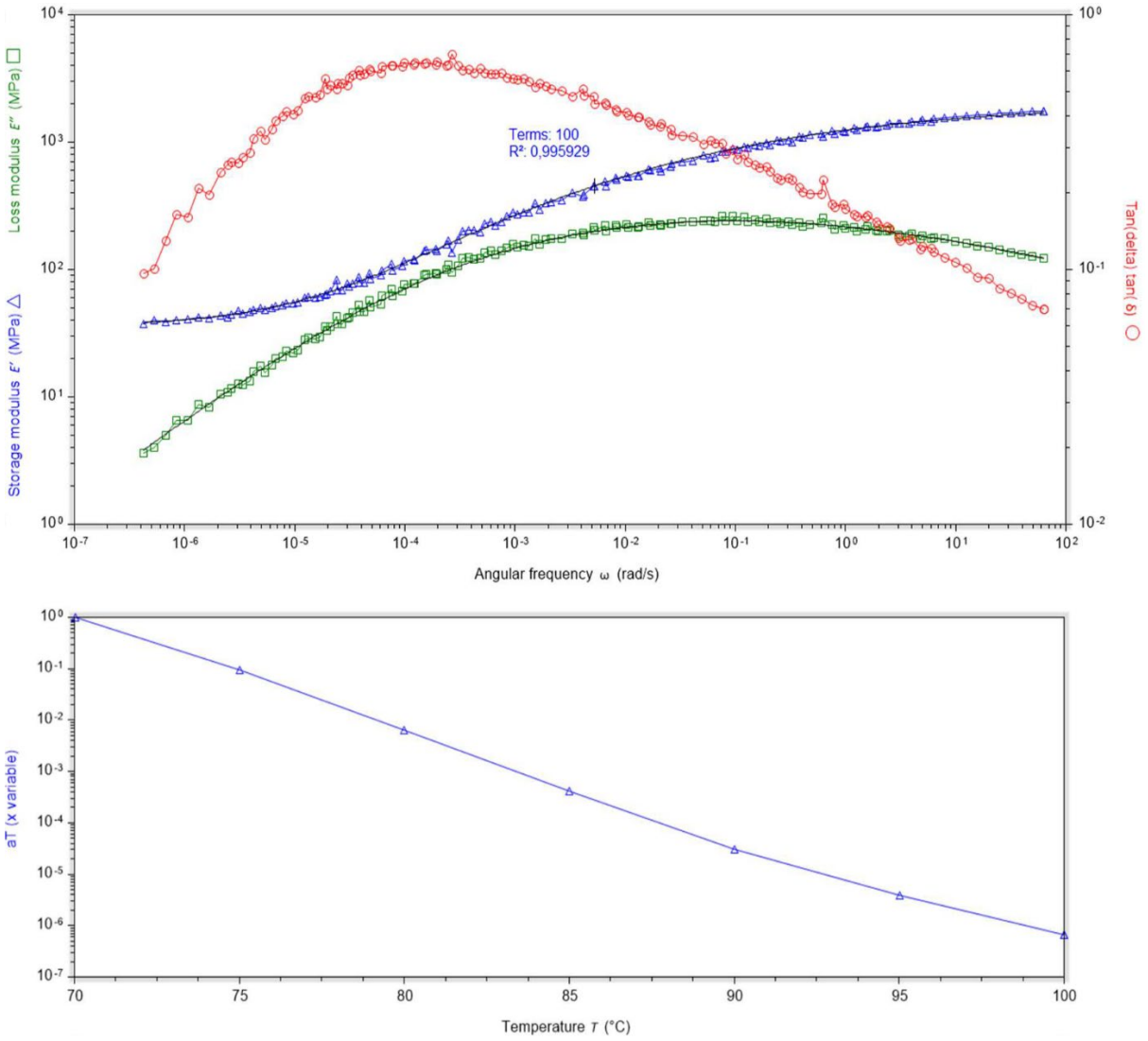

Figure B 8 *Reduced TTS master curve and horizontal shift factors a_T for: fully PD SH epoxy #2. T_{ref} = 70°C.*

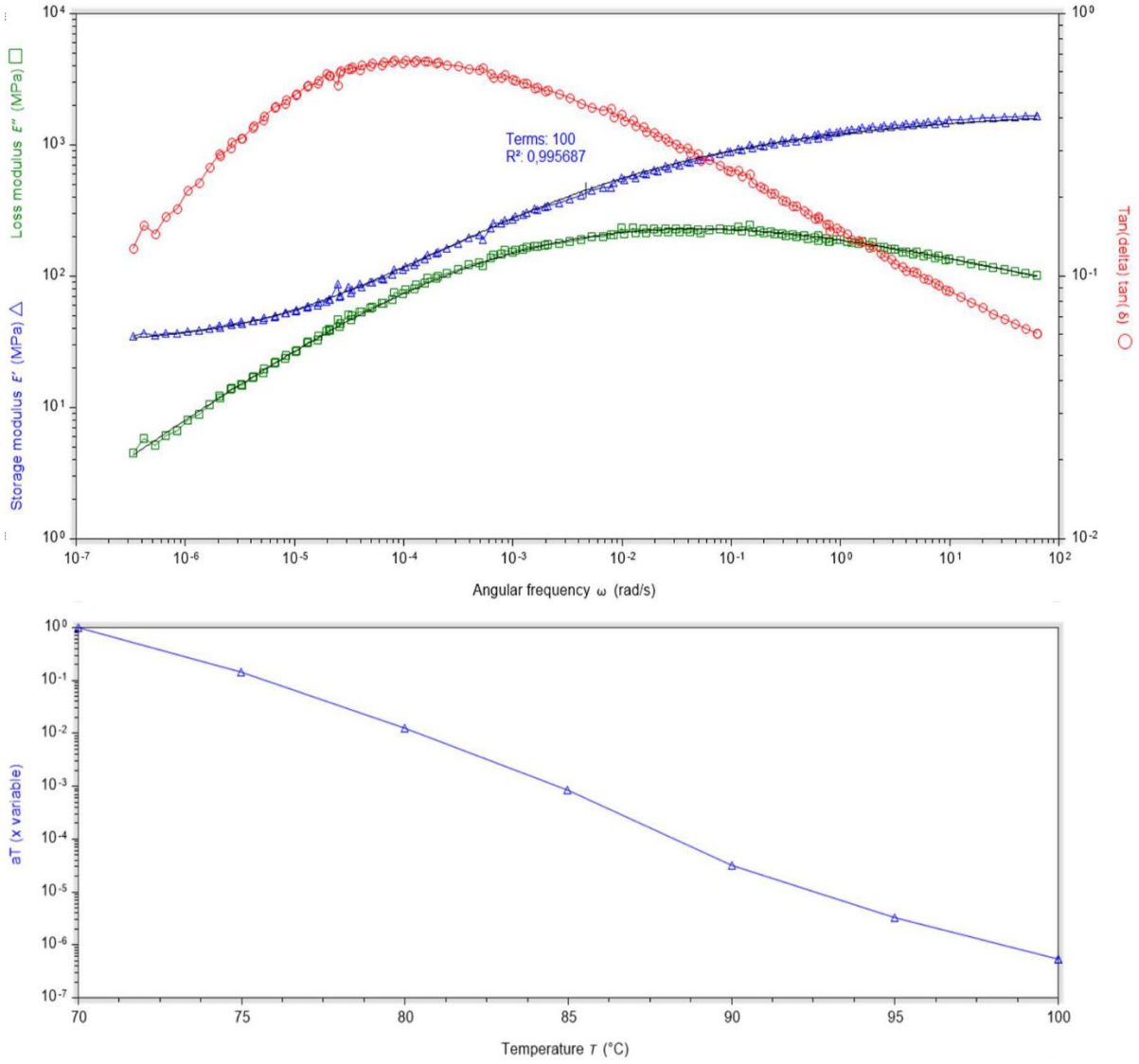

Figure B 9 *Reduced TTS master curve and horizontal shift factors a_T for: fully PD SH epoxy #3. T_{ref} = 70°C.*

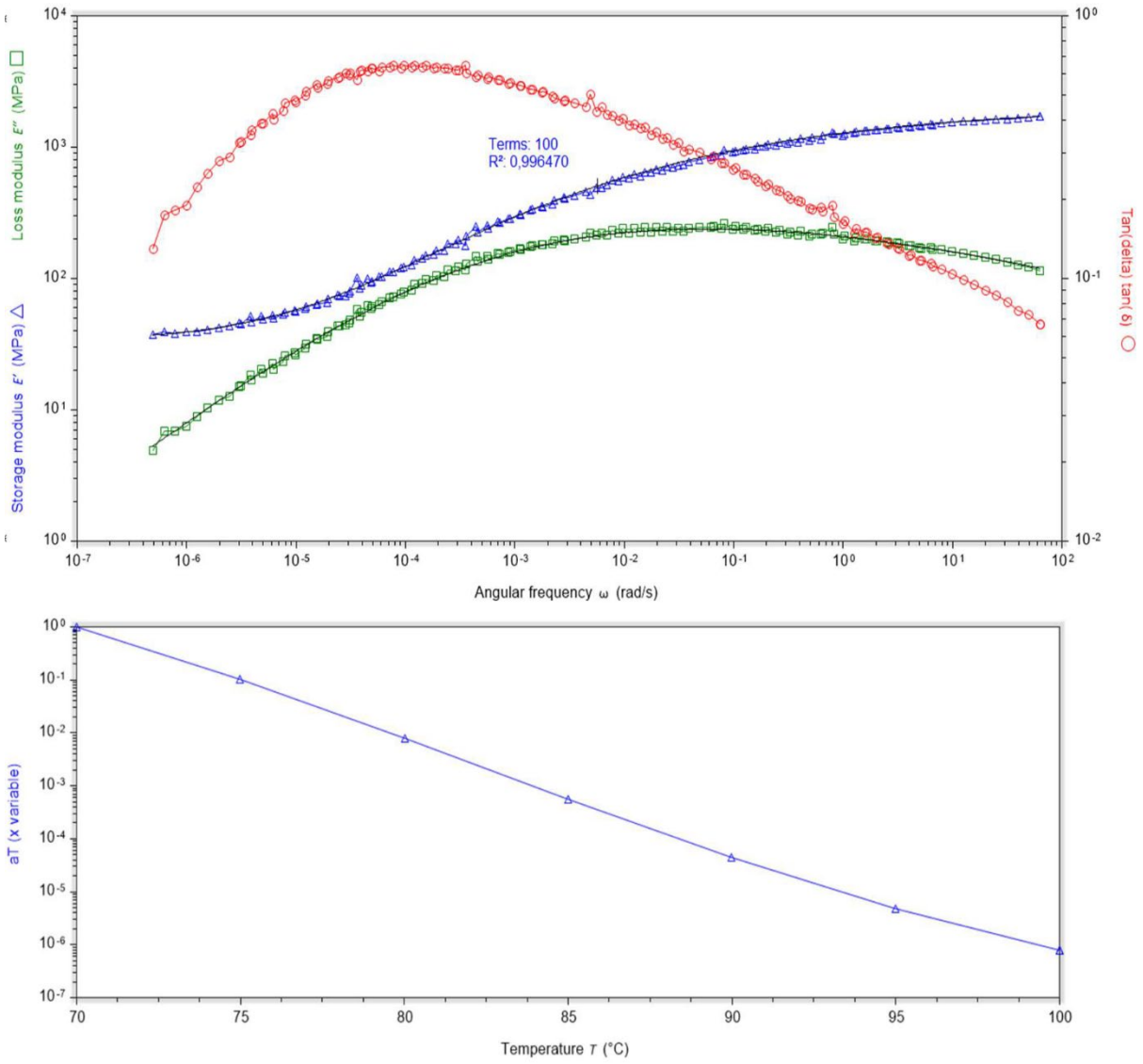

Figure B 10 *Reduced TTS master curve and horizontal shift factors a_T for: pristine SH epoxy before oven. T_{ref} = 70°C.*

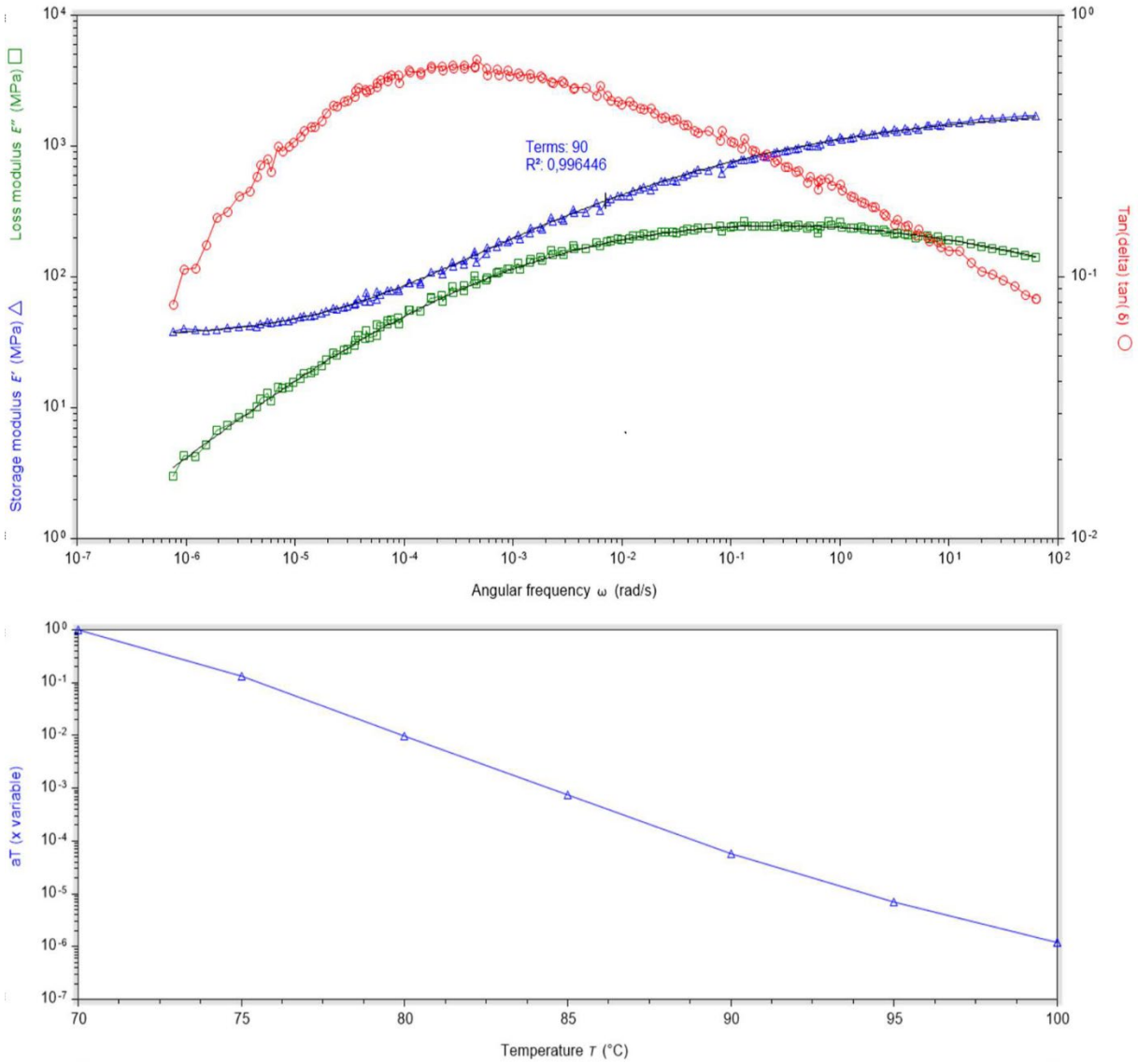

Figure B 11 *Reduced TTS master curve and horizontal shift factors a_T for: pristine SH epoxy after oven. T_{ref} = 70°C.*

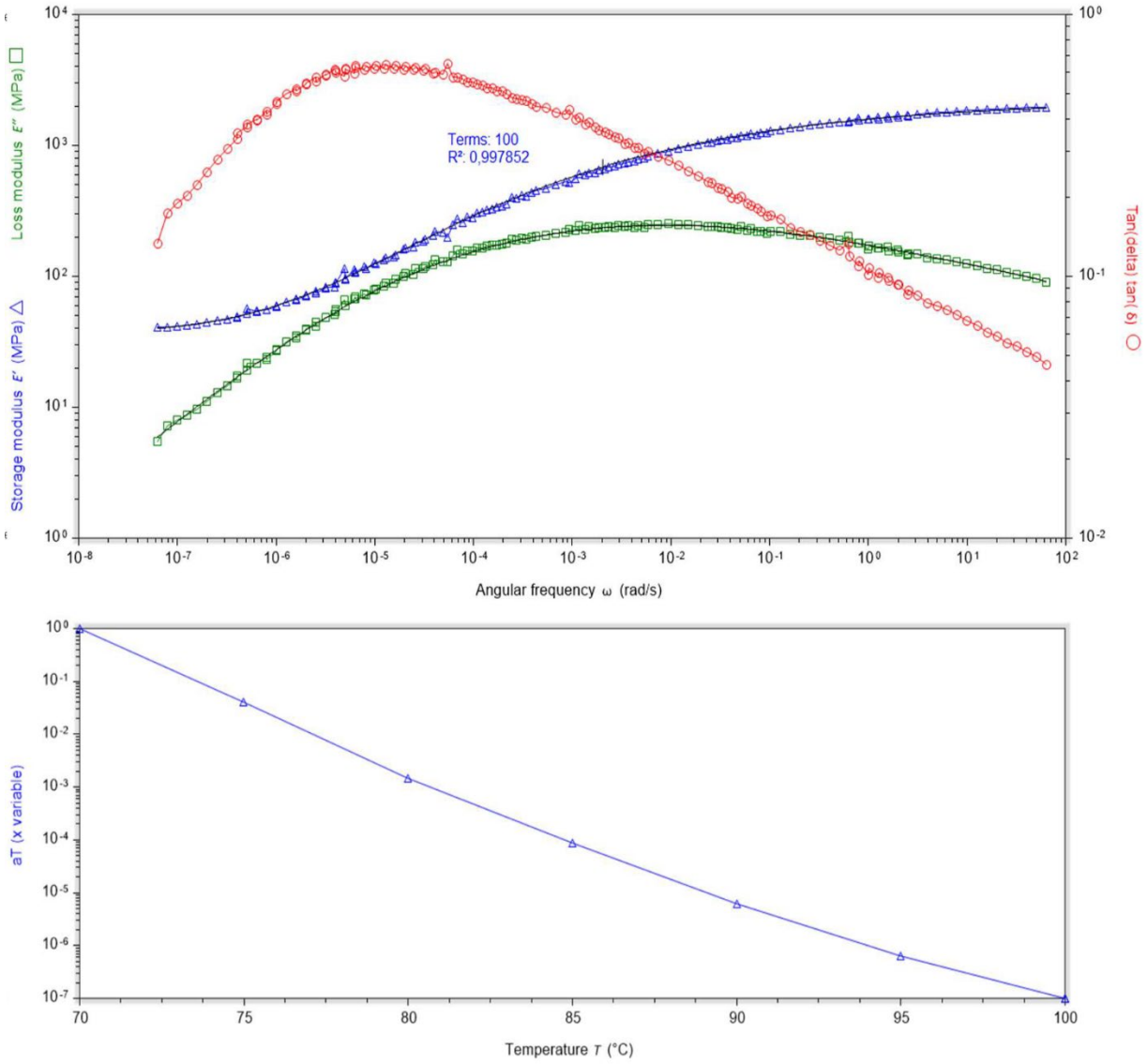

Figure B 12 *Reduced TTS master curve and horizontal shift factors a_T for: fully PD SH epoxy before oven. T_{ref} = 70°C.*

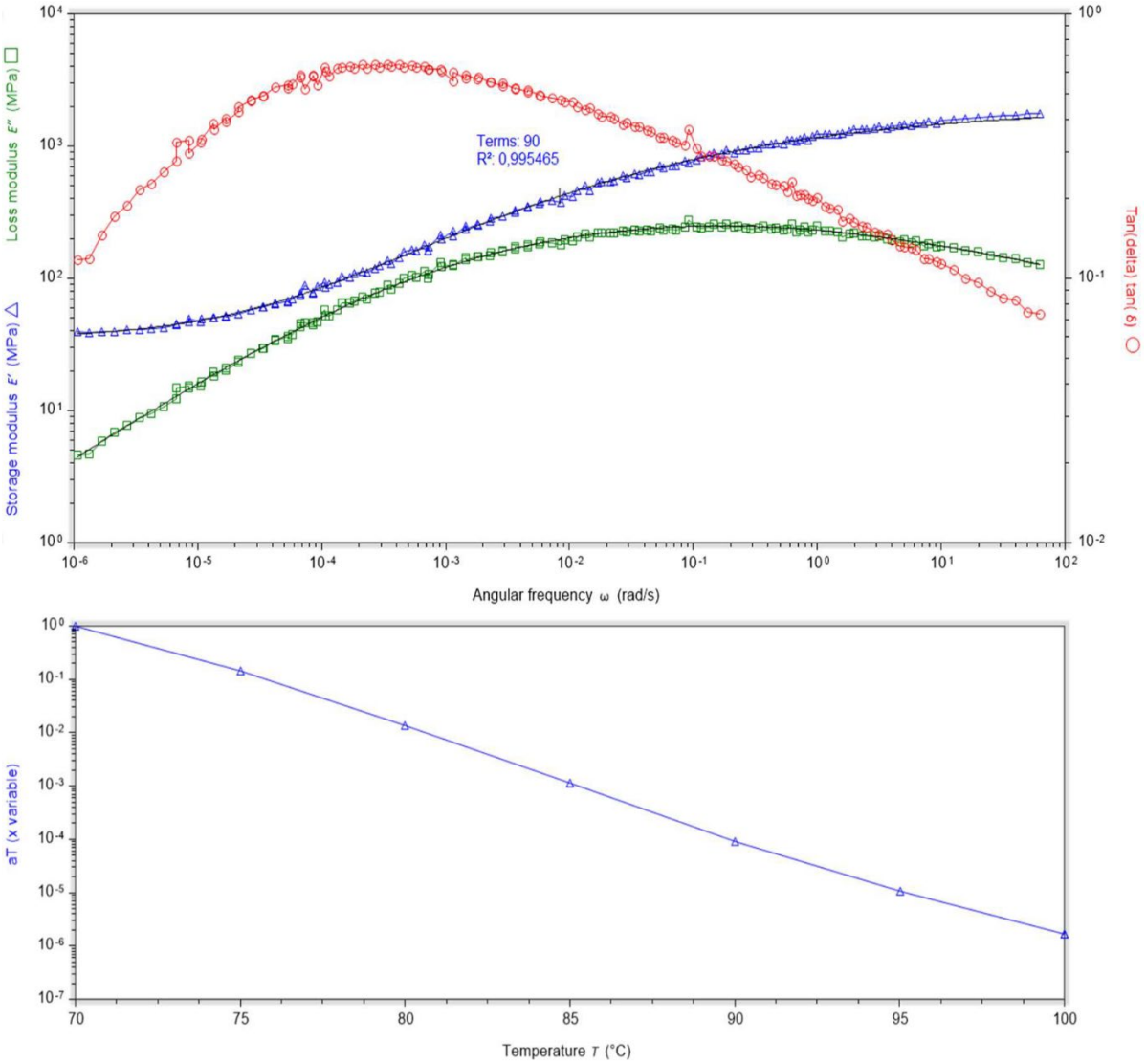

Figure B 13 *Reduced TTS master curve and horizontal shift factors a_T for: fully PD SH epoxy after oven. T_{ref} = 70°C.*

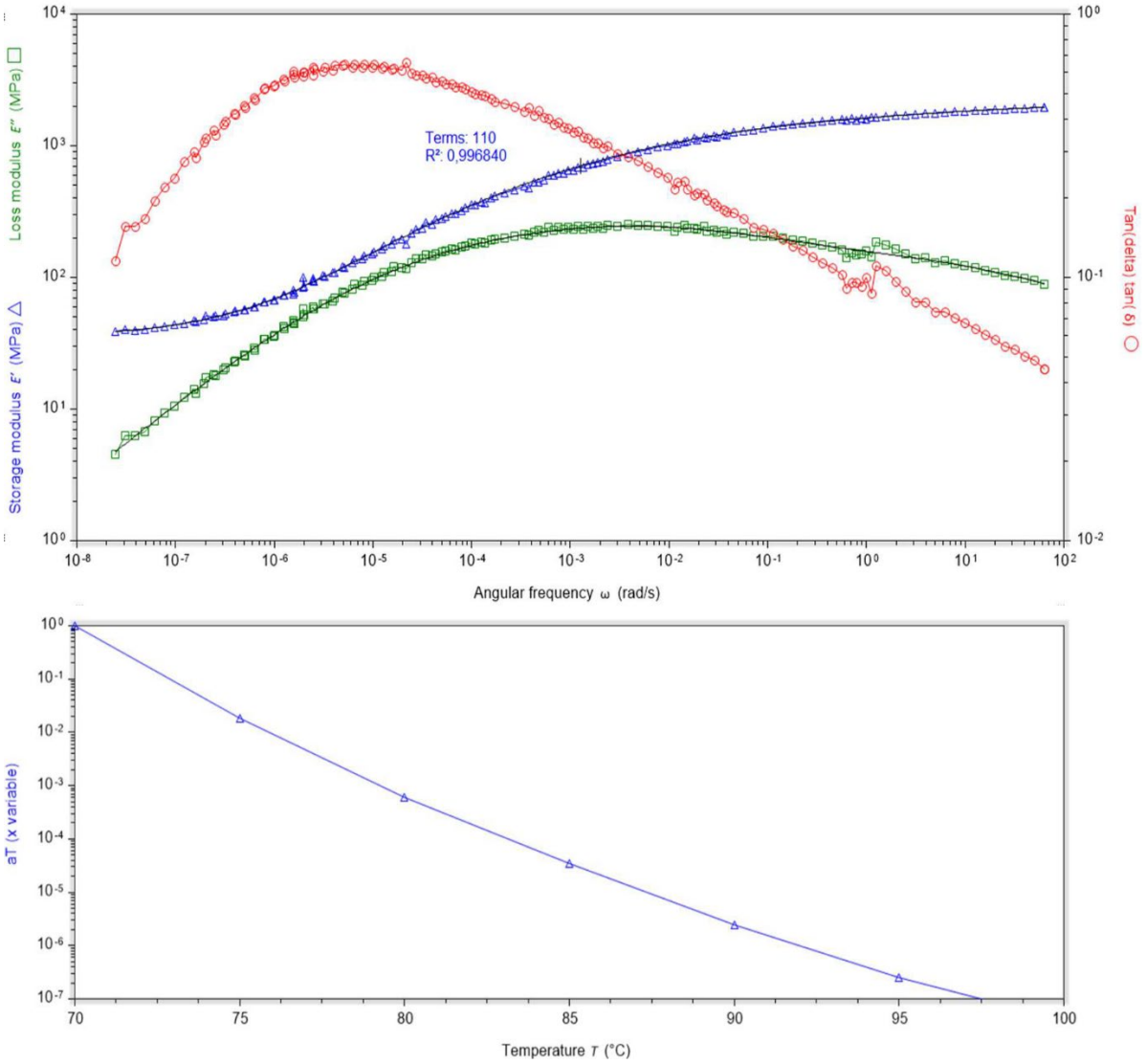

Figure B 14 *Reduced TTS master curve and horizontal shift factors a_T for: pristine NH epoxy before oven. T_{ref} = 70°C.*

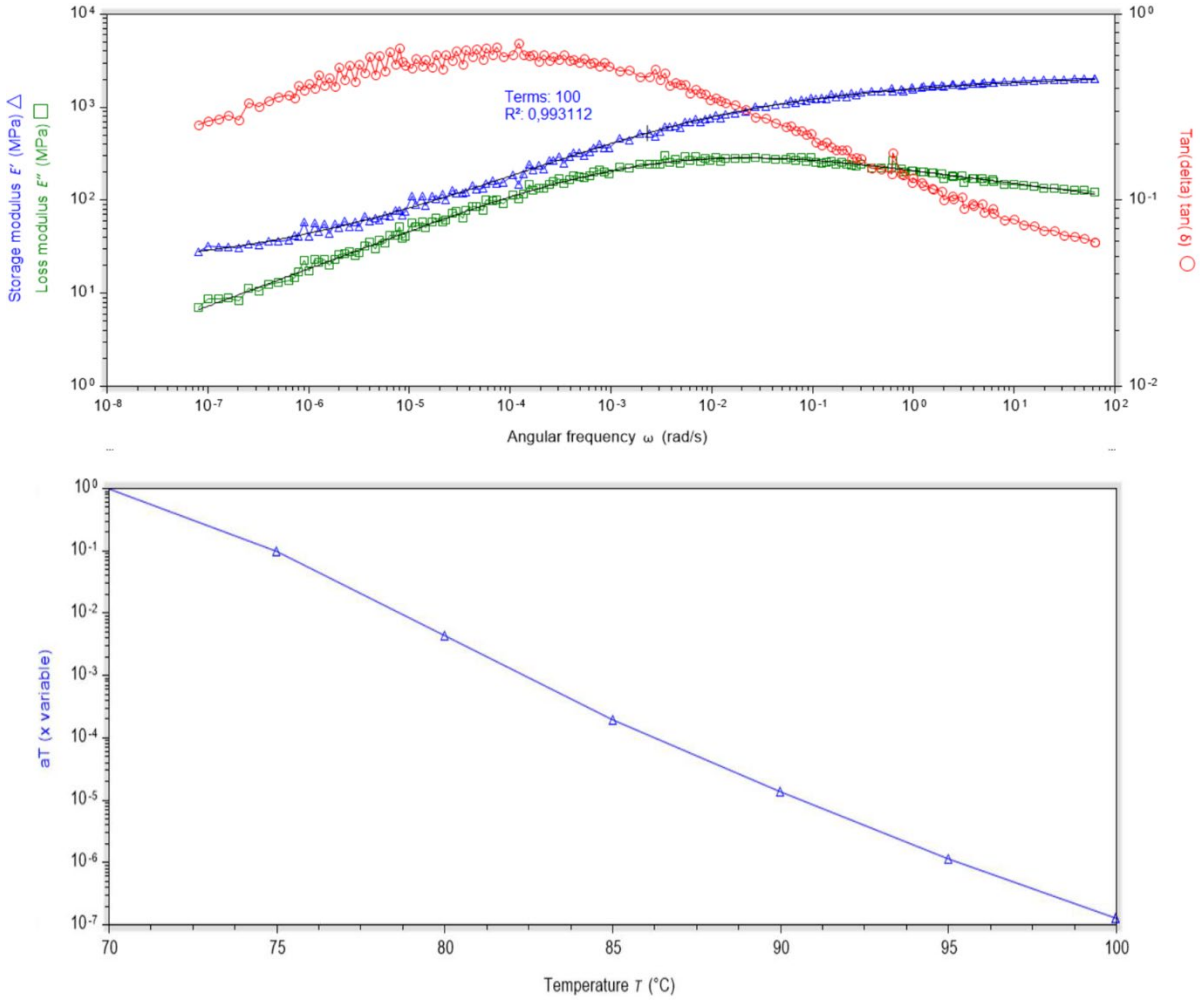

Figure B 15 *Reduced TTS master curve and horizontal shift factors a_T for: pristine NH epoxy after oven. T_{ref} = 70°C.*

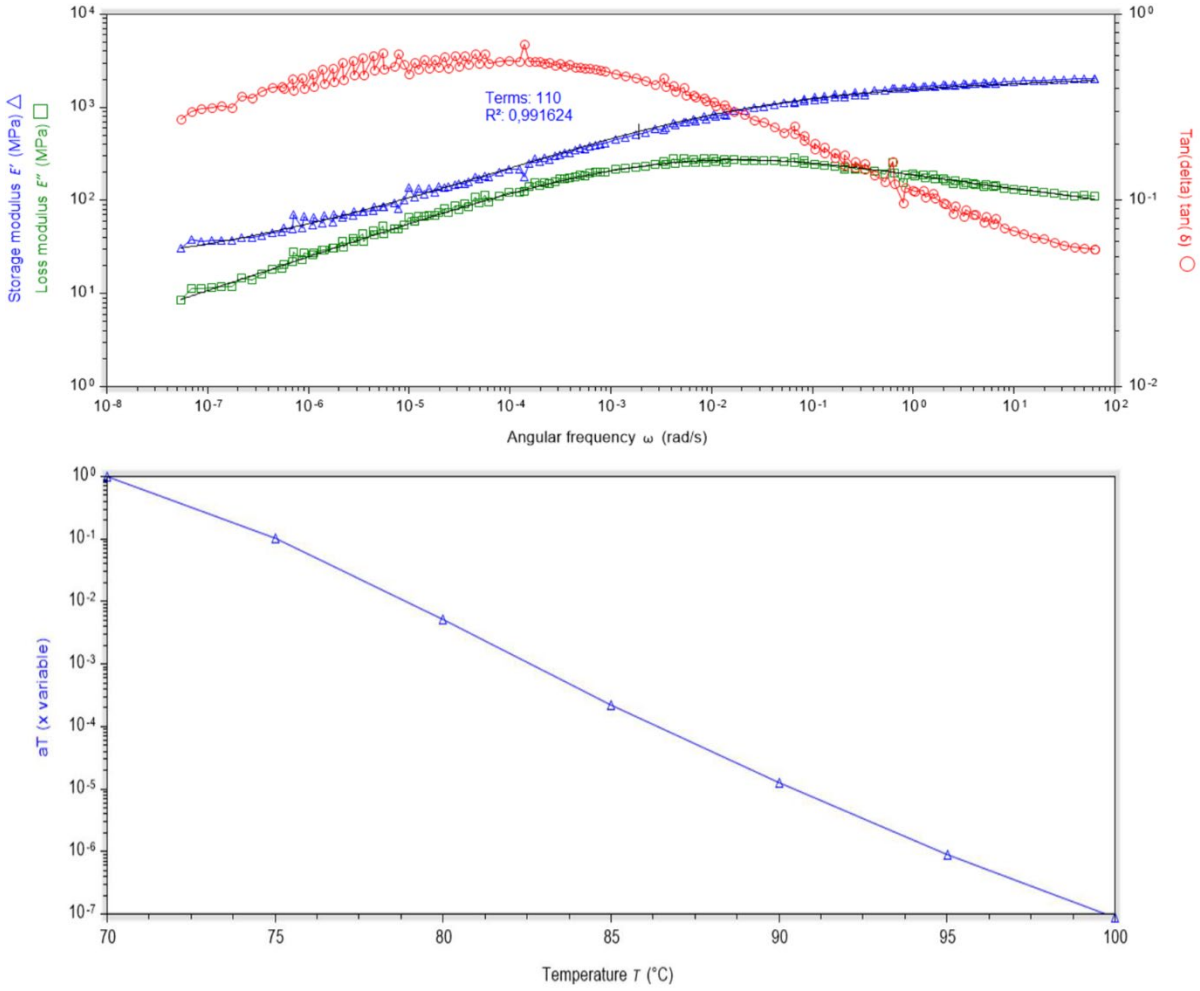

Figure B 16 *Reduced TTS master curve and horizontal shift factors a_T for: fully PD SH epoxy, no oven 1st TF sweep. T_{ref} = 70°C.*

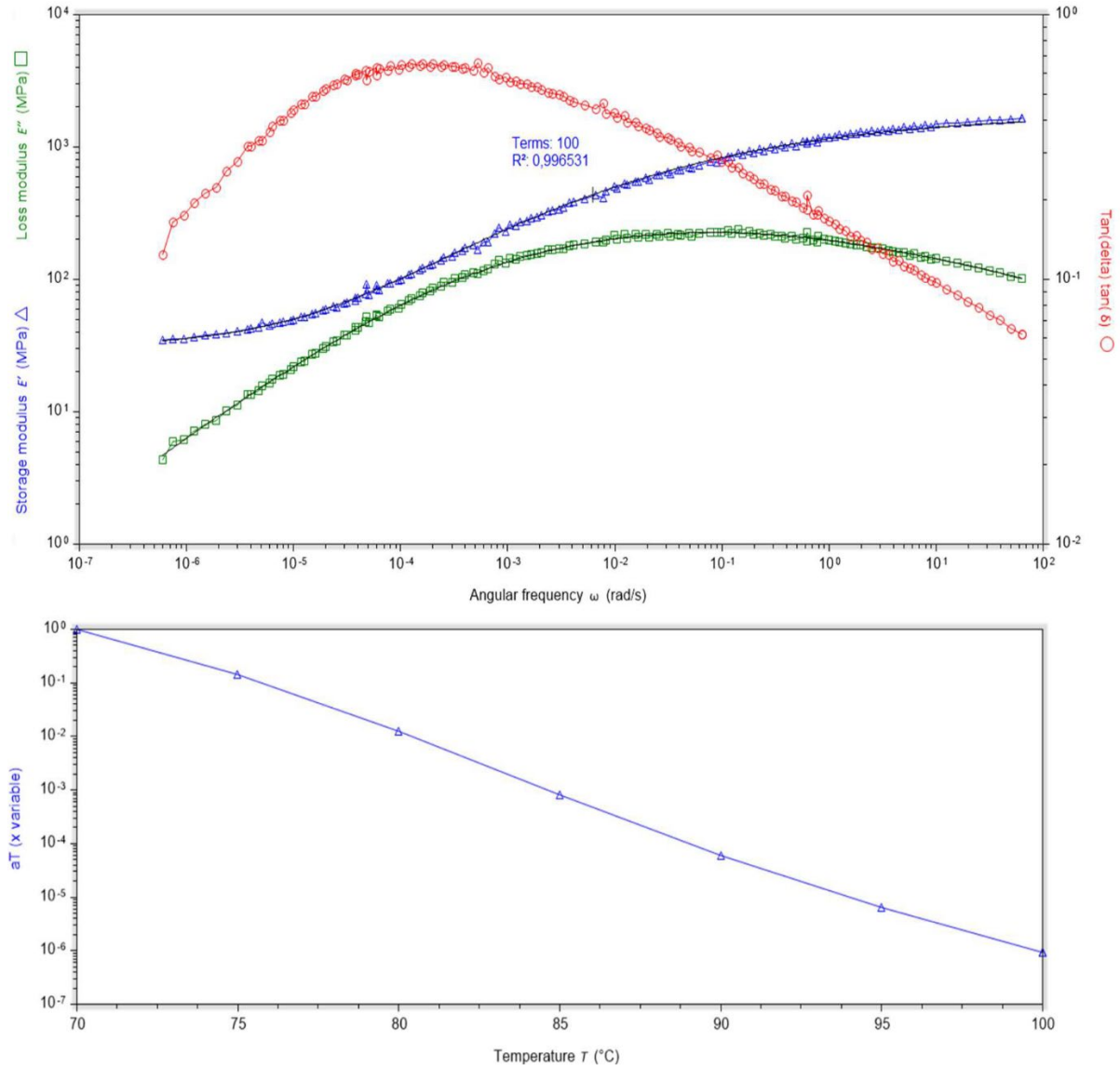

Figure B 17 *Reduced TTS master curve and horizontal shift factors a_T for: fully PD SH epoxy, no oven 2nd TF sweep. T_{ref} = 70°C.*

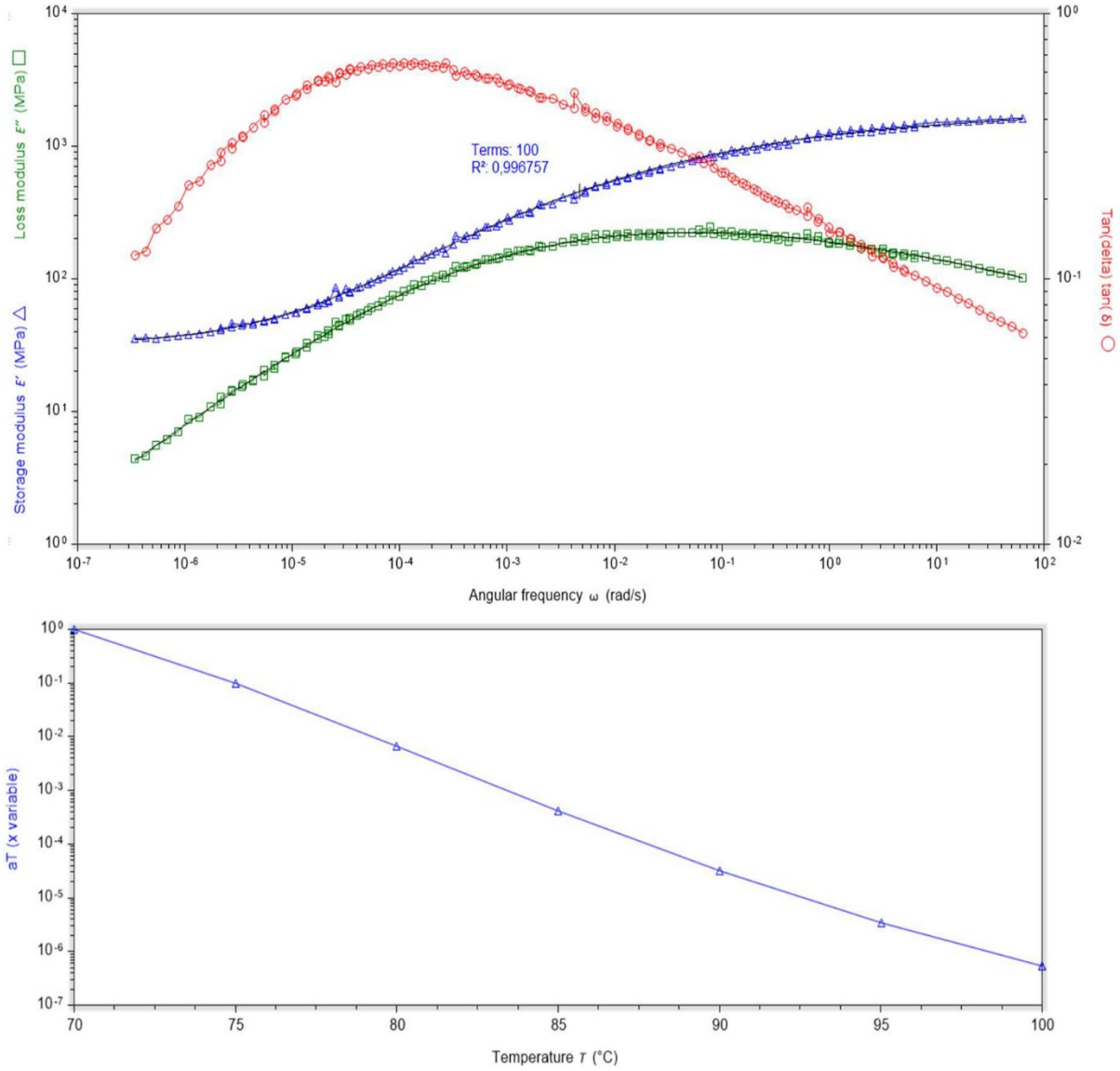

Figure B 18 *Reduced TTS master curve and horizontal shift factors a_T for: fully PD SH epoxy, after oven, before one week recovery. T_{ref} = 70°C.*

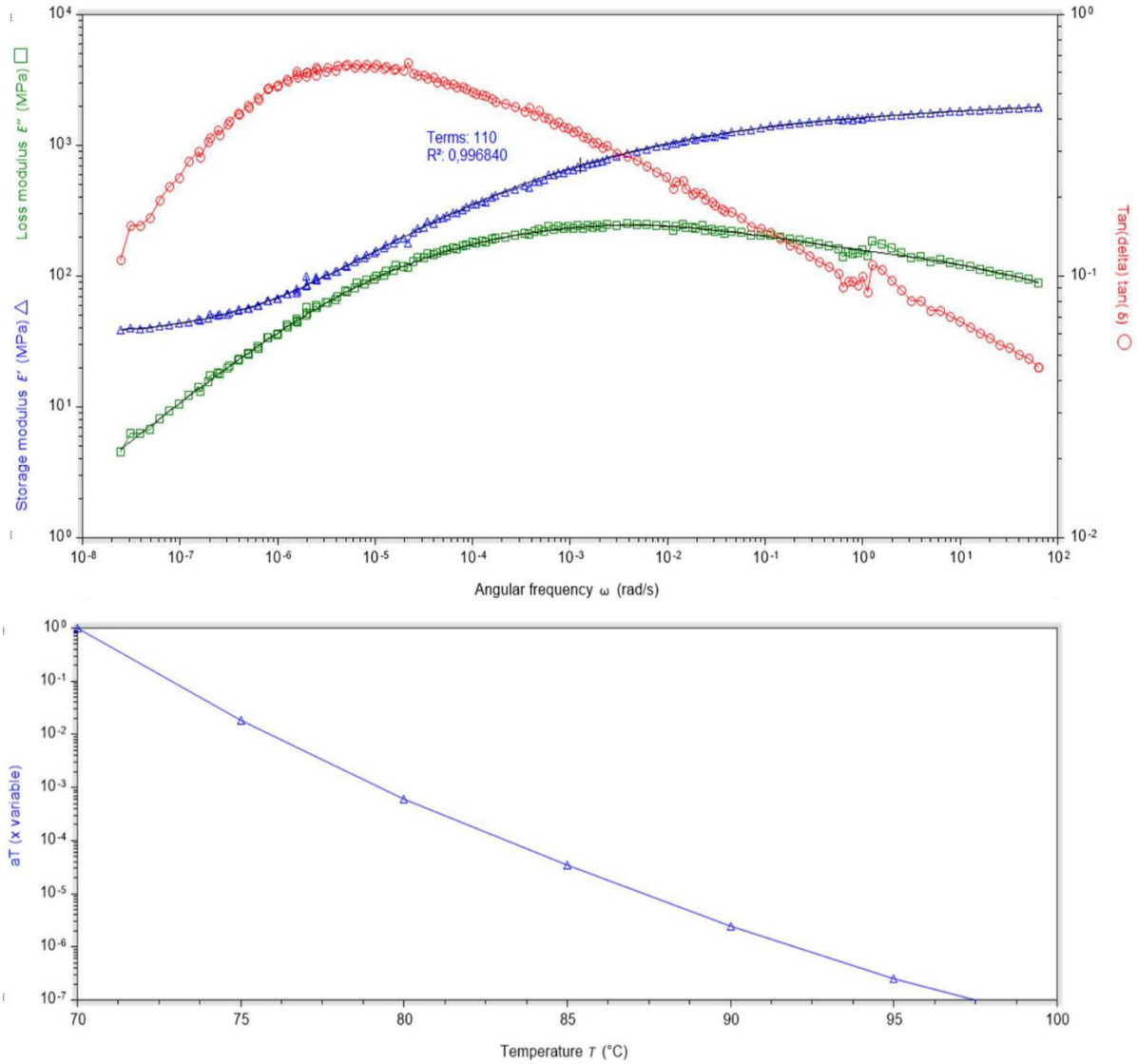

Figure B 19 *Reduced TTS master curve and horizontal shift factors a_T for: fully PD SH epoxy, after oven, after one week recovery. T_{ref} = 70°C.*

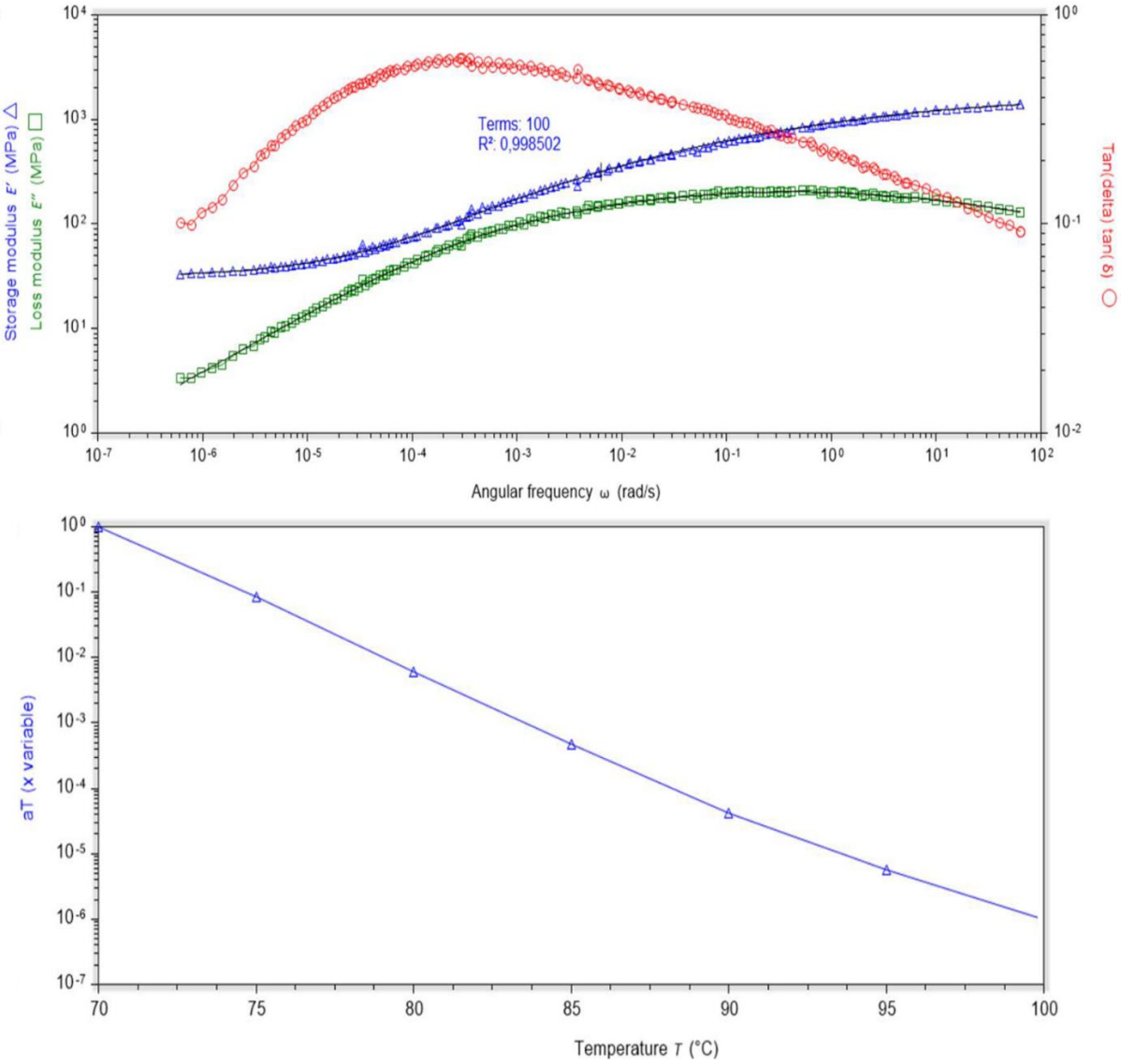

Figure B 20 *Full TTS master curve and horizontal shift factors a_T for: pristine SH epoxy. T_{ref} = 70°C.*

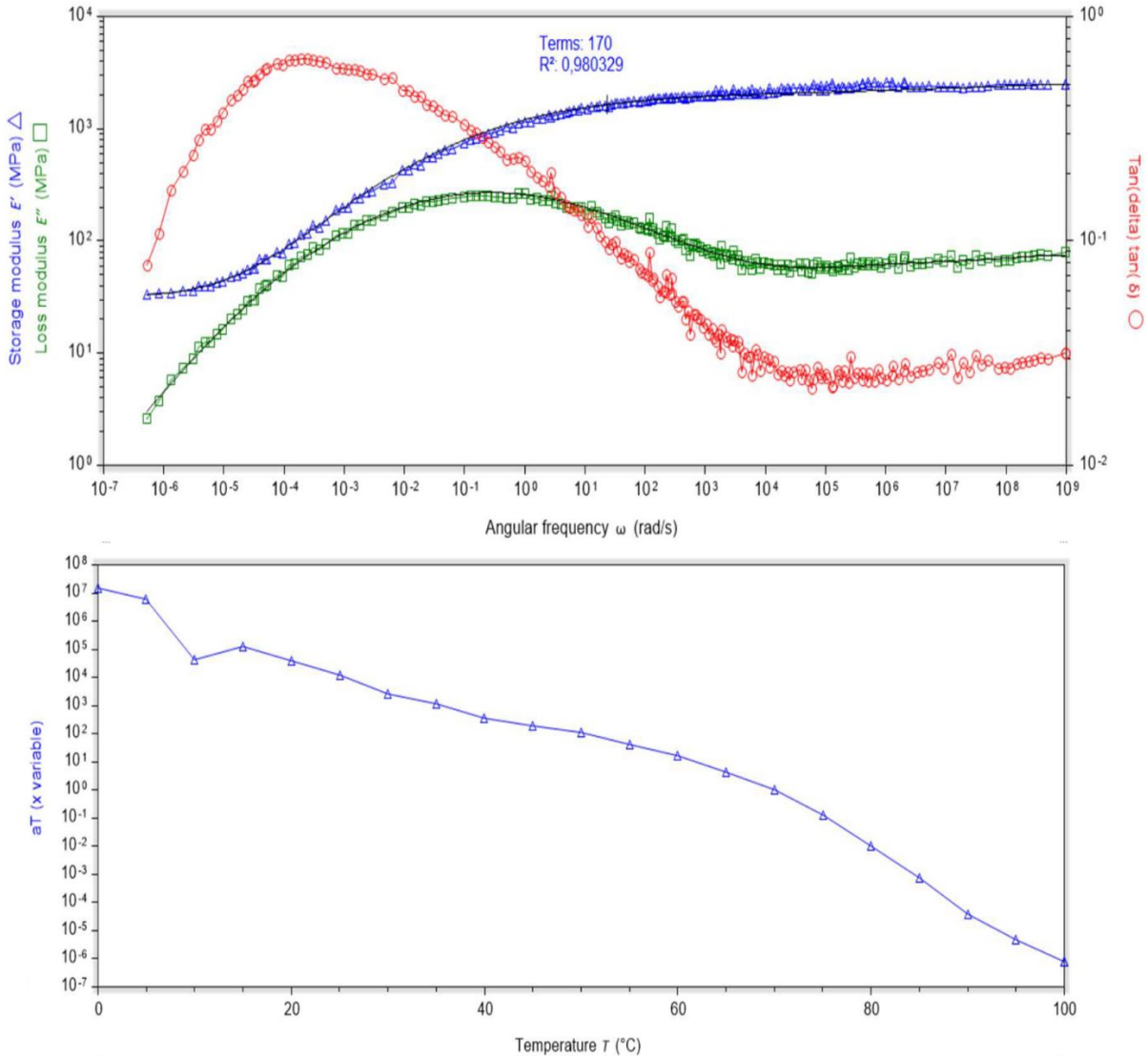

Figure B 21 *Full TTS master curve and horizontal shift factors a_T for: pristine NH epoxy. T_{ref} = 70°C.*

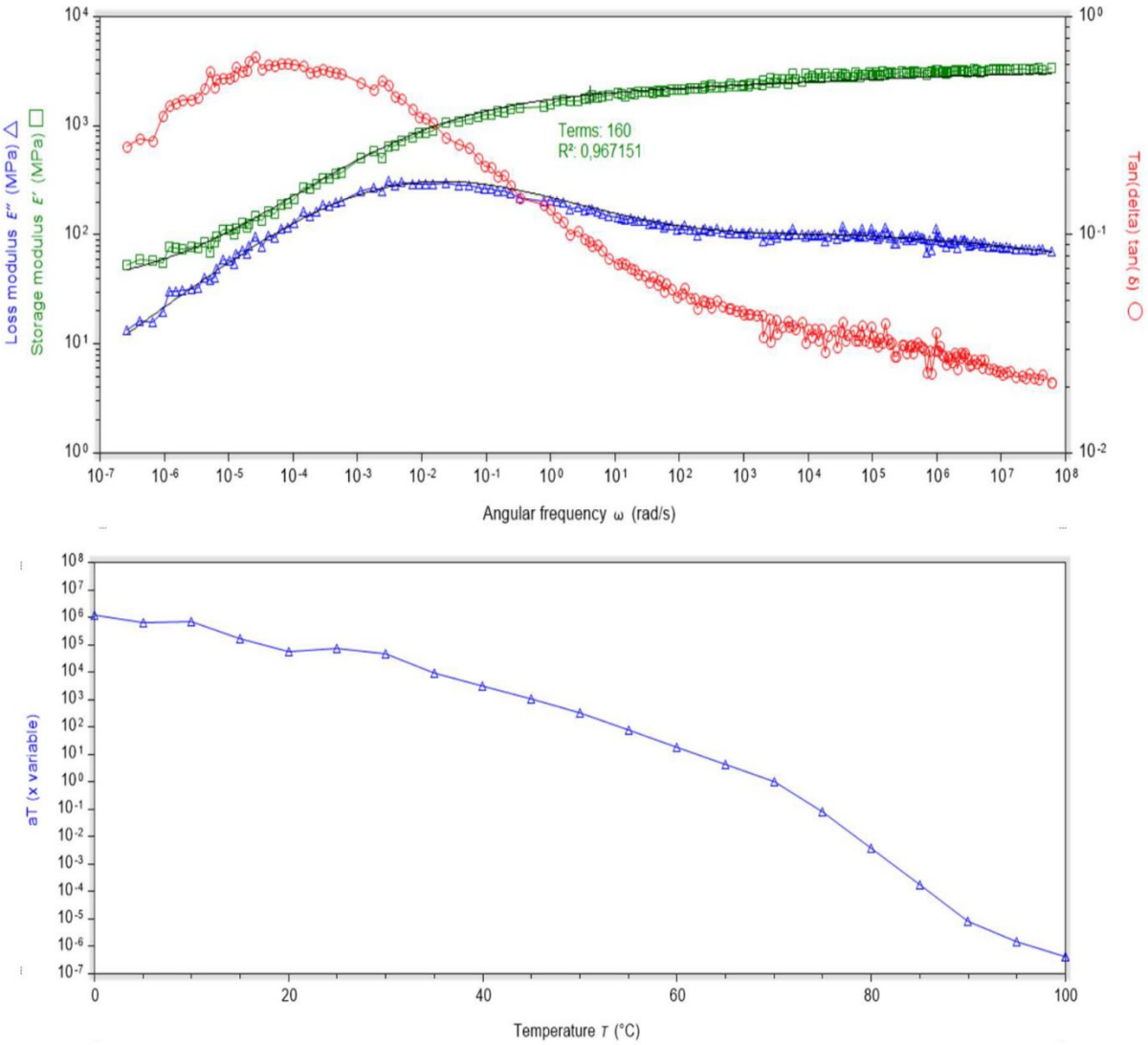

Figure B 22 *TTS master curve data from alternative DMA device. T_{ref} = 70°C.*